The influence of oceanic oxidation on serpentinite dehydration during subduction

Annette Bretscher, Joerg Hermann, Thomas Pettke*

University of Bern, Institute of Geological Sciences, Baltzerstrasse 1&3, CH-3012 Bern, Switzerland

*corresponding author: Thomas Pettke (pettke@geo.unibe.ch)

Please cite this paper as:

Bretscher, A., Hermann, J., Pettke, T.,(2018) The influence of oceanic oxidation on serpentinite dehydration during subduction. EPSL 499, 173–184

DOI: 10.1016/j.epsl.2018.07.017

If you wish to receive the journal reprint, please drop a line at:

pettke@geo.unibe.ch

Abstract

Serpentinites are central to carry water and fluid-mobile elements down subduction zones. The breakdown of antigorite represents the most prominent aqueous fluid release, boosting fluid-mediated element cycling from the slab to the mantle wedge. At Cerro del Almirez, Spain, an antigorite dehydration reaction front is preserved in subducted serpentinites. Bulk rock and mineral major element chemistry linked to detailed petrography reveals that silicate mineral Mg# ((100*[Mg/(Mg+Fe)]$_{molar}$) are higher than bulk rocks due to the presence of magnetite, and olivine Mg# are lower in Chl-harzburgite than in Atg-serpentinite. The amount of magnetite is lower in Chl-harzburgite (1.4 vol%) than in Atg-serpentinite (2.8 vol%), resulting in reactive bulk rock compositions with Mg# of 92.7 and 96.0, respectively. Pseudosection modelling employing these reactive bulk compositions yields a small temperature field at 670°C, 1.6 GPa where Atg-serpentinite and Chl-harzburgite coexist at the same metamorphic conditions. Thus, the antigorite dehydration front represents a compositional boundary rather than a thermal front (isograd). We suggest that this compositional boundary represents an oxidation front established upon serpentinisation at the ocean floor. Previous studies have shown that with increasing extent of serpentinisation increasing amounts of magnetite are formed concomitant with an increase in the Mg# of coexisting silicates. During subduction of such heterogeneous ultramafic rocks antigorite dehydration will be a continuous reaction that can occur over up to ~40 °C, controlled by variations in Mg# of the reactant silicates. The difference in the amount of magnetite between Atg-serpentinite and Chl-harzburgite is thus not related to a change in redox budget of subducting serpentinites at Almirez imposed by the antigorite dehydration reaction. Rather, mass balance considerations suggest that ferric iron from antigorite may actually be the most prominent contribution to the redox budget of the antigorite dehydration reaction. Our findings also imply that direct comparison between Atg-serpentinites and Chl-harzburgites to infer geochemical changes associated with prograde dehydration reactions may lead to erroneous conclusions, including estimates on element loss mediated by aqueous fluid escape and associated changes in redox budget based on Fe^{3+}/Fe_{tot}.

Keywords

- Subduction
- Serpentinite
- Redox
- Metamorphic dehydration
- Mineral chemistry
- Oceanic alteration

1. Introduction

Serpentinites play a major role in the fluid-mediated element cycling in subduction zones, owing to their capacity of carrying water and fluid mobile elements to subarc depths (e.g., Ulmer and Trommsdorff, 1995; Scambelluri and Philippot, 2001; Rüpke et al., 2004; Scambelluri et al., 2004, 2014; Hattori and Guillot, 2007; Kendrick et al., 2011, 2013; Deschamps et al., 2013). Upon serpentinite dehydration (antigorite-out and chlorite-out reactions) occurring somewhere between ~50 and 150 km depth (e.g., Ulmer and Trommsdorff, 1999), up to 13 wt% H_2O (depending on the degree of initial hydration) along with fluid mobile elements are released (van Keken et al., 2011), to eventually trigger arc magmatism via fluid-fluxed melting in the overlying mantle wedge, and to affect rheological and seismic properties of the subducting slab and the slab to wedge interface (e.g., Spandler and Pirard, 2013; Konrad-Schmolke et al., 2016).

Hydrated mantle rocks are among the simplest rock compositions to study metamorphic dehydration reactions when compared to metapelitic or metamafic rocks. In mafic and pelitic rocks, there is a large variation in bulk rock composition, especially in the Mg# ($100*[Mg/(Mg+Fe)]_{molar}$, where all Fe is considered to be Fe^{2+}), leading to continuous dehydration reactions over large temperature intervals (Thompson, 1976). In contrast, hydrated mantle rocks such as serpentinites have a limited compositional range and Mg# is nearly constant at 90 (Niu, 2004). Because of this high Mg#, phase relations in serpentinites have often been approached in the simplified MgO-SiO_2-H_2O (MSH) system (e.g., Ulmer and Trommsdorff, 1999; Wunder and Schreyer, 1997), resulting in univariant (discontinuous) dehydration reactions. However, results obtained from experimental petrology using a natural serpentinite composition (e.g., Ulmer and Trommsdorff, 1995) and, specifically, on the effect of Mg# on serpentine dehydration (Padrón-Navarta et al., 2010), as well as calculations on the increase of serpentine stability by incorporation of Al (Padrón-Navarta et al., 2013) all indicate that small variations of bulk rock compositions may influence the positions and temperature intervals of dehydration reactions.

Variations in bulk rock composition of mantle rocks are mainly driven by melt depletion trends, leading to reduction in Al and Ca and a small increase in Mg# (e.g., Niu, 2004). It has been proposed that the major element bulk rock composition of hydrated mantle rocks largely corresponds to its precursor peridotite except for addition of carbonates and H_2O and possible loss of CaO in case of carbonate-

73 free serpentinites (e.g., Niu, 2004). However, ocean floor hydration of peridotites can significantly
74 modify the distribution of major elements between minerals, including the formation of magnetite,
75 hydrous silicates such as brucite [$(Mg,Fe)(OH)_2$] and chlorite, and sometimes carbonates (e.g.,
76 Kodolanyi et al., 2012) and therefore generates significant heterogeneity at mm to km scales along
77 with orders of magnitude variations in trace element signatures (e.g., Bonatti et al., 1984; Kodolanyi et
78 al., 2012; Niu, 2004; Paulick et al., 2006; Savov et al., 2005).

79 In this paper we address the question to what extent chemical variations induced by serpentinisation
80 and oxidation at the seafloor influence metamorphic dehydration reactions during subduction. We
81 investigated the well-studied locality at Cerro del Almirez (Betic Cordillera, S-Spain), where a contact
82 between Atg-serpentinite and Chl-harzburgite is preserved in subducted ultramafic rocks. This field
83 occurrence has thus become the type locality to study the petrology (Padrón-Navarta et al., 2010;
84 Trommsdorff et al., 1998), and the evolution of chemistry and parameters (e.g., redox, element
85 mobility in antigorite dehydration fluid) across the antigorite-out reaction by a simple comparison
86 between reactant Atg-serpentinites and product Chl-harzburgites (e.g., Alt et al., 2012, 2013; Debret
87 et al., 2014, 2015; Garrido et al., 2005; Harvey et al., 2014; Marchesi et al., 2013; Padrón-Navarta et
88 al., 2010, 2011; Scambelluri et al., 2004). We performed detailed petrography, bulk rock and mineral
89 chemistry and combined this with thermodynamic modelling, in order to evaluate the role of changing
90 magnetite contents acquired during oceanic serpentinisation of the mantle rocks on the nature of the
91 reaction front at high pressures from Atg-serpentinite to Chl-harzburgite at Cerro del Almirez.

92

93 2. Geological setting

94 The hydrous mantle rock units at Cerro del Almirez belong to the Nevado-Filábride Complex, the
95 lowermost tectonometamorphic unit of the Internal Zone of the Betic Cordillera (southern Spain; Fig.
96 1), being part of the Betic Ophiolite Association that represents exhumed slices of the Piemont-
97 Ligurian Ocean (Puga et al., 1999; Trommsdorff et al., 1998). The Almirez Atg-serpentinites and Chl-
98 harzburgites occur intercalated with metasediments (quartzite, micaschist, marble) and, locally,
99 orthogneiss (Schönbächler, 1999). Breakdown of antigorite at eclogite facies conditions (1.6-1.9 GPa
100 and 680-710 °C; Padrón-Navarta et al., 2010) was driven by Alpine subduction in the middle Miocene

as revealed by U-Pb zircon ages of 15.0 ± 0.6 Ma in meta-clinopyroxenite from Cerro del Almirez (López Sánchez-Vizcaíno et al., 2001). An oceanic origin of the Almirez hydrous mantle rocks is indicated by the occurrence of meta-rodingites (Trommsdorff et al., 1998), by specific trace element systematics (Scambelluri et al., 2004; Peters et al., 2017), and by the composition of H-C-O-S isotopes (Alt et al., 2012).

At Cerro del Almirez three bodies of Atg-serpentinites associated with Chl-harzburgites crop out, the largest of which measuring 1.1 x 2.5 km from which all but one of our samples originate (illustrated in Fig. 1). The lithologies at Cerro del Almirez preserve the high-pressure antigorite dehydration as a tectonically undisturbed contact between variably foliated Atg-serpentinites and massive Chl-harzburgites that developed obliquely to the foliation of the Atg−serpentinite and is well exposed in the field (Schönbächler, 1999; Trommsdorff et al., 1998; Padrón-Navarta et al., 2011).

3. Samples and Results

3.1. Petrography of the hydrous mantle rocks

Mineral assemblages of 15 samples were investigated that illustrate the successive prograde growth stages of the various minerals across the antigorite-out mineral reaction. Rocks are referred to as Atg-serpentinites, two transitional lithologies, and Chl-harzburgites (following Padrón-Navarta et al., 2011; mineral abbreviations after Whitney and Evans, 2010). Rocks showing prominent late retrograde formation of serpentine filling cracks were discarded from further investigation; however, retrograde serpentinisation along cracks was observed in most transitional lithologies and Chl-harzburgites. Textures and mineral abundances are summarized in Table 1, and a sequence of mineral parageneses along the transition is illustrated in Figure 2.

Antigorite serpentinites: Atg-serpentinites are texturally heterogeneous. Weakly to strongly foliated types predominate over massive serpentinites, and mineralogy and modal abundances are variable (Table 1). Atg-serpentinites consist of antigorite, olivine, clinopyroxene, rare tremolite, magnetite clots rarely associated with chlorite, and titanoclinohumite. Porphyroblastic Ol-1 is variably fragmented and commonly rich in opaque and antigorite inclusions. Texturally it cannot be distinguished if olivine

formed from the reaction of brucite with antigorite (Ol-1a) or from the reaction of diopside and antigorite (Ol-1b; Fig. 2). Atg-1 forms the variably foliated rock matrix, and larger antigorite blades are less well oriented and may grow over inclusion-rich olivine or clinopyroxene but not tremolite. Dusty Cpx-1 (Fig. 3a) is the only relic mantle mineral, showing occasional magnetite lamellae. Prograde Cpx-2 forms clear rims on Cpx-1 or isolated clear neoblasts. Euhedral Tr-1 may overgrow clinopyroxene (Fig. 3b) or is rarely present as up to 700 µm sized rhombohedral, unoriented crystals that may grow over Ol-1 and the Atg-1 matrix. Chlorite occurs either as a fine-grained felt associated with magnetite (Chl-1, <0.5 vol%) or as inclusions in recrystallized relic clinopyroxene (Chl-2). Ti-chu-1 forms small grains dispersed throughout the matrix. Opaque phases include Cr-rich magnetite (up to 500 µm), subordinate Fe-Ni sulphide, and a Fe-Ti-oxide. Orthopyroxene crystals (Padrón-Navarta et al., 2011) were not observed in our Atg-serpentinite samples.

Chlorite serpentinite and Atg-Chl-Opx-Ol rock: These lithologies characterise the cm to m thick, irregular reaction front between Atg-serpentinites and Chl-harzburgites and document the progressive replacement of antigorite from Atg-serpentinite by antigorite + chlorite, followed by growth of orthopyroxene and olivine until complete antigorite exhaustion. Contacts to the neighbouring rocks are gradational at cm to dm scale and oblique to the regional foliation.

Chl-serpentinite represents the recrystallisation product of foliated Atg-1 from Atg-serpentinite into coarser grained and randomly oriented Atg-2 and Chl-3. The most conspicuous features are (i) euhedral Chl-3 flakes of up to 1 mm, topotactically overgrown by Atg-2 (Fig. 3c and d), and (ii) the absence of clinopyroxene. Tr-1 occurs either as euhedral crystals containing microscopic inclusions of olivine, or interstitially between Chl-3 - Atg-2 intergrowths. Ol-2 forms mm-sized aggregates of individual, clear crystals. Atg-2 grain boundaries against talc are irregular.

Atg-Chl-Opx-Ol rock (i) represents the appearance of orthopyroxene (Opx-1), (ii) has abundant flaky Chl-3 not overgrown by antigorite, (iii) is characterised by reduction in Atg-content to below 10 vol% along with disappearance of fine-grained Atg-1, and (iv) often shows the development of a granular texture similar to that of the granular Chl-harzburgite (see below). Opx-1 is either granular-anhedral and associated with granular-anhedral olivine (Ol-2/Ol-3, Fig. 3e), or Opx-1 forms radial aggregates of thin laths. Olivine is granular, colourless (Ol-2), and may have subordinate brown rims (Ol-3). Rarely, brown olivine grains (Ol-3) can also be observed, and colourless rims (Ol-4) on brown Ol-3 may also

occur. Unoriented Chl-3 flakes not overgrown by antigorite are distributed throughout the rock, while the Chl-3 - Atg-2 intergrowths have a higher chlorite to antigorite ratio compared to those of the Chl-serpentinite. Few, randomly oriented antigorite blades (<1.25 mm) grow over chlorite, olivine and orthopyroxene. Atg-2 and Opx-1 grain boundaries against talc are irregular.

Chlorite harzburgite: Chl-harzburgite occurs as a granular or a spinifex-textured rock (Schönbächler, 1999; Trommsdorff et al., 1998; Padrón-Navarta et al., 2011). Both share an identical mineralogy with only slightly variable modal abundances (Table 1). Their spatial occurrence relative to the contact with Atg-serpentinite is not systematic except that granular rocks are more abundant near the contact to Atg-serpentinites. In fact, granular Chl-harzburgite is texturally very similar to the transitional Atg-Chl-Opx-Ol rock. Transitions between granular and spinifex-textured Chl-harzburgites can be as short as a few centimetres. Rock-forming minerals are randomly oriented.

Brown elongated olivine (up to 10 cm long) predominates in the spinifex-textured Chl-harzburgite, while granular olivine in the granular Chl-harzburgite is exclusively colourless. Opx-1, Chl-3, and magnetite fill the interstices between these olivine crystals. Olivine in variable modal abundances occurs in three growth stages. Clear Ol-2 sometimes form cores of brown Ol-3 (Fig. 3f) that itself may be overgrown by a clear Ol-4 rim. Clear small isometric Ol-4 crystals showing equilibrium texture may also occur in the matrix (Fig. 3f). Clinopyroxene is absent, and Ti-clinohumite is very rare in our samples. Rare tremolite displays equilibrium textures with Chl-3 (Fig. 3h) or overgrows brown Ol-3 or Opx-1. Inclusions of orthopyroxene and olivine in euhedral tremolite were confirmed by RAMAN spectroscopy. Retrograde talc variably replaces orthopyroxene (e.g. Fig. 3g).

Magnetite occurrence and contents: Magnetite modes are higher for Atg-serpentinites (2.8 vol%) than for Chl-harzburgites (1.4 vol%); however, variations within a given rock type are prominent (Atg-serpentinites: 2 - 4 vol%; Chl-harzburgites: 0.4 - 2 vol%). Modes of opaque minerals determined by point counting (Table 1) thereby reflect mostly magnetite for Atg-serpentinites, while the fraction of sulphides in the opaque part can amount to some 30% in Chl-harzburgites. Texturally, magnetite is overgrown by Atg-1 and Ol-1 in Atg-serpentinites (Fig. 4a), testifying to its crystallisation upon ocean floor hydration (Fig. 2). Granular magnetite in Chl-harzburgite (Fig. 4b) commonly displays sharp and even grain boundaries and is also included in Chl-3 and Ol-3 (and Opx-1; not illustrated) resulting from the antigorite breakdown reaction. This equilibrium texture suggests that ocean floor magnetite

may have partially equilibrated upon antigorite breakdown, possibly in association with Fe-sulphide crystallisation. Traces of other oxides (not further investigated) were also observed (compare Debret et al., 2015). Variations in magnetite modes between Atg-serpentinites and Chl-harzburgites at Almirez were also recognized by other studies (Debret et al., 2015; Marchesi et al., 2013; Padrón-Navarta et al., 2011).

3.2. Bulk rock major element concentrations

Major element data acquired for 15 bulk rock samples that cover all lithotypes across the antigorite-out reaction are reported in Supplementary Table 1, employing the methods explained in the Supplementary Material 1. Measured loss on ignition (LOI) values determine bulk rock water contents (subordinate carbonate cannot be excluded), which decrease across the antigorite-out reaction from 11.3 wt% H_2O in Atg-serpentinites typical for complete hydration down to 4.1 wt% H_2O in Chl-harzburgites. Bulk rock major element systematics reveal the combined effects of (i) magmatic mantle history, (ii) oceanic metasomatism, and (iii) partial metamorphic dehydration, of which the magmatic mantle history exerts a dominant control. The mantle rocks are variably refractory and narrowly range in Mg# from 87.7 to 90.9 (all Fe as FeO), typical for upper mantle rocks. In a plot of Al_2O_3/SiO_2 vs. MgO/SiO_2 (Fig. 5a), the samples follow the trend of residual mantle rocks following melt extraction. Some of the samples possess variably low MgO/SiO_2 for their given Al_2O_3/SiO_2 (compare Marchesi et al., 2013) that is typical for abyssal serpentinized peridotites, indicating either addition of SiO_2 or removal of Mg (and Fe) that may have balanced antigorite growth at the expense of chrysotile (e.g., Kodolányi and Pettke, 2011). Alternatively, this may reflect MgO loss during low temperature seafloor alteration (e.g., Niu, 2004). Al_2O_3/SiO_2 ratios are considered to remain unmodified during serpentinization (e.g., Niu, 2004). Alumina concentrations tend to be low, resulting in Al_2O_3/SiO_2 ratios that are typical for abyssal peridotites ($0.01 < Al_2O_3/SiO_2 < 0.07$; Niu, 2004) but higher than most mantle wedge serpentinites ($Al_2O_3/SiO_2 < 0.03$; Deschamps et al., 2013). Despite significant amounts of retrograde talc present in partial to complete antigorite breakdown product rocks, bulk rock SiO_2 concentrations do not show an absolute enrichment relative to the peridotite melting residue trend. Al_2O_3 and SiO_2 show a positive trend across the lithotypes from Atg-serpentinites to Chl-harzburgites, both Al_2O_3 and SiO_2 being higher in Chl-harzburgites compared to all other lithologies. FeO_{tot}

concentrations (for lack of information on Fe^{3+}/Fe^{2+} in our samples we refer to FeO_{tot}) are fairly uniform between 6.9 and 8.7 wt% (except for Atg-Chl-Opx-Ol-rock Alm06-086) as is typical for abyssal peridotites (e.g., Niu, 2004). FeO_{tot} concentrations do not show any trend in Mg# with rock type (Fig. 5b). None of the rocks investigated contains prominent carbonate; elevated CaO concentrations correlate to a first order with clinopyroxene abundance. Very low CaO concentrations result from loss of CaO upon seafloor hydration while Al_2O_3 is retained (Fig. 5c; Table 1, Supplementary Table 1), as is observed in abyssal serpentinites (Paulick et al., 2006).

3.3. Mineral major element concentrations

Electron probe microanalysis (EPMA) measurements were performed on antigorite, chlorite, tremolite, olivine, orthopyroxene, clinopyroxene, Ti-clinohumite, and retrograde talc (for methods see Supplementary Material 1). The complete dataset of major and minor element mineral compositions is reported in Supplementary Table 2. Trace element systematics will be presented elsewhere because these do not affect phase stability systematics. Olivine, antigorite, chlorite, and tremolite of transitional lithologies all have distinctly lower Mg# than those of the Atg-serpentinite (Fig. 6).

Mg# of all olivine growth stages range between 88 and 93.5, similar to those reported in Padrón-Navarta et al. (2011). In a plot of Mg# versus Ni, different textural types of olivine form distinct clusters (Fig. 6a). The highest Mg# of up to 93.5 at low Ni are observed for clear Ol-1 from Atg-serpentinites. In contrast, clear olivine cores from spinifex-textured Chl-harzburgites and clear olivine from Chl-serpentinites (Ol-2) have Mg# extending down to 88 (i.e., the lowest measured), at higher Ni. Brown Ol-3 and its clear Ol-4 overgrowth from spinifex-textured Chl-harzburgites range narrowly between 90.0 and 91.5 and overlap with the most Mg-rich clear olivine cores from this rock. Finally, colourless olivine from granular Chl-harzburgite clusters around $89.5 < Mg\# < 91.0$ and shows the narrowest range (at variable Ni).

Antigorite from transitional lithologies also shows lower Mg# compared to that from Atg-serpentinites (Fig. 6b). Successive antigorite crystallization stages in the Atg-serpentinites and the transitional lithologies delineate a compositional range along a negative Si-Al correlation (not shown) that reflects Tschermak exchange $Al_2Mg_{-1}Si_{-1}$ (1.89-1.97 Si pfu, 0.09-0.23 Al pfu, corresponding to 39.91-44.12

243 SiO_2 and 1.82-4.26 Al_2O_3). The trend in Mg# between Atg-serpentinite and transitional lithologies is
244 less distinct than for chlorite (Fig. 6c) but maintained. Chlorite in Chl-harzburgites shows Mg# identical
245 to those of Atg-Chl-Opx-Ol rocks but extends to higher values for spinifex-textured Chl-harzburgites
246 along with increased Al_2O_3. The Mg# of orthopyroxene ranges from 89 to 91 (Fig. 6d) and thus varies
247 considerably less than that for the other silicates. Average compositions are $En_{83.48}Fs_{16.44}Wo_{0.07}$ for
248 transitional lithologies, $En_{83.56}Fs_{15.28}Wo_{0.16}$ for granular and $En_{83.74}Fs_{16.11}Wo_{0.15}$ for spinifex-textured
249 Chl-harzburgites.

250 Talc is characterized by 97.6<Mg#<99.6 and scatters somewhat more for Chl-serpentinite than for the
251 other rock types. Clinopyroxene Mg# are between 94 and 99, with a few measurements extending
252 down to 91, mainly for mantle relics. Metamorphic Cpx-2 neoblasts cluster at the high Mg# end.
253 Tremolite is also characterised by high Mg#, highest for Atg-serpentinites (98 - 99.3), marginally lower
254 for Chl-harzburgites (97.6 - 98.8) and distinctly lower for transitional lithologies (96.2 - 97.4). Rare Ti-
255 clinohumite in Atg-serpentinite has TiO_2 concentrations of 4.5 to 5.5 wt%, FeO_{tot} ranges between 6
256 and 8 wt%.

257

258 **3.4. Phase diagram modelling**

259 Equilibrium phase diagrams for different bulk compositions were calculated with Perple_X (Connolly,
260 2005) for the CFMASH system at H_2O saturation. Modelling input parameters and reasoning are
261 provided in Supplementary Material 1.

262 Modelling of pseudosections for Atg-serpentinite and Chl-harzburgite requires the determination of
263 reactive bulk compositions for the mineral reactions concerned (compare discussion section below).
264 Reactive bulk compositions are obtained by subtracting the contribution of non-reactive and relic
265 minerals from measured bulk rock compositions. For Atg-serpentinite, 6 vol% relic clinopyroxene
266 (based on the EPMA analyses reported in this study) and 2.8 vol% magnetite (by converting the
267 Fe_2O_3 fraction of magnetite to FeO) were subtracted from average measured bulk rock compositions;
268 for Chl-harzburgite this was 1.4 vol% magnetite only (no relic clinopyroxene observed). This
269 procedure resulted in a significantly lower reactive bulk Mg# for the Chl-harzburgite (92.7) compared
270 to Atg-serpentinite (96.0; Supplementary Table 3); recall that their measured bulk rock Mg# (based on

total iron only) vary little and non-systematically around 90 (Fig. 5b). Pseudosections calculated including 6 vol% clinopyroxene (not shown here) display different phase proportions but returned basically the same topologies and are thus not further considered here.

Figures 7a,b show the calculated phase diagrams for the two reactive bulk compositions together with the Mg# isopleths of olivine that forms at dehydration reactions. The blue arrow shows the prograde PT path of the Almirez hydrous mantle massif consistent with petrography and with peak PT estimations of Padrón-Navarta et al. (2010). The overall topology of the two phase diagrams is very similar.

The first metamorphic olivine is formed at the reaction (reaction a in Fig. 2)

$$Atg + Brc \rightarrow Ol \pm Chl + H_2O \quad (1)$$

This reaction is univariant in the MASH system. The addition of Fe (FMASH system) translates the univariant line into a divariant field, where all phases are stable. Within this field (Fig. 7a), the Mg# of all phases increases with increasing temperature. The first olivine formed at ~460°C has a Mg# of below 80 whereas at the brucite-out location at ~510°C, olivine Mg# has increased to 91. For a reactive bulk Mg# of 92.7, the olivine Mg# of 82 at brucite-out is significantly lower (Fig. 7b).

Tremolite is then formed via the reaction (c in Fig. 2):

$$Atg + Di \rightarrow Ol + Tr + Chl + H_2O \quad (2)$$

The onset of this reaction is also sensitive to the Mg# of the reactive bulk composition, occurring at about 640°C for the Chl-harzburgite and at 660°C for the Atg-serpentinite compositions at 1.6 GPa. Mg# of olivine in equilibrium has increased to 93 for the reactive bulk Mg# of 96.0 (Fig. 7a), while it is 84 for the reactive bulk Mg# of 92.7 (Fig. 7b). We note that this reaction is sluggish and does not run to completion in the serpentinites as relic diopside is common.

The final antigorite breakdown reaction (e in Fig. 2)

$$Atg \rightarrow Ol + Opx + Chl + H_2O \quad (3)$$

is again divariant in the FMASH system. However, for the reactive bulk Mg# of 96.0 it is restricted to a very narrow field at 1.6 GPa, starting at 671°C (orthopyroxene-in) and ending at 676°C. In contrast, the temperature range is larger and at distinctly lower temperature for the reactive bulk Mg# of 92.7,

between 653 and 668 °C (Fig. 7b). Olivine at the antigorite-out boundary has a Mg# of 95 and 91, respectively, approaching the corresponding Mg# of the reactive bulk compositions.

4. Discussion

Comparison between modelling and observations

Comparison between the phase diagrams for the two different bulk compositions (Fig. 7c) identifies the stable coexistence of Atg-serpentinite and Chl-harzburgite within a small temperature interval. There is a narrow field of less than 10°C, where antigorite already disappeared in the Chl-harzburgite with a lower reactive bulk Mg# of 92.7 whereas orthopyroxene has not yet formed in the serpentinite with a higher reactive bulk Mg# of 96.0. A dependence of the onset of antigorite breakdown (orthopyroxene-in) on bulk Mg# has been discussed by Padrón-Navarta et al. (2010, their Fig. 8b) for a rare Opx-bearing Atg-serpentinite ("Si-enriched" Atg-serpentinite) occurring within the Atg-serpentinites at Cerro del Almirez. They found that lowering the Mg# of the reactive bulk of this Si-enriched composition renders the field between the orthopyroxene-in reaction and the antigorite-out reaction larger, thus bringing the onset of antigorite dehydration to lower temperatures, in line with our findings. These observations open the question whether the antigorite dehydration reaction is mainly controlled by the variation in Mg# of the two reactive bulk compositions.

The peak metamorphic pressure is limited to <1.8 GPa by the presence of tremolite in Atg-serpentinites and Chl-harzburgites, in agreement with previous studies (Trommsdorff et al., 1998; Padrón-Navarta et al., 2010). Tremolite plus olivine occur first in the Chl-harzburgite (at 640°C, 1.6 GPa) due to the lower Mg# of the reactive bulk rock composition of Chl-harzburgite. This reaction occurs at 660°C in the Atg-serpentinites, providing a minimum temperature for this rock type. Figure 8 illustrates how the locations of the orthopyroxene-in, the olivine-in, and the antigorite-out boundaries vary as a function of Mg# and temperature at a fixed pressure of 1.6 GPa. In the Fe-free system, the reaction is univariant and orthopyroxene-in occurs at 685°C (Fig. 8a). With increasing amount of Fe, antigorite-out and orthopyroxene-in boundaries diverge and move to lower temperatures. For a typical mantle Mg# of 90, antigorite-out would occur at ~660°C. The increase in the reactive bulk Mg# due to sequestration of Fe into non-reactive magnetite elevates the antigorite-out boundary to 668°C for the

326 Chl-harzburgite. Interestingly at this temperature, the Atg-serpentinite is still below the orthopyroxene-
327 in boundary of reaction 3. Together, this constrains the theoretic peak temperatures reached by the
328 Almirez hydrous mantle rocks tightly to between 668 and 671°C. It is important to stress that the
329 determination of absolute temperatures of metamorphism also depends on the choice of
330 thermodynamic data and solution models and thus likely has an uncertainty of at least 20 °C.
331 However, the result that the temperature difference between all investigated rock types was small
332 (<10°C) is robust.

333 An independent test for this equilibrium modelling result is provided by the measured Mg# of olivine in
334 the two rock types. In Atg-serpentinites Ol-1a and Ol-1b, formed along reactions (1) and (2), have a
335 measured Mg# of between 90 and 93.5 (Fig. 6a). This is in excellent agreement with the calculations
336 that show an Mg# = 91 of olivine at the brucite-out and of 93 at the tremolite-in reactions. (Fig. 7a).
337 Olivine that would have formed upon the antigorite-out reaction would have a Mg# of 95, higher than
338 any of the olivine measurements obtained. To the contrary, the olivine that formed in the Chl-
339 harzburgite from antigorite dehydration displays an overall lower Mg# of between 88 and 91.5 (Fig.
340 6a), in agreement with the more Fe-rich reactive bulk composition (Fig. 8). The lowest Mg# of 88 is
341 found in Ol-2 (Fig. 6a), texturally the oldest olivine associated with the onset of antigorite dehydration
342 (orthopyroxene-in), which is slightly higher than the calculated value of 85. The texturally youngest
343 olivine in Chl-harzburgite (Ol-4) has the overall highest Mg# with a narrow range near 91, closely
344 approaching the predicted value of 91.4 for the antigorite-out boundary. The excellent agreement
345 between measured and calculated olivine compositions for the two different reactive bulk
346 compositions characteristic of Atg-serpentinite and Chl-harzburgite provides strong evidence that the
347 Mg# determines the temperature at which antigorite dehydration occurs, thus controlling water
348 liberation from subducting hydrous mantle rocks.

349 That dehydration of antigorite depends on the Mg# of reactant silicates alone hinges on the
350 assumption that magnetite was not involved in the metamorphic reaction. Let us assume that the
351 original magnetite content was the same in Atg-serpentinites and the protolith of the Chl-harzburgites
352 and that magnetite reacted partially away during the breakdown of antigorite. In this scenario, the core
353 of olivine crystals in the Chl-harzburgite would have an Mg# > 93, and at least some olivine crystals
354 should reveal a reversed zoning with lower Mg# rims around higher Mg# cores when magnetite would
355 progressively be decomposed. The absence of such high Mg# cores and the normal zoning of Mg# in

356 successive olivine generations thus shows that magnetite dissolution during antigorite breakdown was
357 minor at best. It is possible that some magnetite and pentlandite were involved during the formation of
358 Ol-4 (see below) as this olivine generation displays a marked increase in Ni (Fig. 6a). Participation of
359 magnetite at the later stages of the reaction would mean that at the onset of antigorite breakdown, the
360 reactive bulk had a slightly higher Mg#, shifting the "opx-in" boundary to higher temperatures (Fig. 8).
361 The temperature of the "antigorite-out" boundary remains identical, however, as this is constrained by
362 the measured residual magnetite content in the Chl-harzburgites.

363 A further test for the influence of Mg# on metamorphic assemblages can be obtained from the
364 transitional lithologies, the Chl-serpentinite and the Atg-Chl-Opx-Ol-rocks. The newly formed olivine in
365 these rock types covers the same range as in the Chl-harzburgite (Fig. 6a), suggesting that also these
366 rocks originate from a reactive bulk rock with a lower Mg# than the Atg-serpentinites. Indeed,
367 antigorite is still stable in these rocks and its Mg# is significantly lower than the Mg# of antigorite in
368 Atg-serpentinites (Fig. 6b). Therefore, our study reveals that variation in reactive bulk Mg# may be the
369 cause for preservation of the observed antigorite dehydration reaction front that can stably exist at
370 constant peak temperature of about 670°C.

371

372 **4.1. Origin of the antigorite dehydration reaction front**

373 The reaction front of Atg-serpentinite to Chl-harzburgite at Cerro del Almirez developed obliquely to
374 the foliation of the Atg-serpentinite and shows no signs of tectonic activity or offset. For these reasons
375 this contact was interpreted to represent an undisturbed reaction front of antigorite dehydration
376 (Trommsdorff et al., 1998). Over the past 20 years there have been fundamentally different
377 explanations for this dehydration front. The results of our study now add an additional, new
378 hypothesis.

379 *4.1.1. Thermal front*

380 Classically, this front has been regarded as a metamorphic isograd (Garrido et al., 2005; Harvey et
381 al., 2014; Marchesi et al., 2013; Padrón−Navarta et al., 2010, 2011; Trommsdorff et al., 1998), similar
382 to what is observed in contact aureoles (for hydrous mantle rocks see e.g., Trommsdorff and
383 Connolly, 1996). Conceptually, such a view implies that the bulk rock compositions of Atg-
384 serpentinites and Chl-harzburgites are identical except for the loss of water and elements dissolved in

it. Moreover, an isograd would imply a temperature gradient of about 20 °C across a less than 5 m thick, tectonically undisturbed contact zone.

4.1.2. Kinetic front

Padrón−Navarta et al. (2011, p. 2074) have interpreted the sharp contact between Atg-serpentinite and Chl-harzburgite as a reaction front with an approach based on reaction kinetics. If the dehydrating system is not drained (no escape of the Atg−dehydration fluid) the fluid pressure in the system increases. This leads to a drastic decrease of the reaction rate because in such a scenario the reaction path of the rock evolves at increasing fluid pressure parallel to the Clapeyron slopes of the reaction curves (chlorite−in and orthopyroxene−in) and the advancement of the reaction front may come to a halt (metastable overpressure domains). In case of catastrophic rock failure (dehydration embrittlement), fluid overpressure drops back to lithostatic pressure, thus fostering instantaneous crystallisation of spinifex-textured Chl-harzburgites. For cases where no significant fluid overpressure was established, slower reaction rates can be expected to have formed the granular Chl-harzburgites. Such a scenario can elegantly explain the difference between spinifex-textured and granular Chl-harzburgites. However, it is more difficult to maintain supralithostatic fluid pressure at the boundary between Atg-serpentinite and Chl-harzburgite over time without rupturing the rocks; hence, the antigorite dehydration reaction can be delayed but not terminated. Moreover, a thermal gradient is also needed in this model.

4.1.3. Oceanic oxidation front - our preferred explanation

Our results show that the antigorite dehydration reaction front can be explained by different *reactive bulk compositions*, thus emphasising the concept that metamorphic reactions are strictly driven by the compositions of reactant phases (Tracy, 1982, and discussed in Lanari and Engi, 2017). The measured bulk rock FeO_{tot} content is indistinguishable between the Atg-serpentinites and the Chl-harzburgites (Fig. 5b), thus indicating that the chemical depletion trends caused by mantle melting are comparable for Atg-serpentinites and Chl-harzburgites. What can prominently vary, however, are the petrological characteristics and the chemical effects generated upon ocean floor peridotite hydration and oxidation. This is a multistage process, at least in part out of equilibrium, producing highly variable modes of magnetite (0 - 6 %), and highly variable Fe^{3+}/Fe_{tot} in serpentine minerals and bulk

413 rocks, at micro to macro scales (e.g., Andreani et al., 2013; Bach et al., 2006; Bonnemains et al.,
414 2016; Frost et al., 2013; Früh-Green et al., 2004; Klein et al., 2014).

415 Progressive ocean floor serpentinisation leads to the oxidation of ferrous (Fe^{2+}) mantle minerals into
416 ferric (Fe^{3+}-rich) serpentines and magnetite (e.g., Andreani et al., 2013) that can for example be
417 summarised as:

418 olivine + orthopyroxene + $H_2O \rightarrow$ serpentine + magnetite + $H_{2(aq)}$ (4)

419 At early stages of serpentinisation (low water/rock ratios) the ferric iron produced via H_2O reduction is
420 incorporated into serpentine while hardly any magnetite forms. At advanced serpentinisation stages at
421 higher water/rock ratios, progressively higher amounts of magnetite are produced resulting in an
422 increase in Mg# of coexisting serpentine and possibly brucite (Andreani et al., 2013; Bach et al.,
423 2006; Frost et al., 2013; Oufi et al., 2002). Consequently, the total iron content in serpentine minerals
424 correlates inversely with modal magnetite and serpentine mineral Mg# (Andreani et al., 2013;
425 O'Hanley and Dyar, 1993; Bonnemains et al., 2016), starting from peridotites with uniform bulk rock
426 Mg# of around 90. Magnetite content thus increases with increasing water/rock ratio during oceanic
427 serpentinisation. Bulk rock Fe^{3+} content increases almost linearly with progressive serpentinisation too
428 (Andreani et al., 2013). That magnetite modes of oceanic serpentinites vary from 0 to 7 % is also
429 reflected by prominent variations in serpentinite magnetic susceptibility (e.g., Toft et al., 1990; Oufi et
430 al., 2002; Bonnemains et al., 2016). It is thus indisputable that mineralogical and chemical
431 compositions of hydrated mantle rocks entering subduction are extremely diverse, at all scales;
432 hence, the different Mg# of the reactive bulk used in our approach are the product of variable extents
433 of ocean floor hydration and not of variable Fe_{tot} in peridotites prior to ocean floor hydration.

434 For Almirez, ocean floor hydration is indicated by the presence of rodingites (Trommsdorff et al.,
435 1998), by characteristic fluid-mobile element enrichments including B, U, alkali and chalcophile
436 elements (e.g., Peters et al., 2017), and halogen abundances (Kendrick et al., 2011). Geochemical
437 data document prominent variability among the hydrous mantle rocks that is also expressed by their
438 sulphur and carbon isotope systematics (Alt et al., 2012).

439 Consequently, the Atg-serpentinite dehydration reaction front at Almirez images a compositional
440 boundary between (1) moderately oxidised ocean floor serpentinites with low magnetite modes and
441 low antigorite Mg#, produced at low water/rock ratios, i.e., rock-buffered conditions (now dehydrated

442 to Chl-harzburgites), and (2) highly oxidised ocean floor serpentinites with high magnetite modes and
443 high antigorite Mg#, formed at high water/rock ratios, i.e., fluid-buffered conditions (still preserved as
444 Atg-serpentinites). Our model does not consider a possible effect of variable Fe^{3+}/Fe_{tot} in antigorite
445 (e.g., Andreani et al., 2013, Debret et al., 2015) on its stability.

446

447 5. Implications

448 The results presented here clearly demonstrate that Atg-serpentinite and Chl-harzburgite possess
449 different reactive bulk compositions imposed by variations in degree of oceanic serpentinisation that
450 controls whether a given serpentinite rock mass devolatilised or not at Almirez. In this sense the
451 reaction front now cropping out at Almirez represents an inherited oceanic oxidation front, whereby
452 variable degrees of serpentinisation at the seafloor resulted in different amounts of magnetite and
453 different reactive bulk Mg#. Such prominent initial heterogeneity evidently survived prograde mineral
454 transformations up to and including antigorite dehydration. This has prominent consequences.

455 First, it implies that magnetite has remained passive during subduction metamorphism of the studied
456 rocks, at least to antigorite dehydration. However, Debret et al. (2014) have recently suggested that
457 redox reactions critically affect magnetite stability during subduction. Based on comparison of
458 lizardite/chrysotile serpentinites with Atg-serpentinites from locations far away from each other these
459 authors concluded that the amount of magnetite formed during oceanic serpentinisation decreases
460 during early subduction stages. Moreover, Debret et al. (2015) interpret the lower magnetite content in
461 Chl-harzburgites compared to the Atg-serpentinites at Almirez as a result of magnetite dissolution
462 during antigorite breakdown, based on direct comparison of magnetite modes in Atg-serpentinites and
463 Chl-harzburgites. Petrographic inspection of our rocks reveals, however, that magnetite occurs both
464 as inclusions in prograde olivine or forms an equilibrium texture with olivine and chlorite showing
465 sharp grain boundaries (Fig. 4). Hence, magnetite is stable in Chl-harzburgite at Almirez and
466 elsewhere (e.g., Scambelluri et al., 2014). The observation that olivine Mg# is progressively
467 increasing with successive olivine growth generations (Fig. 6a) and the excellent agreement between
468 calculated and measured Mg# in olivine for both Atg-serpentinites and Chl-harzburgites (compare Fig.

8) do not support the addition of significant amounts of iron to silicates during prograde metamorphism via consumption of magnetite.

The question arises, why this oceanic oxidation front has been preserved during subduction up to antigorite decomposition. Seafloor alteration occurs in an open system with variable fluid-rock ratios and a great potential to oxidise iron during serpentinisation (e.g., Andreani et al., 2013). During this process, sulphate from seawater is reduced to form Fe-Ni-sulphides. Recent experiments have shown that magnetite dissolution can occur in serpentinite upon progressive subduction, in the presence of hydrogen as a suitable redox-couple (Merkulova et al., 2016). Apparently, during subduction, there is limited reaction/availability of reduced species such as S in Fe-Ni-sulphides and graphite to invert the oxidation signature acquired during seafloor alteration. Only upon antigorite dehydration a fraction of sulphur may be lost as sulphate (e.g., Alt et al., 2012) according to the following generalized redox reaction (oxidation states in exponent):

$$Fe^{3+}{}_2Fe^{2+}O_4 \text{ (magnetite)} + (Fe^{2+},Ni^{2+})S^{2-} \text{ (sulphide)} \rightarrow Fe^{2+}(Ni^{2+})O \text{ (silicate)} + (S^{6+}O_4)^{2-} \text{ (fluid)} \quad (5)$$

Assuming partial loss of 260 µg g^{-1} S during antigorite dehydration as proposed by Alt et al. (2012) — noting however that this is based on the questionable comparison between Atg-serpentinites and Chl-harzburgites — would result in the consumption of about 0.8 wt% of magnetite (equation 5). Less sulphur oxidation could for example produce pyrite with no sulphur loss to the system:

$$Fe^{3+}{}_2Fe^{2+}O_4 \text{ (magnetite)} + (Fe^{2+},Ni^{2+})S^{2-} \text{ (sulphide)} \rightarrow Fe^{2+}(Ni^{2+})O \text{ (silicate)} + Fe^{2+}S^{1-}{}_2 \text{ (pyrite)} \quad (6)$$

In this case, eight times less magnetite (i.e., 0.1 wt%) is needed to accommodate this electron transfer. Both these reactions can explain the observed increase in Ni in Ol-4 (Fig. 6a).

Either way, the amount of magnetite consumed is not enough to account for the observed differences in magnetite abundances between Chl-harzburgite and Atg-serpentinite, supporting our hypothesis that the boundary reflects an initial redox front.

Ferric iron from antigorite will contribute as well to the redox budget of the antigorite dehydration reaction, via the generalized reaction

$$(Mg,Fe^{2+}/Fe^{3+}) \text{ (antigorite)} + (Fe^{2+},Ni^{2+})S^{2-} \text{ (sulphide)} \rightarrow (Mg,Fe^{2+}/Fe^{3+}) \text{ (chl)} + Mg,Fe^{2+}(Ni^{2+})O \text{ (ol/opx)} + (S^{6+}O_4)^{2-} \text{ (fluid)} \quad (7)$$

496 The first step is to assess how much Fe^{3+} is transferred from antigorite to chlorite. Antigorite and
497 chlorite from Almirez have within error indistinguishable Fe^{3+}/Fe_{tot} of 0.5 (Debret et al., 2015) and
498 FeO_{tot} of ~3.5 wt% (Table 2). From Al mass balance it follows that there is about 4 times less chlorite
499 (13 wt% Al_2O_3) than antigorite (3.5 wt% Al_2O_3). Thus, during reaction (7) 1.3 wt% antigorite-bound
500 Fe_2O_3 has to be reduced and transferred to FeO in olivine/orthopyroxene. This redox budget would be
501 sufficient to oxidise ~600 µg g^{-1} S^{2-} to $(S^{6+}O_4)^{2-}$, more than double the sulphate loss proposed by Alt et
502 al. (2012). Consequently, it may actually be the ferric iron of antigorite that has the largest effect on
503 the redox budget of the antigorite dehydration reaction.

504 Second, our data emphasise that prograde dehydration in serpentinites traditionally seen as
505 discontinuous reactions are in fact continuous reactions as a function of Mg#. Consequently, the
506 depth range during which antigorite dehydration fluid is liberated is smeared out by compositional
507 heterogeneities in Mg# inherited from sea floor hydration, in addition to the strong thermal gradients in
508 the subducting plate perpendicular to its surface. For serpentinites with variable amounts of
509 magnetite, fluid liberation over an interval of up to 40°C is indicated by our modelling results combined
510 with previous results that extend down to lower Mg# of 90 (Padron Navarta et al., 2010).

511 Another question to address is why the dehydration front did not progress further, i.e., including the
512 dehydration of the serpentinites with higher Mg#. One possibility is that the extensive fluid release by
513 the conversion of the serpentinites with low Mg# to Chl-harzburgite led to mechanical instability that
514 triggered the exhumation of the ultramafic bodies, preventing further subduction and thus heating of
515 the high Mg# Atg-serpentinites that would have resulted in complete dehydration. In this sense the
516 preservation of the reaction boundary is not a coincidence but governed by the first voluminous part of
517 ultramafic rocks (with the lowest magnetite content) that underwent dehydration.

518 Finally, our findings fundamentally question approaches that directly compare characteristics of Atg-
519 serpentinites and Chl-harzburgites to infer geochemical changes associated with prograde
520 dehydration reactions. Unless there is independent evidence for identical composition between
521 reactants (serpentinites) and products (Chl-harzburgites) with progressive subduction, estimates on
522 element loss mediated by aqueous fluid escape and associated changes in redox budget based on
523 Fe^{3+}/Fe_{tot}, may lead to erroneous conclusions. Constraining parameters based on reaction products
524 alone thus seems to be much more reliable, e.g., the determination of element mobility based on
525 element distribution coefficients between reaction product phases.

Acknowledgments

We thank Carl Spandler and Janos Kodolanyi for great field work, Pierre Lanari for support with Perple_X modelling, members of our thin section preparation lab for their excellent work, Martin Robyr for assistance during electron probe analysis, and Maria Schönbächler for sharing her MSc work with us. We thank E. Kempf for fruitful discussions, Ralf Halama and anonymous for thoughtful reviews, and Tamsin Mather for excellent editorial handling. This work was supported by the Swiss National Science Foundation [grant numbers 137686 and 160076 to TP].

References

Andreani, M., Munoz, M., Marcaillou, C., and Delacour, A., 2013. mu XANES study of iron redox state in serpentine during oceanic serpentinization. Lithos 178, 70-83. Alt, J.C., Garrido, C.J., Shanks III, W.C., Turchyn, A., Padrón-Navarta, J.A., López Sánchez-Vizcaíno, V., Gómez-Pugnaire, M.T., Marchesi, C., 2012. Recycling of water, carbon, and sulfur during subduction of serpentinites: a stable isotope study of Cerro del Almirez, Spain. Earth and Planetary Science Letters 327-328, 50-60.

Alt, J. C., Garrido, C. J., Shanks, W. C., Turchyn, A., Padrón-Navarta, J. A., Sanchez-Vizcaino, V. L., Pugnaire, M. T. G., and Marchesi, C., 2012. Recycling of water, carbon, and sulfur during subduction of serpentinites: A stable isotope study of Cerro del Almirez, Spain. Earth and Planetary Science Letters 327, 50-60.

Alt, J. C., Schwarzenbach, E. M., Frueh-Green, G. L., Shanks, W. C., Bernasconi, S. M., Garrido, C. J., Crispini, L., Gaggero, L., Padrón-Navarta, J. A., and Marchesi, C., 2013. The role of serpentinites in cycling of carbon and sulfur: Seafloor serpentinization and subduction metamorphism. Lithos 178, 40-54.

Bach, W., Paulick, H., Garrido, C. J., Ildefonse, B., Meurer, W. P., and Humphris, S. E., 2006. Unraveling the sequence of serpentinization reactions: petrography, mineral chemistry, and petrophysics of serpentinites from MAR 15 degrees N (ODP Leg 209, Site 1274). Geophysical Research Letters 33.

Bonatti, E., Lawrence, J. R., and Morandi, N., 1984. Serpentinization of oceanic peridotites - temperature-dependence of mineralogy and boron content. Earth and Planetary Science Letters 70, 88-94.

Bonnemains, D., Carlut, J., Escartin, J., Mevel, C., Andreani, M., and Debret, B., 2016. Magnetic signatures of serpentinization at ophiolite complexes. Geochemistry Geophysics Geosystems 17, 2969-2986.

Bromiley, G. D. and Pawley, A. R., 2003. The stability of antigorite in the systems MgO-SiO2-H2O (MSH) and MgO-Al2O3-SiO2-H2O (MASH): The effects of Al3+ substitution on high-pressure stability. American Mineralogist 88, 99-108.

563 Connolly, J. A. D., 2005. Computation of phase equilibria by linear programming: A tool for
564 geodynamic modeling and its application to subduction zone decarbonation. Earth and Planetary
565 Science Letters 236, 524-541.

566 Debret, B., Andreani, M., Munoz, M., Bolfan-Casanova, N., Carlut, J., Nicollet, C., Schwartz, S.,
567 Trcera, N., 2014. Evolution of Fe redox state in serpentine during subduction. Earth and Planetary
568 Science Letters 400, 206-218.

569 Debret, B., Bolfan-Casanova, N., Padrón-Navarta, J.A., Martin‐Hernandez, F., Andreani, M., Garrido,
570 C.J., López Sánchez-Vizcaíno, V., Gómez-Pugnaire, M.T., Muñoz, M., Trcera, N., 2015. Redox
571 state of iron during high-pressure serpentinite dehydration. Contributions to Mineralogy and
572 Petrology 169, 36.

573 Deschamps, F., Godard, M., Guillot, S., Hattori, K.H., 2013. Geochemistry of subduction zone
574 serpentinites: a review. Lithos 178, 96-127.

575 Frost, B. R., Evans, K. A., Swapp, S. M., Beard, J. S., and Mothersole, F. E., 2013. The process of
576 serpentinization in dunite from New Caledonia. Lithos 178, 24-39.

577 Früh-Green, G. L., Connolly, J. A. D., Plas, A., Kelley, D. S., and Grobety, B., 2004. Serpentinization
578 of oceanic peridotites: Implications for geochemical cycles and biological activity. In: Wilcock, W.
579 S. D., DeLong, E. F., Kelley, D. S., Baross, J. A., and Cary, S. C. Eds.), Subseafloor Biosphere at
580 Mid-Ocean Ranges.

581 Garrido, C.J., López Sánchez-Vizcaíno, V., Gómez-Pugnaire, M.T., Trommsdorff, V., Alard, O.,
582 Bodinier, J.-L., Godard, M., 2005. Enrichment of HFSE in chlorite harzburgite produced by high-
583 pressure dehydration of antigorite-serpentinite: implications for subduction magmatism.
584 Geochemistry Geophysics Geosystems 6.

585 Harvey, J., Garrido, C. J., Savov, I., Agostini, S., Padrón-Navarta, J. A., Marchesi, C., Sanchez-
586 Vizcaino, V. L., and Gomez-Pugnaire, M. T., 2014. B-11-rich fluids in subduction zones: The role
587 of antigorite dehydration in subducting slabs and boron isotope heterogeneity in the mantle.
588 Chemical Geology 376, 20-30.

589 Hattori, K. H. and Guillot, S., 2007. Geochemical character of serpentinites associated with high- to
590 ultrahigh-pressure metamorphic rocks in the Alps, Cuba, and the Himalayas: Recycling of
591 elements in subduction zones. Geochemistry Geophysics Geosystems 8.

592 Kendrick, M.A., Scambelluri, M., Honda, M., Phillips, D., 2011. High abundance of noble gas and
593 chlorine delivered to the mantle by serpentinite subduction. Nature Geoscience 4, 807-812.

594 Kendrick, M.A., Honda, M., Pettke, T., Scambelluri, M., Phillips, D., Giuliani, A., 2013. Subduction
595 zone fluxes of halogens and noble gases in seafloor and forearc serpentinites. Earth and Planetary
596 Science Letters 365, 86-96.

597 Klein, F., Bach, W., Humphris, S. E., Kahl, W. A., Jons, N., Moskowitz, B., and Berquo, T. S., 2014.
598 Magnetite in seafloor serpentinite-Some like it hot. Geology 42, 135-138.

599 Kodolanyi, J. and Pettke, T., 2011. Loss of trace elements from serpentinites during fluid-assisted
600 transformation of chrysotile to antigorite - An example from Guatemala. Chemical Geology 284,
601 351-362.

602 Kodolányi, J., Pettke, T., Spandler, C., Kamber, B.S., Gméling, K., 2012. Geochemistry of ocean floor
603 and fore-arc serpentinites: constraints on the ultrabasic input to subduction zones. Journal of
604 Petrology 53, 235-270.

605 Konrad-Schmolke, M., Halama, R., Manea, V. C., 2016. Slab mantle dehydrates beneath
606 Kamchatka—Yet recycles water into the deep mantle. Geochemistry Geophysics Geosystems 17,
607 2987-3007.

608 Lanari, P., Engi, M. (2017). Local bulk composition effects on metamorphic mineral assemblages, in:
609 Kohn, M., Engi, M., Lanari, P. (Eds), Petrochronology: Methods and Applications. Reviews in
610 Mineralogy and Geochemistry, 83, 55-102.

611 López Sánchez-Vizcaíno, V., Rubatto, D., Gómez-Pugnaire, M.T., Trommsdorff, V., Müntener, O.,
612 2001. Middle Miocene high-pressure metamorphism and fast exhumation of the Nevado-Filábride
613 Complex, SE Spain. Terra Nova 13, 327-332.

614 Marchesi, C., Garrido, C.J., Padrón-Navarta, J.A., López Sánchez-Vizcaíno, V., Gómez-Pugnaire,
615 M.T., 2013. Element mobility from seafloor serpentinization to high-pressure dehydration of

616 antigorite in subducted serpentinite: insight from the Cerro del Almirez ultrabasic massif (southern
617 Spain). Lithos 178, 128–142.

618 Merkulova, M., Munoz, M., Vidal, O., and Brunet, F., 2016. Role of iron content on serpentinite
619 dehydration depth in subduction zones: Experiments and thermodynamic modeling. Lithos 264,
620 441-452.

621 Niu, Y. L., 2004. Bulk-rock major and trace element compositions of abyssal peridotites: Implications
622 for mantle melting, melt extraction and post-melting processes beneath mid-ocean ridges. Journal
623 of Petrology 45, 2423-2458.

624 O'Hanley, D. S. and Dyar, M. D., 1993. The composition of lizardite 1T and the formation of magnetite
625 in serpentinites. American Mineralogist 78, 391-404.

626 Niu, Y., 2004. Bulk-rock major and trace element compositions of abyssal peridotites: implications for
627 mantle melting, melt extraction and post-melting processes beneath mid-ocean ridges. Journal of
628 Petrology 45, 2423-2458.

629 Oufi, O., Cannat, M., and Horen, H., 2002. Magnetic properties of variably serpentinized abyssal
630 peridotites. Journal of Geophysical Research-Solid Earth 107.

631 Padrón-Navarta, J.A., Hermann, J., Garrido, C.J., López Sánchez-Vizcaíno, V., Gómez-Pugnaire,
632 M.T., 2010. An experimental investigation of antigorite dehydration in natural silica-enriched
633 serpentinite. Contributions to Mineralogy and Petrology 159, 25-42.

634 Padrón-Navarta, J.A., López Sánchez-Vizcaíno, V., Garrido, C.J., Gómez-Pugnaire, M.T., 2011.
635 Metamorphic record of high-pressure dehydration of antigorite serpentinite to chlorite harzburgite
636 in a subduction setting (Cerro del Almirez, Nevado-Filábride Complex, Southern Spain). Journal of
637 Petrology 52, 2047-2078.

638 Padrón-Navarta, J.A., López Sánchez-Vizcaíno, V., Hermann, J., Connolly, J.A.D., Garrido, C.J.,
639 Gómez-Pugnaire, M.T., Marchesi, C., 2013. Tschermak's substitution in antigorite and
640 consequences for phase relations and water liberation in high-grade serpentinites. Lithos 178,
641 186–196.

642 Palme, H., O'Neill, H. S. C., 2014. Cosmochemical estimates of mantle composition. Treatise on
643 Geochemistry, 2nd Edition, Vol. 3 Mantle and Core, paper 3.1.

644 Paulick, H., Bach, W., Godard, M., De Hoog, J. C. M., Suhr, G., and Harvey, J., 2006. Geochemistry
645 of abyssal peridotites (Mid-Atlantic Ridge, 15 degrees 20 ' N, ODP Leg 209): Implications for
646 fluid/rock interaction in slow spreading environments. Chemical Geology 234, 179-210.

647 Peters, D., Bretscher, A., John, T., Scambelluri, M., and Pettke, T., 2017. Fluid-mobile elements in
648 serpentinites: Constraints on serpentinisation environments and element cycling in subduction
649 zones. Chemical Geology 466, 654-666.

650 Puga, E., Nieto, J.M., Díaz de Federico, A., Bodinier, J.L., Morten, L., 1999. Petrology and
651 metamorphic evolution of ultrabasic rocks and dolerite dykes of the Betic Ophiolitic Association
652 (Mulhacén Complex, SE Spain): evidence of eo-Alpine subduction following an ocean-floor
653 metasomatic process. Lithos 49, 23-56.

654 Rüpke, L. H., Morgan, J. P., Hort, M., and Connolly, J. A. D., 2004. Serpentine and the subduction
655 zone water cycle. Earth and Planetary Science Letters 223, 17-34.

656 Savov, I. P., Ryan, J. G., D'Antonio, M., Kelley, K., and Mattie, P., 2005. Geochemistry of
657 serpentinized peridotites from the Mariana Forearc Conical Seamount, ODP Leg 125: Implications
658 for the elemental recycling at subduction zones. Geochemistry Geophysics Geosystems 6.

659 Scambelluri, M., Philippot, P., 2001. Deep fluids in subduction zones. Lithos 55, 213-227.

660 Scambelluri, M., Müntener, O., Ottolini, L., Pettke, T., Vannucci, R., 2004. The fate of B, Cl and Li in
661 the subducted oceanic mantle and in the antigorite breakdown fluids. Earth and Planetary Science
662 Letters 222, 217-234.

663 Scambelluri, M., Pettke, T., Rampone, E., Godard, M., Reusser, E., 2014. Petrology and trace
664 element budgets of high-pressure peridotites indicate subduction dehydration of serpentinized
665 mantle (Cima di Gagnone, Central Alps, Switzerland). Journal of Petrology 55, 459-498.

666 Schönbächler, M., 1999. Die Hochdruckmetamorphose der Ultramafika und der angrenzenden
667 Nebengesteine am Cerro del Almirez, Sierra Nevada, Südspanien (Teil 1). Diplomarbeit der
668 Abteilung CX (Erdwissenschaften) der Eidgenössischen Technischen Hochschule, pp. 153.

669 Spandler, C., Pirard, C., 2013. Element recycling from subducting slabs to arc crust: a review. Lithos
670 170, 208-223.

671 Thompson, A.B. 1976. Mineral reactions in pelitic rocks: I. Prediction of P-T-X(Fe-Mg) phase relations.
672 American Journal of Science 276, 401-424.

673 Toft, P. B., Arkanihamed, J., and Haggerty, S. E., 1990. The effects of serpentinization on density and
674 magnetic-susceptibility - a petrophysical model. Physics of the Earth and Planetary Interiors 65,
675 137-157.

676 Tracy, R.J. 1982. Compositional zoning and inclusions in metamorphic minerals. In: Ferry, JM (Ed.):
677 Characterisation of metamorphism through mineral equilibria. Mineralogical Society of America.
678 Reviews in Mineralogy and Geochemistry 10, 355-397.

679 Trommsdorff, V. and Connolly, J. A. D., 1996. The ultramafic contact aureole about the Bregaglia
680 (Bergell) tonalite: Isograds and a thermal model. Schweizerische Mineralogische Und
681 Petrographische Mitteilungen 76, 537-547.

682 Trommsdorff, V., Evans, B., 1972. Progressive metamorphism of antigorite schist in the Bergell
683 tonalite aureole (Italy). American Journal of Science 272, 423-437.

684 Trommsdorff, V., López Sánchez-Vizcaíno, V., Gómez-Pugnaire, M.T., Müntener, O., 1998. High
685 pressure breakdown of antigorite to spinifex-textured olivine and orthopyroxene, SE Spain.
686 Contributions to Mineralogy and Petrology 132, 139-148.

687 Ulmer, P., Trommsdorff, V., 1995. Serpentine stability to mantle depths and subduction-related
688 magmatism. Science 268, 858-861.

689 Ulmer, P., Trommsdorff, V., 1999. Phase relations of hydrous mantle subducting to 300 km. In: Mantle
690 Petrology: Field observations and high pressure experimentation: A tribute to Francis R. (Joe)
691 Boyd. The Geochemical Society, Speccial Publication No. 6, 259-281.

692 van Keken, P. E., Hacker, B. R., Syracuse, E. M., Abers, G. A., 2011. Subduction factory: 4. Depth-
693 dependent flux of H_2O from subducting slabs worldwide. Journal of Geophysical Research-Solid
694 Earth 116.

695 Whitney, D.L., Evans, B.W., 2010. Abbreviations for names of rock-forming minerals. American
696 Mineralogist 95, 185-187.

697 Wunder, B. and Schreyer, W., 1997. Antigorite: High pressure stability in the system MgO-SiO2-H2O
698 (MSH). Lithos 41, 213-227.

Figure captions

- all figures in colour

- Figs. 1, 2, 3, 4, 6, 8 are 2-column fitting

- Fig. 5, 7 are single column fitting

Fig. 1. (a) Geological overview map. The Nevado-Filábride Complex in the Betic Cordillera (southern Spain) with the location of Cerro del Almirez ultramafic body (taken from Marchesi et al., 2013). (b) Geological outcrop map of the main ultramafic body at Cerro del Almirez (coloured lithologies: Atg-serpentinites, transitional lithologies and Chl-harzburgites) and associated metarodingites and metasediments (redrawn from Schönbächler, 1999). Colour-coded dots and numbers represent ultramafic rocks investigated in detail in this study (Alm06-XXX). The Chl-harzburgite sample Alm06-029 was taken from one of the two minor Chl-harzburgite bodies located to the west of the main body. Samples taken from boulders are marked with a "b" in the exponent.

Fig. 2. Schematic evolution of prograde mineral growth stages at Almirez. First appearance of a mineral is marked with an arrowhead and labelled. Thicknesses of the lines are proportional to average modal abundances of the minerals. Dotted lines indicate stability of the respective minerals that were not observed in our samples. Opaque minerals other than magnetite, and retrograde talc are omitted for simplicity. (a) to (e) mark the appearance or disappearance of a diagnostic mineral (mineral isograd). Olivine 1a and Olivine 1b derive from different prograde reactions, but are not distinguishable based on textural observations. The blue shaded background marks stages for which fluid saturation of the rocks is implied. Mineral abbreviations are after Whitney and Evans (2010).

Fig. 3. Transmitted light thin section micrographs. Selected petrographic features of Almirez lithologies are illustrated with crossed polarizers ((a)-(e) and (g)-(h)) and with single polarizer (f). Mineral growth stages as defined in Fig. 2.
(a) Atg-serpentinite: Relic dusty clinopyroxene (Cpx-1) core with recrystallized inclusion-poor metamorphic rim (Cpx-2). Such relic clinopyroxene cores are common in clinopyroxene-bearing Atg-serpentinites (samples Alm06-094/107/109).
(b) Atg-serpentinite: Neoblastic columnar clinopyroxene (Cpx-2) overgrown by euhedral tremolite crystals (Tr-1), both growing over a fine-grained Atg-1 matrix.

(c) Transitional Chl-serpentinite: Chlorite cores (Chl-3) overgrown by antigorite (Atg-2). These overgrowths are randomly oriented within the rock, predominantly occurring in domains rich in fine-grained Atg-1 and growing over olivine (Ol-1).
(d) Transitional Chl-serpentinite: Talc located interstitially between coarse antigorite (Atg-2) of Chl-3 - Atg-2 intergrowths. Irregular grain boundaries between antigorite and talc indicate talc growth after Atg-2.
(e) Transitional Atg-Chl-Opx-Ol rock: Granular colourless olivine (Ol-2), first appearance of orthopyroxene (Opx-1), and flaky chlorite (Chl-3) characterise this lithology. The mode of the Chl-3 - Atg-2 intergrowths is reduced and the Atg-2 overgrowths are smaller compared to the Chl-serpentinite.
(f) Spinifex-textured Chl-harzburgite: Three growth stages of olivine are illustrated, colourless granular cores often rich in opaque inclusions (Ol-2), overgrown by brown pennate Ol-3, that in turn is occasionally overgrown by a discontinuous rim of colourless Ol-4 (not shown in the image). Ol-4 also forms equilibrium texture matrix grains. Note that colourless olivine cores and rim overgrowths cannot be distinguished microscopically unless when occurring together.
(g) Granular Chl-harzburgite: talc replacing orthopyroxene (Opx-1) along grain boundaries and fractures.
(h) Granular Chl-harzburgite: rare tremolite lath (Tr-1) in stable coexistence with chlorite (Chl-3), documenting tremolite stability with chlorite as part of the peak assemblage Ol-3/4 + Opx-1 + Chl-3.

Fig. 4. Reflected light thin section micrographs. (a) Atg-serpentinite and (b) Chl-harzburgite. Mineral growth stages as defined in Fig. 2. (a) Note the blades of Atg-1 and granular Ol-1 growing over magnetite in Atg-serpentinite, thus identifying magnetite formation at low-temperature hydration. (b) Magnetite grains are either enclosed in Ol-2 and Ol-3 or show an equilibrium texture with Atg-breakdown product Ol-2 and Ol-3 and Chl-3. Black domains represent holes in the section resulting from broken-out mineral grains.

Fig. 5. Bulk rock major element compositional systematics of the ultramafic lithologies across antigorite-out reaction at Almirez. (a) Al_2O_3/SiO_2 vs. MgO/SiO_2. The thick dark grey arrow represents the compositional trend due to variable melt extraction ("Melting Residue"). The grey field represents the composition of abyssal peridotites after Niu (2004). Primitive mantle composition is from Palme

and O'Neill (2014). (b) Plot of MgO vs. FeO_{tot}, contoured for bulk rock Mg# (Mg# = $100*[Mg/(Mg+Fe)]_{molar}$), demonstrating no systematic variation in bulk rock Mg# between the different rock types. (c) Plot of CaO vs. Al_2O_3, illustrating variations in CaO due to ocean floor hydration. Colouring of symbols defined in (a).

Fig. 6. Selected element compositions as a function of Mg# ($100*[Mg/(Mg+Fe)]_{molar}$) for (a) olivine, (b) antigorite, (c) chlorite, and (d) orthopyroxene of the ultramafic lithologies from Cerro del Almirez. apfu = atoms per formula unit. Note the distinct Mg# clusters for the different mineral growth stages. Data of Padron-Navarta et al. (2011) represent averages of representative samples. S-Chl-harzb stands for spinifex-textured Chl-harzburgite, G-Chl-harzb stands for granular Chl-harzburgite.

Fig. 7. Perple_X modelling. P-T diagrams of the reactive bulk compositions of (a) Mg# = 96.0 for Atg-serpentinite, (b) Mg# = 92.7 for Chl-harzburgite (Mg# = $100*[Mg/(Mg+Fe)]_{molar}$), and their overlay (c). Figures (a) and (b) are contoured for olivine Mg#. Figure (c) shows the preferred clockwise P-T-t path of the Almirez ultramafic massif with tightly constrained peak conditions of 1.8 GPa and 670-680 °C, consistent with results of Padrón-Navarta et al. (2011). The narrow grey band represents the P-T interval where Atg-serpentinite and Chl-harzburgite stably coexist at given P and T. The Chl-harzburgite is already beyond antigorite-out (right of the orange thick curve; compare figure (b)) while the Atg-serpentinite is still within antigorite stability (left of the thick bright green antigorite-out curve; compare figure (a)) and did not reach orthopyroxene-stability (left of the thin dark green orthopyroxene-in curve; compare figure (a)). Reaction (2), tremolite-in, is omitted for simplicity.

Fig. 8. Perple_X modelling. Plots of reactive bulk Mg# versus temperature (°C) at P = 1.6 GPa, comparing the modelled mineral compositions with those measured for the successive mineral growth stages (reaction (2), tremolite-in, is omitted for simplicity). Plot (a) illustrates that the last antigorite in the reactive bulk composition characteristic for Chl-harzburgites dehydrated prior to the first antigorite dehydration (orthopyroxene-in) in Atg-serpentinites. Plot (b) displays for these two reactive bulk compositions the olivine crystallisation with increasing temperatures and compares the results with the measured olivine compositions (thick bands; measurement data illustrated in Fig. 6a). The compositional agreement is excellent.

Figure 1

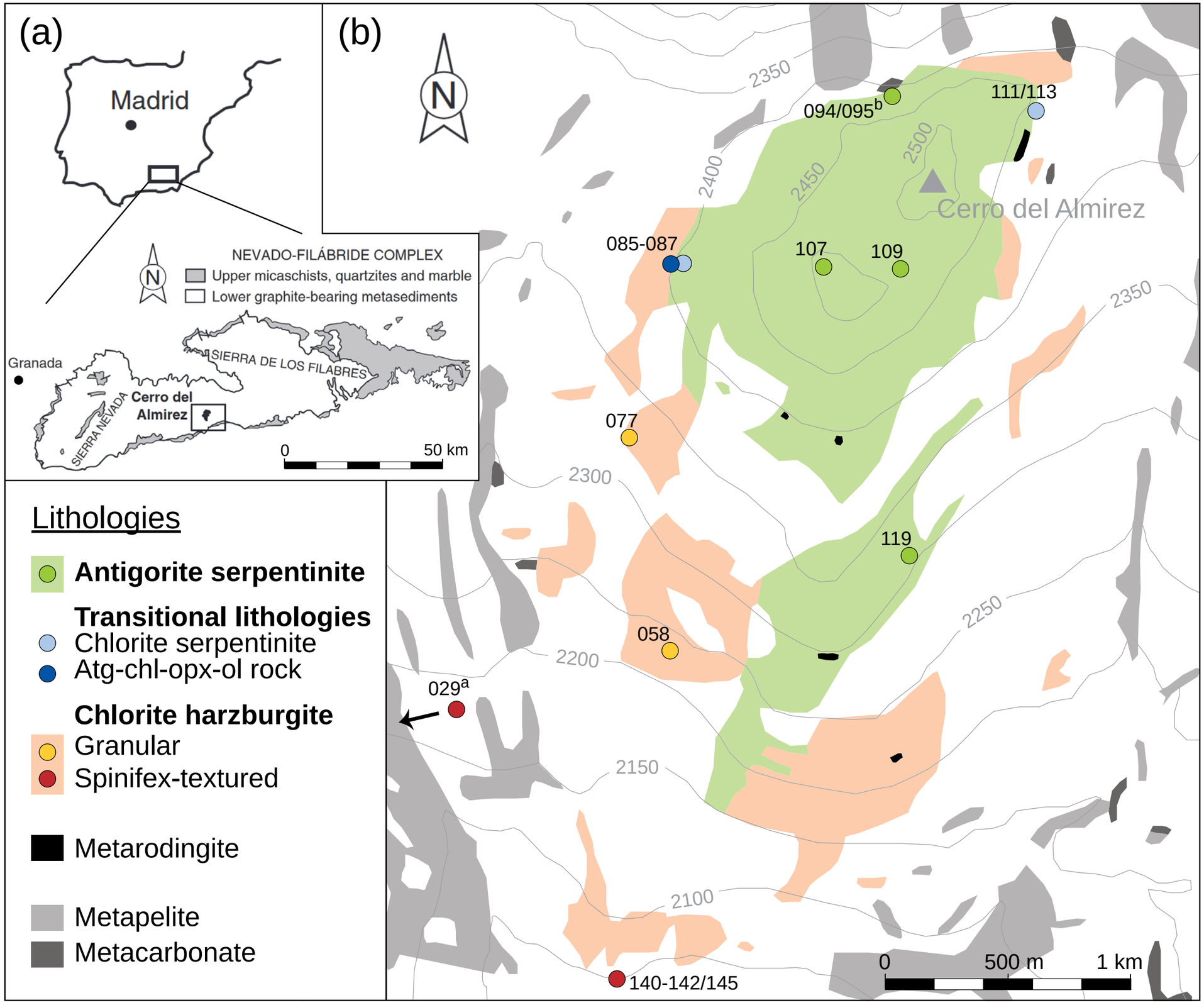
(a)
Madrid
N
NEVADO-FILÁBRIDE COMPLEX
Upper micaschists, quartzites and marble
Lower graphite-bearing metasediments
Granada
SIERRA DE LOS FILABRES
SIERRA NEVADA
Cerro del Almirez
0
50 km
(b)
N
2350
2400
2450
2500
Cerro del Almirez
094/095b
111/113
085-087
107
109
077
2300
119
2250
058
2200
029a
2150
2100
140-142/145
0
500 m
1 km
Lithologies
Antigorite serpentinite
Transitional lithologies
Chlorite serpentinite
Atg-chl-opx-ol rock
Chlorite harzburgite
Granular
Spinifex-textured
Metarodingite
Metapelite
Metacarbonate

Figure 2

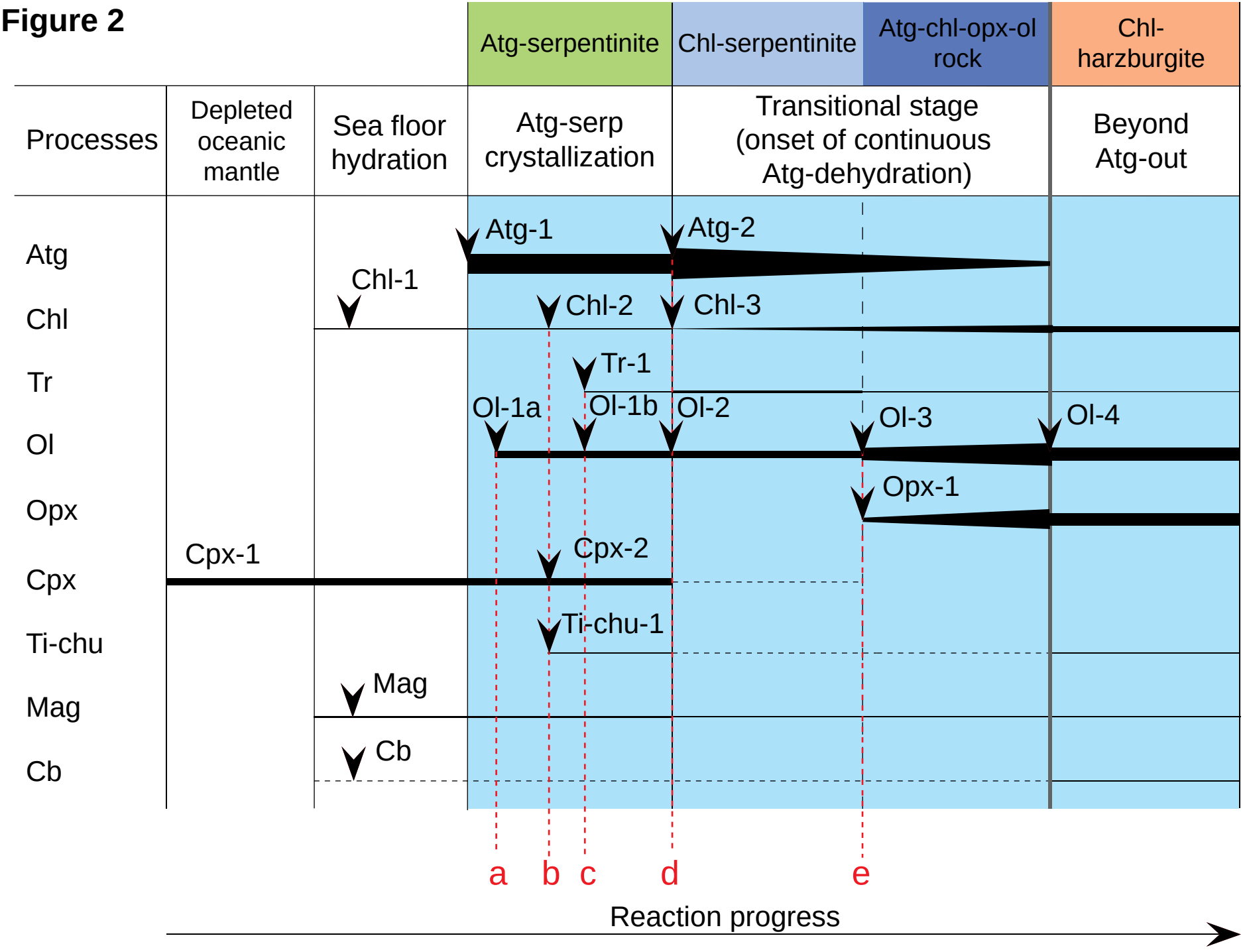
Atg-serpentinite
Chl-serpentinite
Atg-chl-opx-ol rock
Chl-harzburgite
Processes
Depleted oceanic mantle
Sea floor hydration
Atg-serp crystallization
Transitional stage (onset of continuous Atg-dehydration)
Beyond Atg-out
Atg
Chl
Tr
Ol
Opx
Cpx
Ti-chu
Mag
Cb
Atg-1
Atg-2
Chl-1
Chl-2
Chl-3
Tr-1
Ol-1a
Ol-1b
Ol-2
Ol-3
Ol-4
Opx-1
Cpx-1
Cpx-2
Ti-chu-1
Mag
Cb
a
b
c
d
e
Reaction progress

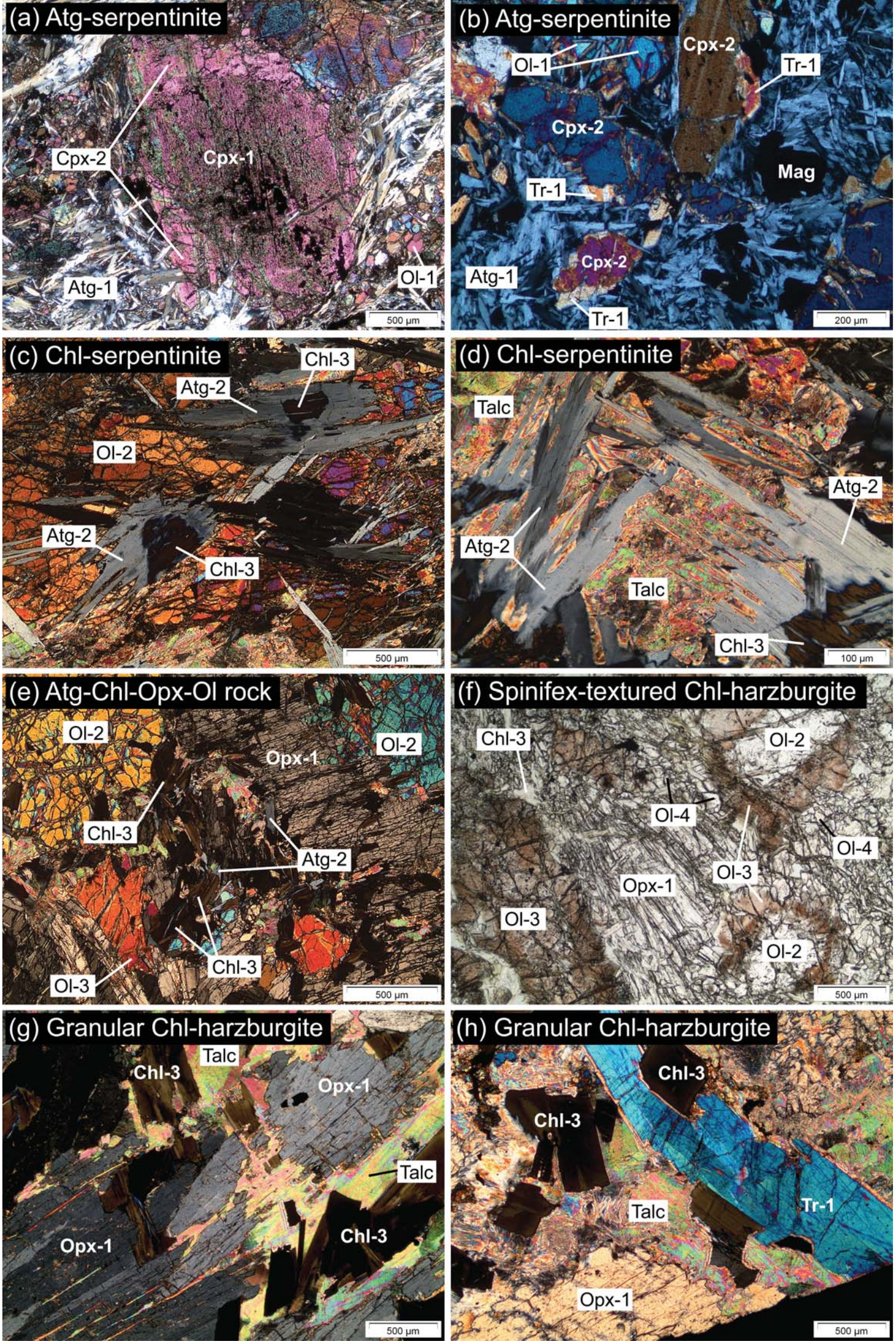
(a) Atg-serpentinite
Cpx-2
Cpx-1
Atg-1
Ol-1
500 μm
(b) Atg-serpentinite
Ol-1
Cpx-2
Tr-1
Cpx-2
Mag
Tr-1
Cpx-2
Atg-1
Tr-1
200 μm
(c) Chl-serpentinite
Chl-3
Atg-2
Ol-2
Atg-2
Chl-3
500 μm
(d) Chl-serpentinite
Talc
Atg-2
Atg-2
Talc
Chl-3
100 μm
(e) Atg-Chl-Opx-Ol rock
Ol-2
Opx-1
Ol-2
Chl-3
Atg-2
Chl-3
Ol-3
500 μm
(f) Spinifex-textured Chl-harzburgite
Chl-3
Ol-2
Ol-4
Ol-4
Ol-3
Opx-1
Ol-3
Ol-2
500 μm
(g) Granular Chl-harzburgite
Talc
Chl-3
Opx-1
Talc
Opx-1
Chl-3
500 μm
(h) Granular Chl-harzburgite
Chl-3
Chl-3
Talc
Tr-1
Opx-1
500 μm

Figure 4

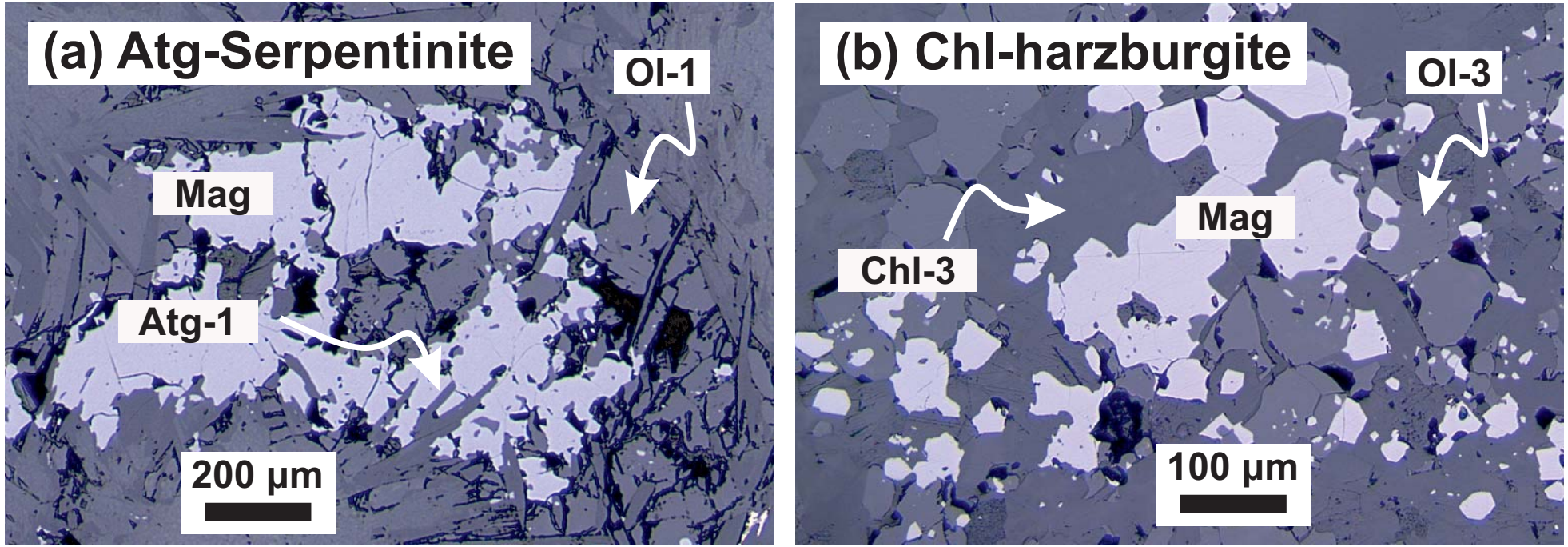
(a) Atg-Serpentinite
Ol-1
Mag
Atg-1
200 μm
(b) Chl-harzburgite
Ol-3
Mag
Chl-3
100 μm

Figure 5

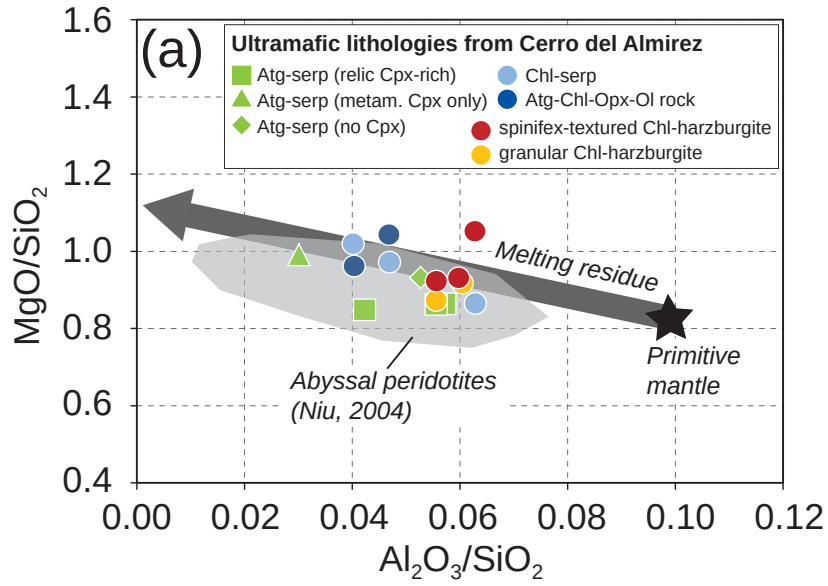
(a)
Ultramafic lithologies from Cerro del Almirez
Atg-serp (relic Cpx-rich)
Atg-serp (metam. Cpx only)
Atg-serp (no Cpx)
Chl-serp
Atg-Chl-Opx-Ol rock
spinifex-textured Chl-harzburgite
granular Chl-harzburgite
Melting residue
Primitive mantle
Abyssal peridotites (Niu, 2004)
MgO/SiO2
Al2O3/SiO2
1.6
1.4
1.2
1.0
0.8
0.6
0.4
0.00
0.02
0.04
0.06
0.08
0.10
0.12

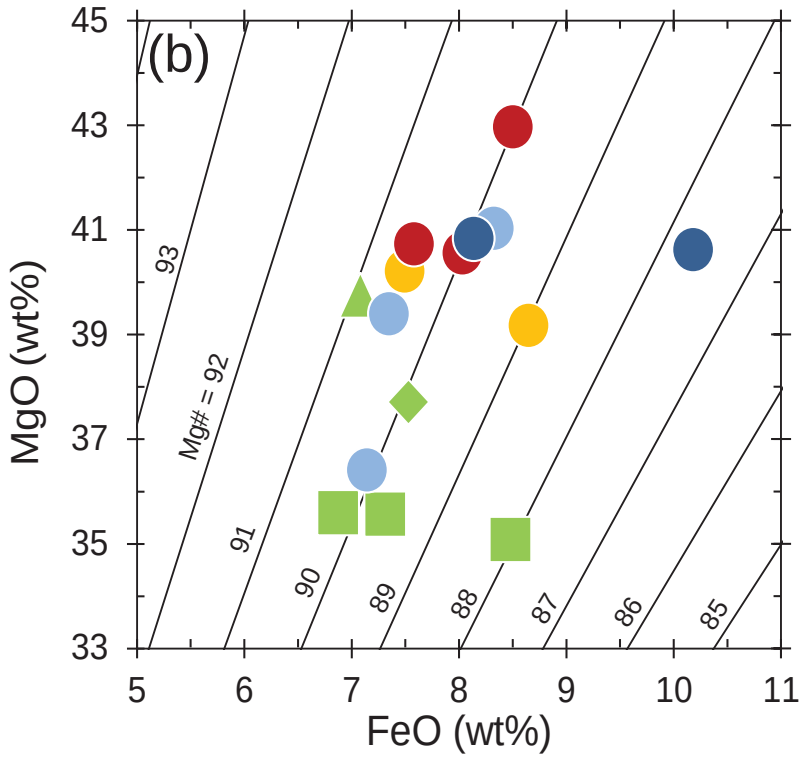
(b)
Mg# = 92
93
91
90
89
88
87
86
85
MgO (wt%)
FeO (wt%)
45
43
41
39
37
35
33
5
6
7
8
9
10
11

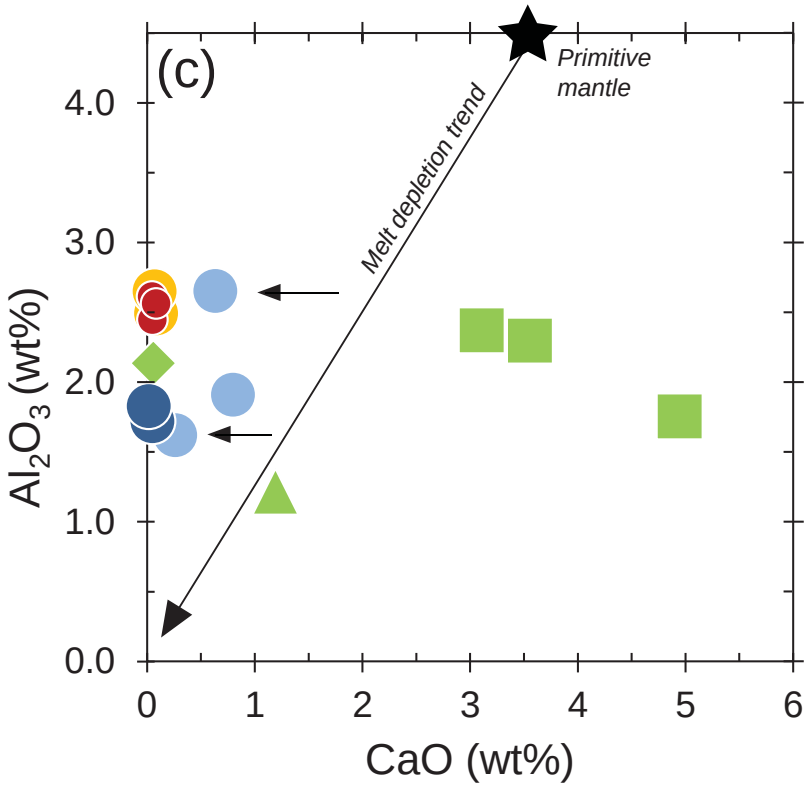
(c)
Primitive mantle
Melt depletion trend
Al2O3 (wt%)
CaO (wt%)
4.0
3.0
2.0
1.0
0.0
0
1
2
3
4
5
6

Figure 6

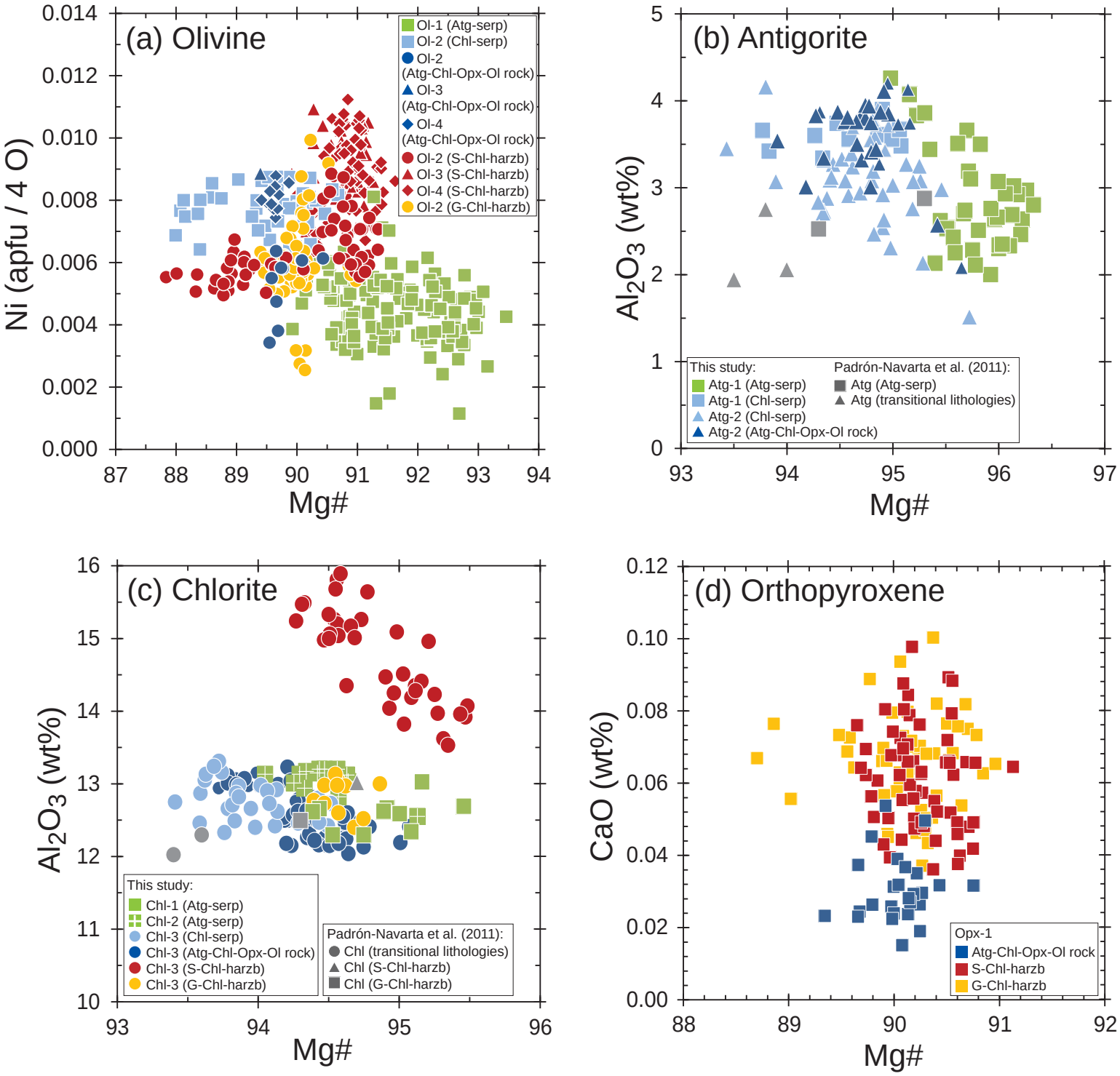
(a) Olivine
Ni (apfu / 4 O)
Mg#
Ol-1 (Atg-serp)
Ol-2 (Chl-serp)
Ol-2 (Atg-Chl-Opx-Ol rock)
Ol-3 (Atg-Chl-Opx-Ol rock)
Ol-4 (Atg-Chl-Opx-Ol rock)
Ol-2 (S-Chl-harzb)
Ol-3 (S-Chl-harzb)
Ol-4 (S-Chl-harzb)
Ol-2 (G-Chl-harzb)
(b) Antigorite
Al2O3 (wt%)
Mg#
This study:
Atg-1 (Atg-serp)
Atg-1 (Chl-serp)
Atg-2 (Chl-serp)
Atg-2 (Atg-Chl-Opx-Ol rock)
Padrón-Navarta et al. (2011):
Atg (Atg-serp)
Atg (transitional lithologies)
(c) Chlorite
Al2O3 (wt%)
Mg#
This study:
Chl-1 (Atg-serp)
Chl-2 (Atg-serp)
Chl-3 (Chl-serp)
Chl-3 (Atg-Chl-Opx-Ol rock)
Chl-3 (S-Chl-harzb)
Chl-3 (G-Chl-harzb)
Padrón-Navarta et al. (2011):
Chl (transitional lithologies)
Chl (S-Chl-harzb)
Chl (G-Chl-harzb)
(d) Orthopyroxene
CaO (wt%)
Mg#
Opx-1
Atg-Chl-Opx-Ol rock
S-Chl-harzb
G-Chl-harzb

Figure 7

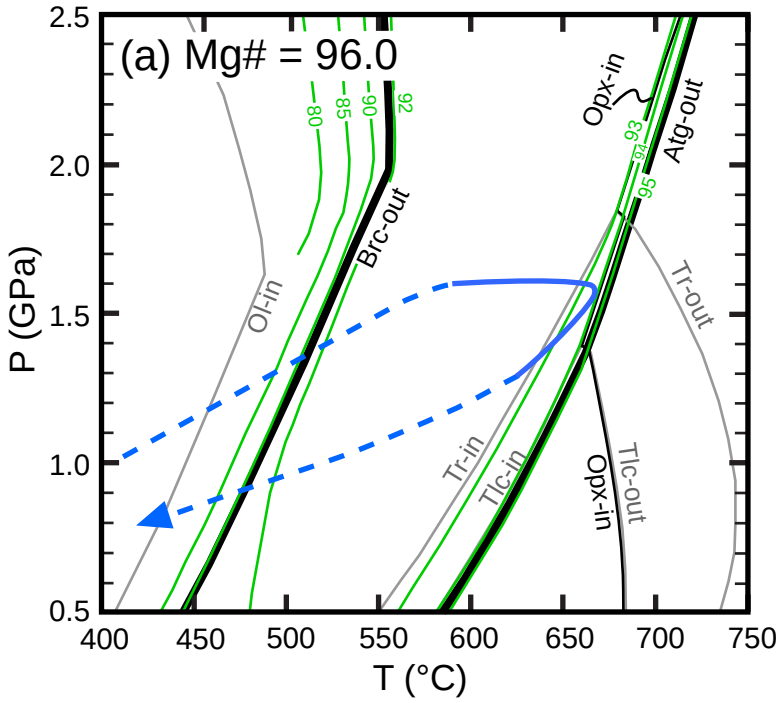
(a) Mg# = 96.0
Opx-in
Atg-out
Brc-out
Ol-in
Tr-out
Tr-in
Tlc-in
Tlc-out
Opx-in
P (GPa)
T (°C)

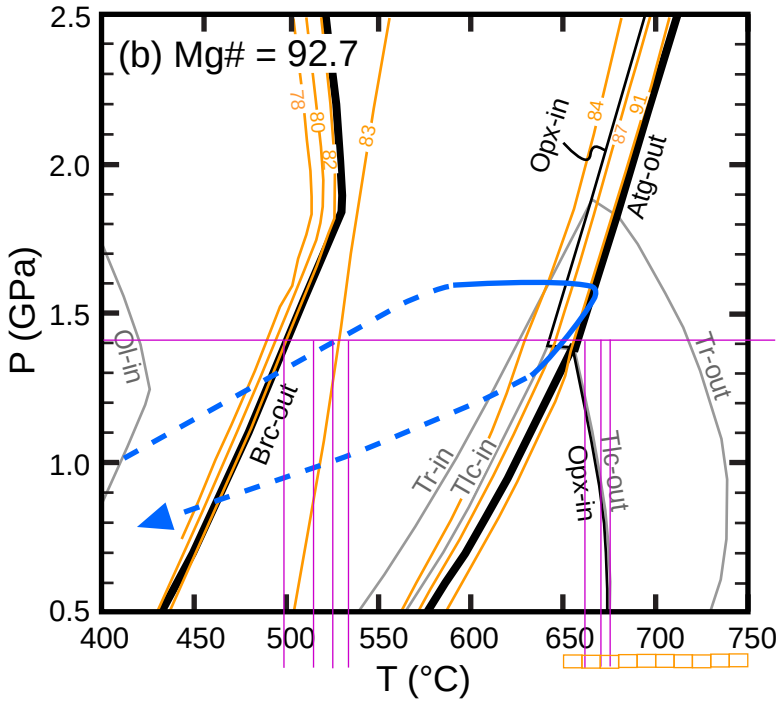
(b) Mg# = 92.7
Opx-in
Atg-out
Brc-out
Ol-in
Tr-out
Tr-in
Tlc-in
Tlc-out
Opx-in
P (GPa)
T (°C)

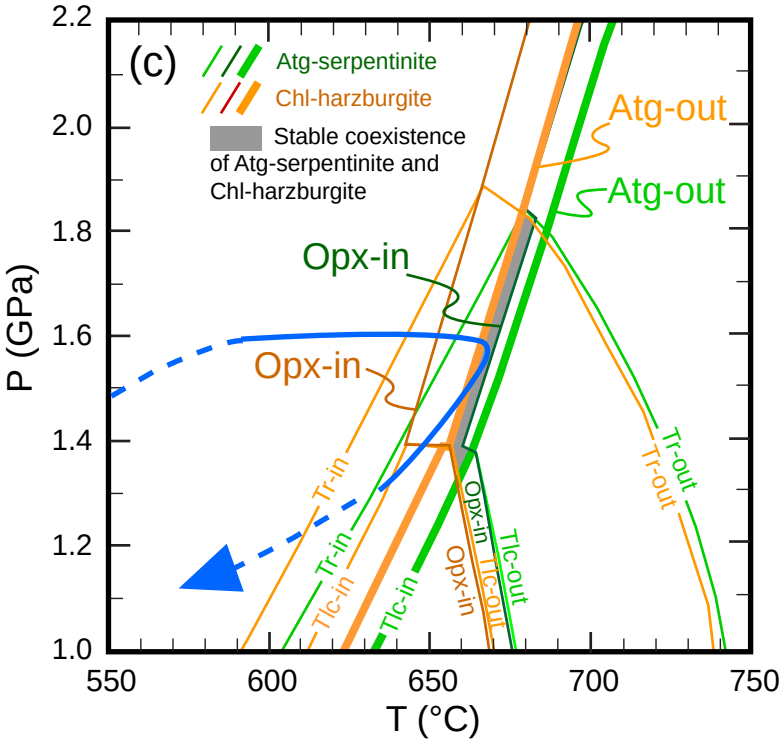
(c)
Atg-serpentinite
Chl-harzburgite
Stable coexistence of Atg-serpentinite and Chl-harzburgite
Atg-out
Atg-out
Opx-in
Opx-in
Tr-in
Tr-in
Tlc-in
Tlc-in
Opx-in
Tlc-out
Opx-in
Tlc-out
Tr-out
Tr-out
P (GPa)
T (°C)

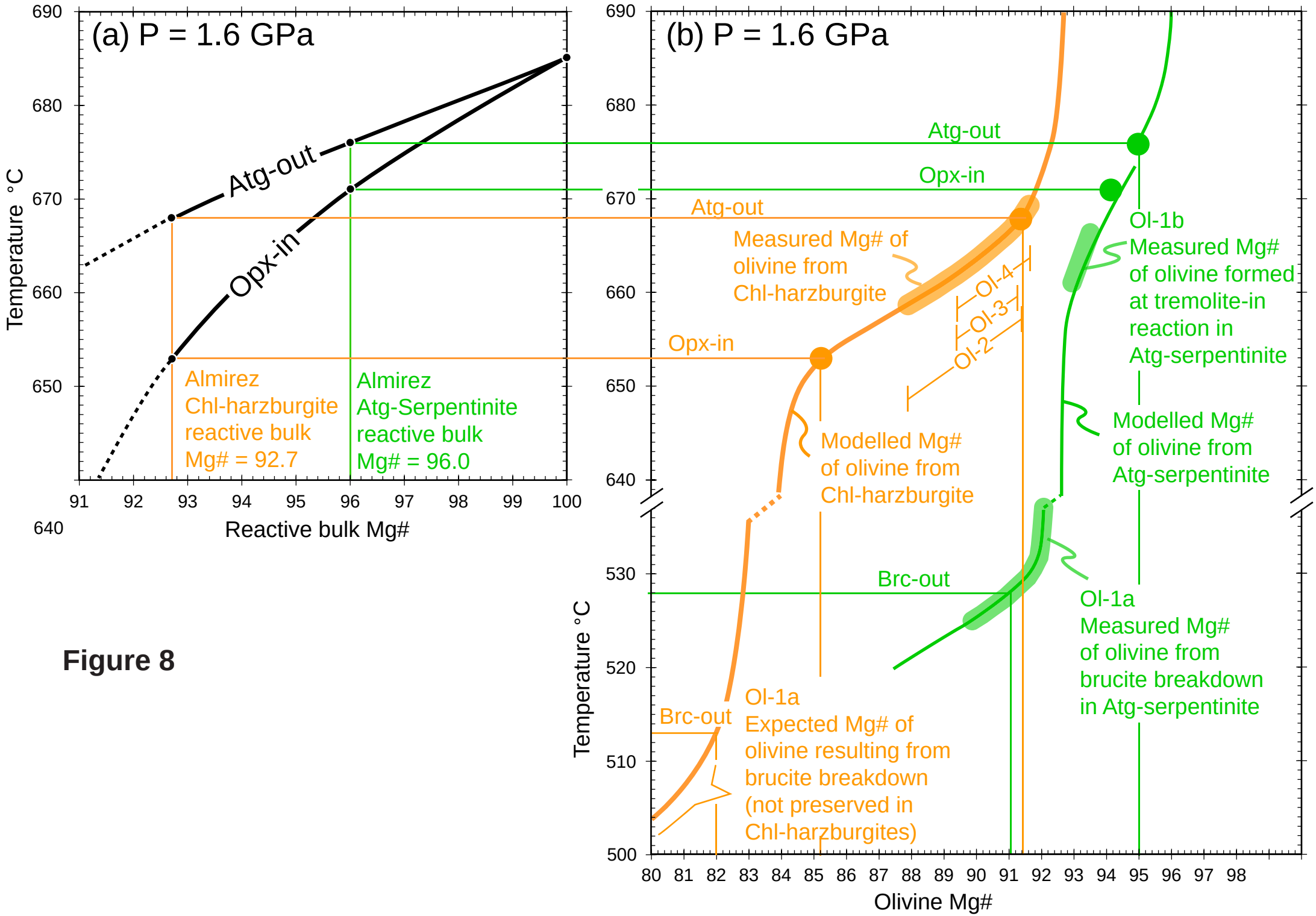
(a) P = 1.6 GPa
Temperature °C
Reactive bulk Mg#
Atg-out
Opx-in
Almirez
Chl-harzburgite
reactive bulk
Mg# = 92.7
Almirez
Atg-Serpentinite
reactive bulk
Mg# = 96.0
(b) P = 1.6 GPa
Olivine Mg#
Atg-out
Opx-in
Atg-out
Measured Mg# of
olivine from
Chl-harzburgite
Ol-4
Ol-3
Ol-2
Opx-in
Modelled Mg#
of olivine from
Chl-harzburgite
Ol-1b
Measured Mg#
of olivine formed
at tremolite-in
reaction in
Atg-serpentinite
Modelled Mg#
of olivine from
Atg-serpentinite
Brc-out
Ol-1a
Measured Mg#
of olivine from
brucite breakdown
in Atg-serpentinite
Brc-out
Ol-1a
Expected Mg# of
olivine resulting from
brucite breakdown
(not preserved in
Chl-harzburgites)

Figure 8

Table 1. Sample list, textures, and mineral abundances

				Modal abundances of minerals (vol%), from point counting												
				Opaque[a]	Atg	Chl	Tr	Ol[b]	Opx	Cpx[b]		Ti-Chu	Tlc	Cb[c]	Srp[d]
Lithology	**Subtype**	**Sample**	**Texture**							relic	metam.				
Atg-Serpentinite	Atg-serpentinite with relic and metamorphic Cpx	Alm06-094	foliated	4	57	0.6	-	27	-	6	5	0.4	-	-	-
		Alm06-107	foliated	3	56	x	x	24	-	9	7.6	-	-	-	0.4
		Alm06-109[e]	foliated	2	72	2	-	12	-	3.6	8	0.2	-	-	0.2
	Atg-serpentinite with metamorphic Cpx only	Alm06-119[e]	massive	2	65	-	1	27.7	-	-	4	0.3	-	-	-
	Cpx-free Ol-Atg-serpentinite	Alm06-095[e]	foliated	3	89	-	0.4	7	-	-	-	0.3	-	-	0.3
Chl-serpentinite		Alm06-085	foliated	2	52	9	5	14	-	-	-	-	7	-	11
		Alm06-111	foliated												
		Alm06-113	foliated	3	55	5	7	30	-	-	-	-	-	-	-
Atg-Chl-Opx-Ol-rock		Alm06-086	weakly foliated	6	10	10	x	46	1	-	-	-	13	-	14
		Alm06-087	massive, granular	2	4	16	x	48	7	-	-	-	11	-	12
Chl-harzburgite	Granular	Alm06-058	massive, granular	1	-	24	x	36	24	-	-		1	x	14
		Alm06-077[e]	massive, granular	1.5	-	23	0.4	22	33	-	-	0.6	9	x	10.5
		Alm06-029	massive, spinifex-textured	3	-	12	2	46	9	-	-	-	22	-	6
		Alm06-140	massive, spinifex-textured	0.4	-	14	0.3	41	36	-	-	-	1	-	7.3
		Alm06-141	massive, spinifex-textured												
		Alm06-142	massive, spinifex-textured	2	-	19	-	37	30	-	-	-	1	-	11
		Alm06-145[e]	massive, spinifex-textured	0.5	-	20	0.3	33	31	-	-	0.2	6	-	9

Notes:

Mineral abbreviations after Whitney and Evans (2010)

- : not observed

x: observed in thin section but not detected during point counting (abundance below 0.5 vol %)

a: mainly magnetite with minor sulphides and rare Fe-Ti-oxide

b: olivine and metamorphic clinopyroxene in Atg-serpentinites were counted as one phase during point counting (due to difficulties in reliably distinguishing them).
The fraction of clinopyroxene was then calculated from the bulk rock CaO, assuming all CaO in clinopyroxene (in absence of carbonate).

c: rare coarse carbonate

d: late retrograde mesh serpentine

e: modal abundances refined based on measured bulk rock data

Supplementary materials to:

The influence of oceanic oxidation on serpentinite dehydration during subduction

Annette Bretscher, Joerg Hermann, Thomas Pettke

University of Bern, Institute of Geological Sciences, Baltzerstrasse 1&3, CH-3012 Bern, Switzerland (pettke@geo.unibe.ch)

Caption to Supplementary Materials:

- **Supplementary Material 1** contains details on the analytical methods and on the modelling parameters employed

- **Supplementary Table A1** contains bulk rock major element compositions

- **Supplementary Table A2** contains major element compositions of rock-forming silicates

- **Supplementary Table A3** contains the reactive bulk rock major element compositions employed for modelling

Supplementary Material 1:

Methods

Samples with minimal weathering were investigated by optical microscopy based on 25 µm thin sections, and mineral identification was assisted by scanning electron microscopy (SEM-EDX) and RAMAN spectroscopy. Modal abundances of opaque minerals (magnetite plus minor sulphides) were obtained by point counting.

Bulk rock compositions

Bulk rock major element measurements were performed with laser ablation (LA) - ICP-MS on pressed powder pellets (PPP) following procedures detailed in Peters and Pettke (2017). Only pristine sample material was used; sawing and weathering surfaces of the samples were chipped away. After crushing the samples in plastic bags to obtain fragments smaller than 5 mm they were dry milled with a RETSCH 250 ml agate planetary ball mill and subsequently wet milled with a RETSCH 50 ml agate planetary ball mill, in order to obtain a single µm sized sample powder. The powder was then mixed with a binder (microcrystalline cellulose), and pressed to pellets of 10 mm diameter and 1 mm thickness. Pellets were measured by LA-ICP-MS with a Geolas Pro 193 nm ArF excimer laser system coupled to an ELAN DRC-e quadrupole ICP-MS instrument at the Institute of Geological Sciences, University of Bern, Switzerland. Instrument optimization procedures and analytical strategies closely followed those outlined in Pettke et al. (2012). Measurement beam size was set at 120 µm, and the surface area of each measurement spot was cleaned by pre-ablation for 5 s employing a 160 µm beam size. External calibration was performed using the trace element doped basaltic glasses GSD-1G or BCR-2G from USGS employing the preferred values listed in Peters and Pettke (2017). Data were reduced employing SILLS, by normalizing to the sum of major element oxides minus water (and rare CO_2) as determined by loss on ignition obtained by heating the dried sample powder at 1050 °C during 1.5 hours. Bulk rock element concentrations reported represent the average and 1 standard deviation of 6 measurement spots per PPP. Quality control was done by measuring a pressed powder pellet of the rock standard MUH-1 (serpentinized harzburgite) provided by

the International Association of Geoanalysts, and the measured concentrations correspond within 2 standard deviation error to the long term average reported in Peters and Pettke (2017).

Mineral major element composition

Major element concentrations of the rock forming minerals olivine, antigorite, orthopyroxene, clinopyroxene, chlorite, tremolite, talc, and Ti-clinohumite were determined by electron probe microanalysis (EPMA) using a JEOL JXA-8200 instrument at the Institute of Geological Sciences, University of Bern. The acceleration voltage was 15 keV and the beam current 20 nA. Beam sizes were 1 µm for olivine, orthopyroxene, clinopyroxene, and Ti-clinohumite, 5 µm for tremolite, and 10 µm for antigorite, talc, and chlorite. Counting times were 20 seconds on peak and 10s on each background position. Natural or synthetic silicate and oxide minerals were used as standards. A PhiRhoZAF routine was used for matrix correction.

Modelling parameters

Chemical model systems are referred to as
- MSH (MgO-SiO_2-H_2O); MASH (MgO-Al_2O_3-SiO_2-H_2O), FMASH (FeO-MgO-Al_2O_3-SiO_2-H_2O), and CFMASH (CaO-FeO-MgO-Al_2O_3-SiO_2-H_2O).

Input reactive bulk compositions:

Thermodynamic component	**Atg-Serpentinite Wt%**	**Chl-harzburgite Wt%**
SiO_2	46.26	45.80
Al_2O_3	2.32	2.80
FeO	3.48	6.34
MgO	46.97	44.97
CaO	0.97	0.08
H_2O	Saturated component	

Solid solution models in Perple_X (Connolly, 2005):

We have chosen the Holland and Powell thermodynamic data set, database hp02ver.dat with the fluid equation of state "X(CO_2) H_2O-CO_2 CORK Holland and Powell 91, 98" (Holland and Powell, 1998), as this allows including the Tschermak ($Al_2Mg_{-1}Si_{-1}$) solid solution in antigorite as given in Padrón-Navarta et al. (2013). Aluminium-substitution in antigorite is important since natural antigorite can host up to several wt% Al_2O_3, and Al-bearing antigorite is stable to higher temperatures compared to Al-free antigorite, due to the effect of minimizing structural misfit among the component octahedral and tetrahedral sheets (Bromiley and Pawley, 2003). The models assume closed system conditions. Minor components (TiO_2, Cr_2O_3, MnO, NiO, Na_2O, K_2O, and P_2O_5) were neglected for simplicity; their impact on the positions of the major dehydration reactions is considered to be subordinate.

Mineral	Solution phase	Reference
Antigorite	Atg(PN)	Padrón-Navarta et al. (2013)
Chlorite	Chl(HP)	Holland et al. (1998)
Talk	Tlc, ideal	
Tremolite	Tr, ideal	
Brucite	Brc, ideal	
Olivine	Ol(HP)	Holland and Powell (1998)
Orthopyroxene	Opx(HP)	Holland and Powell (1996)
Clinopyroxene	Cpx(HP)	Holland and Powell (1996)
Garnet	Grt(HP)	Holland and Powell (1998)

References

Bromiley, G. D. and Pawley, A. R., 2003. The stability of antigorite in the systems $MgO\text{-}SiO_2\text{-}H_2O$ (MSH) and $MgO\text{-}Al_2O_3\text{-}SiO_2\text{-}H_2O$ (MASH): The effects of Al^{3+} substitution on high-pressure stability. American Mineralogist 88, 99-108.

Connolly, J. A. D., 2005. Computation of phase equilibria by linear programming: A tool for geodynamic modeling and its application to subduction zone decarbonation. Earth and Planetary Science Letters 236, 524-541.

Holland, T., Powell, R., 1996. Thermodynamics of order-disorder in minerals. 2. Symmetric formalism applied to solid solutions. American Mineralogist 81, 1425-37.

Holland, T.J.B., Powell, R., 1998. An internally consistent thermodynamic data set for phases of petrological interest. Journal of Metamorphic Geology 16, 309-43.

Holland, T., Baker, J., Powell, R., 1998. Mixing properties and activity-composition relationships of chlorites in the system MgO-FeO-Al2O3-SiO2-H2O. European Journal of Mineralogy 10, 395-406.

Padrón-Navarta, J.A., López Sánchez-Vizcaíno, V., Hermann, J., Connolly, J.A.D., Garrido, C.J., Gómez-Pugnaire, M.T., Marchesi, C., 2013. Tschermak's substitution in antigorite and consequences for phase relations and water liberation in high-grade serpentinites. Lithos 178, 186–196.

Peters, D. and Pettke, T., 2017. Evaluation of Major to Ultra Trace Element Bulk Rock Chemical Analysis of Nanoparticulate Pressed Powder Pellets by LA-ICP-MS. Geostandards and Geoanalytical Research 41, 5-28.

Pettke, T., Oberli, F., Audetat, A., Guillong, M., Simon, A. C., Hanley, J. J., and Klemm, L. M., 2012. Recent developments in element concentration and isotope ratio analysis of individual fluid inclusions by laser ablation single and multiple collector ICP-MS. Ore Geology Reviews 44, 10-38.

Supplementary Table A1. Bulk major element compositions, measured by LA-ICP-MS on pressed powder pellets

	Atg-serpentinites								Chl-serpentinites							
	Alm06-094[a]	2SD%	Alm06-107[a]	2SD%	Alm06-109[a]	2SD%	Alm06-119[a]	2SD%	Alm06-095[a]	2SD%	Alm06-085[a]	2SD%	Alm06-111[a]	2SD%	Alm06-113[a]	2SD%
Major elements in wt% oxides																
SiO_2	41.16	2	41.37	0.4	41.24	1	40.29	1	40.48	1	42.10	1	40.22	1	40.57	1
TiO_2	0.08	6	0.09	10	0.07	16	0.04	12	0.04	15	0.04	10	0.05	15	0.06	13
Al_2O_3	2.37	2	1.75	2	2.29	3	1.22	2	2.14	3	2.65	3	1.62	3	1.91	3
Cr_2O_3	0.38	2	0.36	2	0.37	3	0.32	4	0.37	2	0.32	3	0.38	3	0.42	3
FeO	7.31	3	8.48	3	6.86	2	7.08	1	7.53	3	7.14	1	8.33	2	7.35	2
MnO	0.11	4	0.13	1	0.11	2	0.15	2	0.10	2	0.12	1	0.15	2	0.13	2
NiO	0.24	4	0.25	7	0.26	9	0.28	5	0.27	4	0.23	2	0.29	3	0.29	5
MgO	35.54	2	35.06	0.3	35.57	1	39.75	1	37.69	1	36.39	1	41.02	0.3	39.38	1
CaO	3.11	2	4.95	2	3.56	3	1.19	7	0.06	8	0.64	8	0.26	5	0.80	3
Na_2O	0.013	42	0.025	4	0.01	8	0.004	5	0.002	19	0.015	5	0.009	15	0.020	7
K_2O	0.001	18	0.003	10	0.001	39	0.001	14	0.003	13	0.006	5	0.002	17	0.004	5
P_2O_5	0.002	6	0.003	17	0.003	17	0.004	18	0.002	25	0.009	17	0.007	12	0.011	30
LOI[b]	9.7		7.5		9.7		9.7		11.3		10.3		7.7		9.1	
Total	100.0		100.0		100.0		100.0		100.0		100.0		100.0		100.0	
Mg#[c]	89.7		88.0		90.2		90.9		89.9		90.1		89.8		90.5	

	Atg-Chl-Opx-Ol rock		Spinifex-textured Chl-harzburgites						Granular Chl-harzburgites					
	Alm06-086	2SD%	Alm06-087	2SD%	Alm06-141[a]	2SD%	Alm06-142[a]	2SD%	Alm06-145[a]	2SD%	Alm06-058[a]	2SD%	Alm06-077[a]	2SD%
SiO_2	38.91	1	42.50	1	40.83	3	43.94	0	43.66	1	43.82	1	44.77	1
TiO_2	0.21	10	0.05	11	0.06	20	0.07	9	0.07	10	0.07	6	0.06	8
Al_2O_3	1.82	2	1.72	6	2.56	1	2.45	5	2.61	3	2.65	6	2.49	5
Cr_2O_3	0.90	3	0.44	4	0.40	3	0.42	3	0.43	1	0.38	4	0.40	2
FeO	10.18	3	8.14	2	8.50	2	8.03	3	7.58	1	7.50	1	8.65	2
MnO	0.13	1	0.13	2	0.12	3	0.11	2	0.10	0.4	0.12	1	0.10	1
NiO	0.26	4	0.28	3	0.25	3	0.28	2	0.28	1	0.29	4	0.25	5
MgO	40.61	1	40.83	1	42.96	3	40.55	0.5	40.72	1	40.20	1	39.16	1
CaO	0.02	22	0.05	11	0.09	24	0.05	4	0.05	6	0.07	5	0.02	9
Na_2O	0.010	14	0.011	10	0.008	21	0.006	18	0.009	18	0.006	33	0.016	13
K_2O	0.003	18	0.003	11	0.002	30	<0.0003	94	0.002	8	0.0003	52	0.003	22
P_2O_5	0.004	6	0.012	10	0.001	26	0.003	5	0.003	4	0.011	8	0.027	8
LOI[b]	6.9		5.8		4.2		4.1		4.5		4.9		4.1	
Total	100.0		100.0		100.0		100.0		100.0		100.0		100.0	
Mg#[c]	87.7		89.9		90.0		90.0		90.5		90.5		89.0	

Notes:

Internal standardisation of the LA-ICP-MS measurement data was performed on total oxides, i.e., 100 wt% element oxides minus LOI (wt%); hence, the totals are all 100.0 wt%

[a] Bulk rock data from Peters et al. (2017).

[b] LOI: loss on ignition determined by heating the dried sample pouder at 1050 °C during 1.5 hours

[c] 100 * $[MgO/(MgO+FeO)]_{molar}$

Supplementary Table A2. Major element compositions of antigorite (representative measurements)

Lithology	**Atg-serpentinite**																		
Mineral growth stage	**Atg-1 (matrix, foliated)**									**Atg-1 (matrix, massive)**									
Sample	Alm06-094	Alm06-094	Alm06-093	Alm06-093	Alm06-095	Alm06-095	**Average**	2stdev	2stdev%	Alm06-125	Alm06-125	Alm06-125	Alm06-125	Alm06-125	Alm06-125	**Average**	2stdev	2stdev%
Wt% oxides																		
SiO2	41.99	41.73	41.91	42.33	43.13	42.33	**42.24**	1.00	2.4	43.02	43.07	42.93	42.13	42.40	41.68	**42.54**	1.13	2.7
Al2O3	3.93	4.26	3.66	3.44	2.64	2.80	**3.46**	1.27	36.7	2.46	2.33	2.51	2.30	2.34	2.35	**2.38**	0.17	7.0
FeO_{tot}	3.18	3.57	3.07	3.31	2.68	2.63	**3.07**	0.73	23.7	2.71	2.81	3.01	2.88	2.87	2.86	**2.86**	0.20	6.9
MnO	0.06	0.08	0.04	0.05	0.09	0.05	**0.06**	0.04	62.0	0.05	0.06	0.06	0.05	0.05	0.06	**0.05**	0.01	27.4
MgO	37.87	37.89	38.33	38.07	38.30	38.71	**38.20**	0.64	1.7	38.56	38.87	38.60	38.78	38.67	38.86	**38.72**	0.27	0.7
TiO2	0.03	0.00		0.02	0.01	0.02	**0.01**	0.02	138.9	0.01	0.01	0.03		0.03	0.01	**0.02**	0.03	147.1
CaO		0.01	0.00	0.01	0.01		**0.01**	0.00	27.7	0.01	0.01	0.00	0.02	0.02	0.01	**0.01**	0.01	101.7
Na2O	0.01		0.01		0.02	0.01	**0.01**	0.01	117.0		0.02	0.03				**0.02**	0.01	35.6
K2O	0.00	0.01		0.00	0.01	0.01	**0.01**	0.01	116.7		0.01		0.00	0.01		**0.01**	0.01	72.3
Total	87.07	87.55	87.02	87.22	86.88	86.56	**87.05**	0.66	0.8	86.81	87.20	87.17	86.16	86.38	85.82	**86.59**	1.12	1.3
No. of ions in formula based on 6.824 O																		
Si	1.91	1.89	1.91	1.92	1.96	1.93	**1.92**	0.05	2.4	1.95	1.95	1.95	1.93	1.94	1.92	**1.94**	0.02	1.2
Al	0.21	0.23	0.20	0.18	0.14	0.15	**0.19**	0.07	36.5	0.13	0.12	0.13	0.12	0.13	0.13	**0.13**	0.01	6.3
Fe3+																		
Fe2+	0.12	0.14	0.12	0.13	0.10	0.10	**0.12**	0.03	23.5	0.10	0.11	0.11	0.11	0.11	0.11	**0.11**	0.01	7.1
Mn	0.00	0.00	0.00	0.00	0.00	0.00	**0.00**	0.00	61.7	0.00	0.00	0.00	0.00	0.00	0.00	**0.00**	0.00	27.6
Mg	2.57	2.56	2.60	2.58	2.59	2.63	**2.59**	0.05	2.0	2.61	2.62	2.61	2.65	2.64	2.67	**2.64**	0.05	1.9
Ti	0.00	0.00		0.00	0.00	0.00	**0.00**	0.00	178.4	0.00	0.00	0.00		0.00	0.00	**0.00**	0.00	185.6
Ca		0.00	0.00	0.00	0.00		**0.00**	0.00	158.2	0.00	0.00	0.00	0.00	0.00	0.00	**0.00**	0.00	101.9
Na	0.00		0.00		0.00	0.00	**0.00**	0.00	205.8		0.00	0.00				**0.00**	0.00	313.5
K	0.00	0.00		0.00	0.00	0.00	**0.00**	0.00	159.1		0.00		0.00	0.00		**0.00**	0.00	237.4
Total	4.81	4.82	4.82	4.81	4.80	4.82	**4.81**	0.02	0.4	4.80	4.81	4.81	4.83	4.82	4.84	**4.82**	0.02	0.5
Mg#	95.50	94.98	95.70	95.35	96.22	96.33	**95.68**	1.04	1.1	96.21	96.10	95.81	96.00	96.00	96.04	**96.03**	0.26	0.3

Note:
Antigorite composition in terms of Altotal vs Si, calculated on the basis of the ideal antigorite formula (m=17) and normalized to 6·824 oxygens, following Padron-Navarta et al. (2011).

Atg-1 (single blades over Ol-1)								**Chl-serpentinite** **Atg-1 (fine-grained foliated matrix)**							
Alm06-093	Alm06-093	Alm06-093	Alm06-125	Alm06-125	**Average**	2stdev	2stdev%	Alm06-085	Alm06-085	Alm06-085	Alm06-111	Alm06-111	**Average**	2stdev	2stdev%
42.74	41.73	43.12	42.82	43.48	**42.78**	1.31	3.1	42.79	42.68	42.15	41.29	42.14	**42.21**	1.19	2.8
2.00	3.10	2.62	2.28	2.13	**2.43**	0.88	36.5	3.28	3.34	3.85	3.90	3.61	**3.60**	0.57	15.8
2.91	3.04	3.26	3.07	3.31	**3.12**	0.33	10.6	4.10	4.08	4.46	3.58	3.61	**3.97**	0.74	18.7
0.04	0.04	0.06	0.05	0.09	**0.06**	0.04	65.8	0.06	0.06	0.08	0.06	0.04	**0.06**	0.03	55.0
38.42	38.28	38.35	38.83	38.51	**38.48**	0.43	1.1	37.08	37.62	37.22	37.39	37.35	**37.33**	0.40	1.1
0.01	0.03	0.02		0.01	**0.02**	0.02	123.9	0.02	0.03	0.02	0.00	0.02	**0.02**	0.02	139.0
	0.00	0.01		0.00	**0.00**	0.01	262.5	0.02	0.01	0.01	0.00	0.00	**0.01**	0.01	133.6
0.00											0.01		**0.01**		
0.01	0.01	0.01	0.00	0.00	**0.01**	0.01	108.8	0.00	0.01	0.01			**0.01**	0.01	141.0
86.14	86.24	87.45	87.05	87.53	**86.88**	1.31	1.5	87.35	87.84	87.80	86.23	86.77	**87.20**	1.39	1.6
1.96	1.92	1.95	1.95	1.97	**1.95**	0.04	2.0	1.94	1.93	1.91	1.90	1.92	**1.92**	0.03	1.8
0.11	0.17	0.14	0.12	0.11	**0.13**	0.05	37.1	0.18	0.18	0.21	0.21	0.19	**0.19**	0.03	16.7
0.11	0.12	0.12	0.12	0.13	**0.12**	0.01	9.3	0.16	0.15	0.17	0.14	0.14	**0.15**	0.03	17.7
0.00	0.00	0.00	0.00	0.00	**0.00**	0.00	64.5	0.00	0.00	0.00	0.00	0.00	**0.00**	0.00	54.5
2.63	2.62	2.59	2.63	2.59	**2.61**	0.04	1.5	2.51	2.54	2.52	2.57	2.54	**2.53**	0.04	1.7
0.00	0.00	0.00		0.00	**0.00**	0.00	175.1	0.00	0.00	0.00	0.00	0.00	**0.00**	0.00	138.4
	0.00	0.00		0.00	**0.00**	0.00	358.7	0.00	0.00	0.00	0.00	0.00	**0.00**	0.00	133.2
0.00					**0.00**	0.00	447.2				0.00		**0.00**	0.00	447.2
0.00	0.00	0.00	0.00	0.00	**0.00**	0.00	110.0	0.00	0.00	0.00			**0.00**	0.00	246.6
4.81	4.82	4.80	4.82	4.80	**4.81**	0.02	0.4	4.79	4.80	4.81	4.82	4.80	**4.80**	0.02	0.4
95.92	95.73	95.45	95.75	95.40	**95.65**	0.44	0.5	94.16	94.26	93.70	94.90	94.86	**94.38**	1.01	1.1

Atg-2 (single blades growing over olivine, random orientation)										**Atg-2 (Atg-2-Chl-3-intergrowths)**										
Alm06-111	Alm06-111	Alm06-113	Alm06-113	Alm06-113	Alm06-113	**Average**	2stdev	2stdev%		Alm06-085	Alm06-085	Alm06-085	Alm06-085	Alm06-085	Alm06-111	Alm06-111	Alm06-111	**Average**	2stdev	2stdev%
43.20	42.74	43.49	43.92	42.45	42.56	**43.06**	1.16	2.7		43.10	42.70	41.74	43.34	43.76	40.98	41.71	41.96	**42.41**	1.92	4.5
3.08	3.39	2.56	1.82	3.40	3.05	**2.88**	1.21	42.0		3.07	3.45	4.16	2.91	2.54	3.69	3.54	3.71	**3.38**	1.03	30.5
3.69	3.82	3.42	3.12	4.05	4.06	**3.69**	0.74	20.0		4.37	4.64	4.31	3.85	3.66	3.77	3.68	3.49	**3.97**	0.82	20.8
0.04	0.05	0.06	0.05	0.05	0.04	**0.05**	0.01	24.6		0.04	0.07	0.07	0.05	0.05	0.06	0.04	0.04	**0.05**	0.03	50.9
37.76	37.62	38.77	39.18	37.57	37.72	**38.10**	1.38	3.6		37.71	37.03	36.58	37.70	38.26	37.22	37.51	36.89	**37.36**	1.08	2.9
0.04	0.01	0.01	0.01	0.01	0.02	**0.02**	0.02	145.8			0.00	0.03	0.00	0.01	0.03	0.02	0.03	**0.02**	0.02	151.4
0.00	0.01	0.01	0.00	0.00		**0.01**	0.01	153.7		0.01	0.02	0.01	0.01	0.00	0.01	0.01	0.01	**0.01**	0.01	136.5
	0.01	0.01		0.01	0.02	**0.01**	0.01	69.9		0.00	0.01		0.00		0.00	0.03		**0.01**	0.02	227.0
0.00				0.00		**0.00**	0.00	193.5			0.01	0.01	0.01	0.01	0.00			**0.01**	0.01	98.2
87.82	87.65	88.33	88.09	87.55	87.47	**87.82**	0.67	0.8		88.30	87.94	86.91	87.88	88.29	85.76	86.53	86.12	**87.22**	2.03	2.3
1.95	1.93	1.95	1.97	1.93	1.93	**1.94**	0.03	1.6		1.94	1.93	1.91	1.95	1.96	1.90	1.91	1.93	**1.93**	0.04	2.3
0.16	0.18	0.14	0.10	0.18	0.16	**0.15**	0.07	42.8		0.16	0.18	0.22	0.15	0.13	0.20	0.19	0.20	**0.18**	0.06	32.3
0.14	0.14	0.13	0.12	0.15	0.15	**0.14**	0.03	21.0		0.16	0.18	0.16	0.15	0.14	0.15	0.14	0.13	**0.15**	0.03	20.1
0.00	0.00	0.00	0.00	0.00	0.00	**0.00**	0.00	24.5		0.00	0.00	0.00	0.00	0.00	0.00	0.00	0.00	**0.00**	0.00	51.1
2.54	2.54	2.59	2.62	2.54	2.55	**2.56**	0.07	2.7		2.53	2.50	2.50	2.53	2.56	2.57	2.57	2.53	**2.54**	0.06	2.2
0.00	0.00	0.00	0.00	0.00	0.00	**0.00**	0.00	145.7			0.00	0.00	0.00	0.00	0.00	0.00	0.00	**0.00**	0.00	180.2
0.00	0.00	0.00	0.00	0.00		**0.00**	0.00	191.4		0.00	0.00	0.00	0.00	0.00	0.00	0.00	0.00	**0.00**	0.00	135.5
	0.00	0.00		0.00	0.00	**0.00**	0.00	175.1		0.00	0.00		0.00		0.00	0.00		**0.00**	0.00	322.4
0.00				0.00		**0.00**	0.00	403.8			0.00	0.00	0.00	0.00	0.00			**0.00**	0.00	204.1
4.79	4.80	4.81	4.81	4.81	4.81	**4.80**	0.01	0.3		4.80	4.80	4.80	4.79	4.79	4.82	4.82	4.79	**4.80**	0.02	0.5
94.80	94.61	95.28	95.72	94.30	94.31	**94.84**	1.14	1.2		93.90	93.43	93.80	94.58	94.91	94.62	94.78	94.96	**94.37**	1.16	1.2

Atg-Chl-Opx-Ol rock

Atg-2 (Atg-2-Chl-3-intergrowths)									**Atg-2 (single blades, random orientation)**									
Alm06-086	Alm06-086	Alm06-086	Alm06-086	Alm06-087	Alm06-087	**Average**	2stdev	2stdev%	Alm06-086	Alm06-086	Alm06-087	Alm06-087	Alm06-087	Alm06-087	Alm06-087	**Average**	2stdev	2stdev%
44.12	42.99	41.80	42.38	41.75	42.79	**42.64**	1.77	4.1	42.47	42.30	42.86	43.07	43.92	39.91	40.84	**42.20**	2.75	6.5
2.08	3.27	4.20	3.88	3.83	3.84	**3.52**	1.53	43.5	3.80	4.11	3.01	3.44	2.57	4.04	3.82	**3.54**	1.14	32.2
3.17	3.64	3.48	3.69	4.04	3.75	**3.63**	0.58	16.0	3.71	3.57	3.74	3.66	3.30	4.16	3.83	**3.71**	0.52	14.1
0.03	0.05	0.06	0.06	0.05	0.05	**0.05**	0.02	34.1	0.02	0.05	0.08	0.04	0.02	0.05	0.05	**0.04**	0.04	97.4
39.09	37.79	36.73	37.01	37.32	37.59	**37.59**	1.66	4.4	37.50	37.40	38.18	37.75	38.59	37.02	37.51	**37.71**	1.05	2.8
0.01	0.02	0.00	0.02	0.01	0.02	**0.01**	0.02	127.2	0.02	0.02	0.02	0.02	0.01	0.02	0.03	**0.02**	0.01	59.1
0.01	0.01	0.01	0.00	0.01	0.00	**0.01**	0.01	131.4	0.01	0.01	0.01	0.01	0.00	0.02	0.00	**0.01**	0.01	135.0
0.00					0.01	**0.01**	0.01	152.7		0.01			0.00		0.01	**0.01**	0.01	85.7
		0.00		0.00	0.01	**0.01**	0.01	222.6	0.00	0.00	0.01	0.00			0.00	**0.00**	0.01	179.9
88.51	87.77	86.29	87.04	87.00	88.07	**87.45**	1.63	1.9	87.53	87.48	87.91	87.99	88.41	85.22	86.09	**87.23**	2.30	2.6
1.97	1.94	1.92	1.93	1.91	1.93	**1.93**	0.04	2.2	1.92	1.92	1.93	1.94	1.96	1.87	1.89	**1.92**	0.06	3.3
0.11	0.17	0.23	0.21	0.21	0.20	**0.19**	0.08	44.8	0.20	0.22	0.16	0.18	0.14	0.22	0.21	**0.19**	0.07	34.3
0.12	0.14	0.13	0.14	0.15	0.14	**0.14**	0.02	17.1	0.14	0.14	0.14	0.14	0.12	0.16	0.15	**0.14**	0.02	17.2
0.00	0.00	0.00	0.00	0.00	0.00	**0.00**	0.00	35.2	0.00	0.00	0.00	0.00	0.00	0.00	0.00	**0.00**	0.00	97.4
2.60	2.54	2.51	2.51	2.54	2.52	**2.54**	0.07	2.7	2.53	2.52	2.57	2.53	2.57	2.58	2.58	**2.56**	0.05	2.1
0.00	0.00	0.00	0.00	0.00	0.00	**0.00**	0.00	127.3	0.00	0.00	0.00	0.00	0.00	0.00	0.00	**0.00**	0.00	59.6
0.00	0.00	0.00	0.00	0.00	0.00	**0.00**	0.00	131.8	0.00	0.00	0.00	0.00	0.00	0.00	0.00	**0.00**	0.00	137.7
0.00					0.00	**0.00**	0.00	372.0		0.00			0.00		0.00	**0.00**	0.00	276.3
		0.00		0.00	0.00	**0.00**	0.00	355.2	0.00	0.00	0.00	0.00			0.00	**0.00**	0.00	245.9
4.80	4.80	4.79	4.79	4.81	4.80	**4.80**	0.02	0.3	4.80	4.80	4.81	4.79	4.79	4.84	4.83	**4.81**	0.04	0.8
95.65	94.87	94.95	94.70	94.27	94.70	**94.86**	0.90	1.0	94.74	94.92	94.79	94.84	95.42	94.07	94.58	**94.77**	0.81	0.9

Supplementary Table A2. Major element compositions of chlorite (representative measurements)

Lithology	**Atg-serpentinite**																	
Mineral growth stage	**Chl-1 (fine-grained mass associated with Mag)**								**Chl-2 (flaky inclusions in relic Cpx-1)**									
Sample	Alm06-094	Alm06-094	Alm06-094	Alm06-094	Alm06-094	**Average**	2stdev	2stdev%	Alm06-107	Alm06-107	Alm06-107	Alm06-107	Alm06-107	Alm06-107	**Average**	2stdev	2stdev%	
Wt% oxides																		
SiO2	34.32	34.21	33.95	34.20	34.08	**34.15**	0.28	0.8	35.71	35.60	34.76	34.45	34.40	34.66	**34.93**	1.16	3.3	
Al2O3	13.02	12.68	13.10	13.53	13.05	**13.08**	0.61	4.6	11.94	12.55	13.03	13.15	13.20	13.12	**12.83**	0.99	7.7	
FeO_{tot}	3.22	3.61	3.62	3.16	3.67	**3.46**	0.49	14.2	3.33	3.16	3.51	3.68	3.69	3.54	**3.49**	0.41	11.9	
MnO	0.04	0.03	0.04	0.04	0.04	**0.04**	0.01	32.1	0.04	0.04	0.05	0.05	0.03	0.04	**0.04**	0.02	46.3	
MgO	34.35	34.99	34.46	34.87	34.62	**34.66**	0.54	1.6	35.47	34.63	34.76	34.94	35.37	34.99	**35.03**	0.66	1.9	
TiO2			0.01	0.02		**0.01**	0.00	16.4	0.03	0.03	0.01	0.02	0.02	0.02	**0.02**	0.02	76.7	
CaO	0.01	0.02	0.03	0.00	0.01	**0.01**	0.02	164.8	0.04	1.43	0.04	0.06	0.04	0.03	**0.27**	1.13	413.5	
Na2O			0.00	0.01		**0.01**	0.00	42.0			0.01	0.02			**0.02**	0.01	77.3	
K2O	0.01	0.00	0.01	0.01	0.00	**0.01**	0.01	170.9	0.01	0.00	0.01	0.01			**0.01**	0.00	71.1	
SO3																		
Total	84.97	85.54	85.24	85.83	85.47	**85.41**	0.64	0.8	86.57	87.45	86.18	86.39	86.74	86.39	**86.62**	0.89	1.0	
No. of ions in formula based on 14 O																		
Si	3.30	3.28	3.27	3.26	3.27	**3.27**	0.03	1.0	3.37	3.34	3.30	3.27	3.25	3.28	**3.30**	0.09	2.7	
Al	1.48	1.43	1.48	1.52	1.48	**1.48**	0.06	4.2	1.33	1.39	1.46	1.47	1.47	1.47	**1.43**	0.12	8.3	
Fe2+	0.26	0.29	0.29	0.25	0.29	**0.28**	0.04	14.6	0.26	0.25	0.28	0.29	0.29	0.28	**0.28**	0.03	12.6	
Mn	0.00	0.00	0.00	0.00	0.00	**0.00**	0.00	32.4	0.00	0.00	0.00	0.00	0.00	0.00	**0.00**	0.00	46.5	
Mg	4.92	5.00	4.94	4.95	4.95	**4.95**	0.06	1.1	4.99	4.84	4.92	4.94	4.99	4.94	**4.94**	0.11	2.2	
Ti			0.00	0.00		**0.00**	0.00	274.5	0.00	0.00	0.00	0.00	0.00	0.00	**0.00**	0.00	76.0	
Ca	0.00	0.00	0.00	0.00	0.00	**0.00**	0.00	165.1	0.00	0.14	0.00	0.01	0.00	0.00	**0.03**	0.11	412.8	
Na			0.00	0.00		**0.00**	0.00	278.5			0.00	0.00			**0.00**	0.00	326.7	
K	0.00	0.00	0.00	0.00	0.00	**0.00**	0.00	171.4	0.00	0.00	0.00	0.00			**0.00**	0.00	176.0	
Total	9.96	10.00	9.99	9.98	9.99	**9.99**	0.03	0.3	9.96	9.97	9.97	10.00	10.01	9.98	**9.98**	0.04	0.4	
Mg#	95.00	94.53	94.43	95.16	94.39	**94.70**	0.71	0.7	95.00	95.13	94.64	94.42	94.47	94.63	**94.71**	0.57	0.6	

Chl-serpentinite												**Atg-Chl-Opx-Ol rock**									
Chl-3 (Chl-3-Atg-2-intergrowths)												**Chl-3 (flaky aggregates, no Atg-2-rims)**									
Alm06-085	Alm06-085	Alm06-111	Alm06-111	Alm06-111	Alm06-111	Alm06-113	Alm06-113	**Average**	2stdev	2stdev%		Alm06-086	Alm06-087	Alm06-087	Alm06-086	Alm06-086	Alm06-086	Alm06-087	**Average**	2stdev	2stdev%
34.94	34.70	34.45	33.49	33.62	33.28	34.30	34.75	**34.19**	1.28	3.7		34.07	34.51	34.43	33.81	33.34	33.52	33.53	**33.89**	0.93	2.7
12.97	12.49	12.46	12.42	12.92	13.24	12.73	11.76	**12.62**	0.90	7.2		12.13	12.59	12.16	12.78	12.26	12.35	13.07	**12.48**	0.70	5.6
4.00	3.96	3.69	3.56	3.80	4.04	3.84	3.85	**3.84**	0.32	8.4		3.39	3.49	3.61	3.67	3.65	3.43	3.89	**3.59**	0.34	9.5
0.03	0.04	0.04	0.06	0.04	0.04	0.03	0.06	**0.04**	0.02	49.7		0.04	0.04	0.04	0.05	0.06	0.05	0.02	**0.04**	0.02	50.4
34.32	33.81	34.14	34.28	34.19	33.63	34.23	34.48	**34.14**	0.56	1.6		34.31	34.19	32.96	33.97	34.18	33.73	33.27	**33.80**	1.03	3.0
0.02	0.01		0.01	0.02	0.01	0.02		**0.02**	0.01	44.8		0.02	0.03		0.04	0.02	0.01	0.02	**0.02**	0.02	106.6
0.02		0.00	0.01	0.02	0.02	0.01	0.01	**0.01**	0.01	146.6		0.01	0.01	0.00	0.02		0.01	0.01	**0.01**	0.01	85.2
		0.01		0.00	0.01	0.01		**0.01**	0.01	95.1		0.00	0.02				0.00		**0.01**	0.01	204.9
0.00	0.04		0.01	0.01	0.00	0.00		**0.01**	0.03	284.6		0.01	0.01	0.01	0.00		0.00	0.01	**0.01**	0.01	103.6
86.30	85.05	84.80	83.83	84.61	84.27	85.18	84.90	**84.87**	1.45	1.7		83.99	84.88	83.22	84.34	83.51	83.10	83.82	**83.84**	1.27	1.5
3.32	3.34	3.33	3.28	3.26	3.25	3.30	3.36	**3.30**	0.08	2.4		3.32	3.33	3.38	3.29	3.28	3.30	3.28	**3.31**	0.07	2.2
1.45	1.42	1.42	1.43	1.48	1.52	1.44	1.34	**1.44**	0.11	7.3		1.39	1.43	1.41	1.46	1.42	1.43	1.51	**1.44**	0.08	5.3
0.32	0.32	0.30	0.29	0.31	0.33	0.31	0.31	**0.31**	0.02	7.8		0.28	0.28	0.30	0.30	0.30	0.28	0.32	**0.29**	0.03	9.9
0.00	0.00	0.00	0.00	0.00	0.00	0.00	0.00	**0.00**	0.00	50.6		0.00	0.00	0.00	0.00	0.00	0.00	0.00	**0.00**	0.00	50.6
4.86	4.86	4.92	5.00	4.94	4.89	4.91	4.96	**4.92**	0.10	2.0		4.98	4.91	4.83	4.92	5.01	4.95	4.85	**4.92**	0.13	2.7
0.00	0.00		0.00	0.00	0.00	0.00		**0.00**	0.00	133.1		0.00	0.00		0.00	0.00	0.00	0.00	**0.00**	0.00	143.1
0.00			0.00	0.00	0.00	0.00	0.00	**0.00**	0.00	174.1		0.00	0.00	0.00	0.00		0.00	0.00	**0.00**	0.00	126.6
		0.00		0.00	0.00	0.00		**0.00**	0.00	247.2		0.00	0.00				0.00		**0.00**	0.00	370.6
0.00	0.00		0.00	0.00	0.00	0.00		**0.00**	0.00	342.9		0.00	0.00	0.00	0.00		0.00	0.00	**0.00**	0.00	141.6
9.95	9.95	9.96	10.01	10.00	9.99	9.98	9.97	**9.98**	0.04	0.4		9.98	9.96	9.92	9.98	10.01	9.98	9.96	**9.97**	0.06	0.6
93.86	93.83	94.28	94.49	94.13	93.69	94.08	94.11	**94.06**	0.52	0.6		94.75	94.58	94.21	94.29	94.35	94.60	93.84	**94.38**	0.61	0.6

Chl-3 (Chl-3-Atg-2-intergrowths)										Chl-3 (flaky Chl-inclusions in Opx-1)										
Alm06-086	Alm06-086	Alm06-086	Alm06-086	Alm06-087	Alm06-087	**Average**	2stdev	2stdev%		Alm06-086	Alm06-086	Alm06-086	Alm06-086	Alm06-087	Alm06-087	Alm06-087	Alm06-087	**Average**	2stdev	2stdev%
34.66	34.01	34.56	34.10	34.22	34.11	**34.28**	0.54	1.6		33.74	34.34	34.52	34.09	34.90	34.52	33.44	33.89	**34.18**	0.96	2.8
12.35	12.49	12.38	12.67	12.97	13.15	**12.67**	0.66	5.2		13.01	12.16	12.04	13.07	12.60	12.72	13.04	12.57	**12.65**	0.79	6.2
3.38	3.39	3.63	3.68	3.88	3.85	**3.64**	0.43	11.9		3.96	3.58	3.40	3.86	3.49	3.59	3.69	3.71	**3.66**	0.37	10.1
0.04	0.06	0.06	0.03	0.06	0.04	**0.05**	0.02	50.1		0.06	0.04	0.05	0.04	0.04	0.05	0.04	0.05	**0.05**	0.01	32.0
33.86	33.74	34.02	34.01	33.69	33.77	**33.85**	0.28	0.8		33.53	34.05	33.68	33.35	34.53	34.26	33.81	34.10	**33.91**	0.79	2.3
0.02	0.02	0.01	0.01	0.01	0.01	**0.01**	0.01	77.3		0.03	0.01	0.02	0.02	0.02	0.01	0.01	0.02	**0.02**	0.01	79.8
0.03	0.03	0.01	0.02	0.01	0.04	**0.02**	0.02	92.7		0.02	0.02	0.06		0.01	0.01	0.02	0.00	**0.02**	0.04	198.5
0.02			0.02		0.01	**0.01**	0.01	70.8						0.02	0.00	0.02	0.01	**0.01**	0.02	140.4
	0.01	0.00	0.01	0.00	0.00	**0.00**	0.01	171.0			0.01	0.02	0.01		0.01	0.01		**0.01**	0.01	123.0
84.36	83.75	84.68	84.54	84.84	84.98	**84.52**	0.88	1.0		84.34	84.21	83.80	84.45	85.61	85.17	84.08	84.35	**84.50**	1.19	1.4
3.36	3.32	3.34	3.30	3.31	3.29	**3.32**	0.05	1.5		3.28	3.34	3.37	3.31	3.33	3.32	3.26	3.29	**3.31**	0.07	2.0
1.41	1.44	1.41	1.45	1.48	1.49	**1.45**	0.07	4.8		1.49	1.39	1.38	1.49	1.42	1.44	1.50	1.44	**1.45**	0.09	6.3
0.27	0.28	0.29	0.30	0.31	0.31	**0.29**	0.03	11.3		0.32	0.29	0.28	0.31	0.28	0.29	0.30	0.30	**0.30**	0.03	10.7
0.00	0.00	0.00	0.00	0.00	0.00	**0.00**	0.00	50.4		0.00	0.00	0.00	0.00	0.00	0.00	0.00	0.00	**0.00**	0.00	32.6
4.89	4.91	4.90	4.91	4.85	4.86	**4.89**	0.05	1.1		4.86	4.93	4.90	4.82	4.92	4.91	4.92	4.94	**4.90**	0.08	1.6
0.00	0.00	0.00	0.00	0.00	0.00	**0.00**	0.00	77.7		0.00	0.00	0.00	0.00	0.00	0.00	0.00	0.00	**0.00**	0.00	79.7
0.00	0.00	0.00	0.00	0.00	0.00	**0.00**	0.00	92.7		0.00	0.00	0.01		0.00	0.00	0.00	0.00	**0.00**	0.00	226.0
0.00			0.00		0.00	**0.00**	0.00	236.9						0.00	0.00	0.00	0.00	**0.00**	0.00	281.9
	0.00	0.00	0.00	0.00	0.00	**0.00**	0.00	208.9			0.00	0.00	0.00		0.00	0.00		**0.00**	0.00	223.1
9.94	9.96	9.95	9.97	9.96	9.96	**9.96**	0.02	0.2		9.97	9.96	9.94	9.94	9.96	9.96	9.99	9.98	**9.96**	0.03	0.3
94.70	94.66	94.35	94.28	93.93	93.99	**94.32**	0.65	0.7		93.79	94.43	94.64	93.90	94.63	94.45	94.23	94.25	**94.29**	0.63	0.7

Granular Chl-harzburgite										**Spinifex-textured Chl-harzburgite**								
Chl-3 (flaky chlorite)										**Chl-3 (flaky chlorite)**								
Alm09-001	Alm09-001	Alm09-001	Alm09-001	Alm06-077	Alm06-077	**Average**	2stdev	2stdev%		Alm06-029	Alm06-029	Alm06-029	Alm06-141	Alm06-141	Alm06-141	**Average**	2stdev	2stdev%
32.89	34.43	34.42	34.51	34.46	34.72	**34.24**	1.34	3.9		33.27	34.37	32.27	33.24	32.11	33.04	**33.05**	1.63	4.9
12.67	13.59	13.27	13.02	12.77	12.40	**12.95**	0.86	6.7		14.96	13.62	15.89	13.82	13.53	15.33	**14.53**	2.00	13.8
3.63	3.57	3.30	3.53	3.67	3.49	**3.53**	0.26	7.4		3.06	3.07	3.40	3.10	2.90	3.52	**3.18**	0.47	14.8
0.02	0.01	0.03	0.03	0.03	0.03	**0.02**	0.02	78.2		0.02	0.05	0.04	0.03	0.04	0.01	**0.03**	0.02	74.6
34.01	34.71	34.85	34.31	34.67	34.86	**34.57**	0.68	2.0		34.12	35.03	33.31	33.29	33.34	33.93	**33.84**	1.37	4.0
0.00	0.01		0.02	0.02	0.01	**0.01**	0.01	108.6		0.01	0.00	0.01	0.01		0.02	**0.01**	0.01	136.5
0.00	0.04	0.03	0.05	0.01	0.01	**0.02**	0.04	158.1					0.00	0.01	0.01	**0.01**	0.01	141.7
		0.00	0.01	0.01		**0.01**	0.01	140.6			0.02	0.00		0.01		**0.01**	0.01	165.5
0.01	0.01	0.01	0.00	0.00		**0.00**	0.00	94.0			0.02	0.02				**0.02**	0.01	44.2
83.23	86.37	85.90	85.48	85.64	85.53	**85.36**	2.19	2.6		85.44	86.17	84.93	83.49	81.93	85.86	**84.64**	3.25	3.8
3.24	3.26	3.28	3.30	3.30	3.32	**3.28**	0.06	1.7		3.18	3.26	3.11	3.25	3.20	3.15	**3.19**	0.11	3.6
1.47	1.52	1.49	1.47	1.44	1.40	**1.46**	0.08	5.6		1.69	1.52	1.81	1.59	1.59	1.72	**1.65**	0.21	12.6
0.30	0.28	0.26	0.28	0.29	0.28	**0.28**	0.03	9.0		0.24	0.24	0.27	0.25	0.24	0.28	**0.26**	0.03	13.2
0.00	0.00	0.00	0.00	0.00	0.00	**0.00**	0.00	77.6		0.00	0.00	0.00	0.00	0.00	0.00	**0.00**	0.00	74.3
5.00	4.91	4.95	4.90	4.94	4.97	**4.94**	0.08	1.6		4.86	4.95	4.79	4.85	4.96	4.83	**4.87**	0.14	2.8
0.00	0.00		0.00	0.00	0.00	**0.00**	0.00	152.2		0.00	0.00	0.00	0.00		0.00	**0.00**	0.00	175.2
0.00	0.00	0.00	0.01	0.00	0.00	**0.00**	0.00	158.0					0.00	0.00	0.00	**0.00**	0.00	284.4
		0.00	0.00	0.00		**0.00**	0.00	282.3			0.00	0.00		0.00		**0.00**	0.00	299.5
0.00	0.00	0.00	0.00	0.00		**0.00**	0.00	141.4			0.00	0.00				**0.00**	0.00	314.9
10.02	9.98	9.98	9.96	9.98	9.98	**9.98**	0.04	0.4		9.98	9.98	9.99	9.95	10.00	9.98	**9.98**	0.03	0.3
94.35	94.54	94.96	94.54	94.39	94.68	**94.58**	0.44	0.5		95.21	95.31	94.58	95.04	95.35	94.50	**95.00**	0.74	0.8

Supplementary Table A2. Major element compositions of tremolite (representative measurements)

Lithology	**Atg-serpentinite**																					
Mineral growth stage	**Tr-1 (overgrowths on columnar metamorphic Cpx-2)**							**Tr-1 (isolated grains, not associated with Cpx)**						**Tr-1 (isolated grains, not associated with Cpx)**							
Sample	Alm06-119	Alm06-119	Alm06-119	Alm06-119	**Average**	2stdev	2stdev%	Alm06-119	Alm06-119	Alm06-119	**Average**	2stdev	2stdev%	Alm06-125	Alm06-125	Alm06-125	Alm06-125	Alm06-125	**Average**	2stdev	2stdev%
Wt% oxides																						
SiO2	58.25	58.13	58.35	58.31	**58.26**	0.19	0.3	57.41	58.23	58.66	**58.10**	1.27	2.2	58.15	58.30	58.79	58.75	58.70	**58.54**	0.58	1.0
Al2O3	0.19	0.22	0.27	0.13	**0.20**	0.11	55.5	0.22	0.19	0.18	**0.20**	0.04	18.1	0.35	0.38	0.24	0.12	0.27	**0.27**	0.20	74.6
FeO_{tot}	0.75	0.36	0.81	0.44	**0.59**	0.45	75.7	0.62	0.65	0.28	**0.52**	0.41	80.1	0.84	0.50	0.69	0.65	0.68	**0.67**	0.24	35.6
MnO	0.06	0.07	0.07	0.08	**0.07**	0.02	27.5	0.06	0.06	0.06	**0.06**	0.00	8.3	0.09	0.09	0.10	0.07	0.07	**0.08**	0.03	32.2
MgO	24.05	23.81	23.69	24.07	**23.91**	0.37	1.6	23.87	23.96	23.89	**23.91**	0.09	0.4	23.55	23.73	24.14	23.75	23.22	**23.68**	0.67	2.8
NiO	0.22	0.03			**0.13**	0.26	209.0									0.18	0.10	0.09	**0.12**	0.10	79.3
TiO2	0.02	0.03	0.02	0.02	**0.02**	0.01	37.4	0.03	0.04	0.03	**0.03**	0.02	44.9	0.01	0.03		0.03	0.01	**0.02**	0.02	103.3
CaO	13.63	13.57	13.14	13.70	**13.51**	0.50	3.7	13.47	13.53	13.48	**13.49**	0.06	0.5	12.58	12.55	12.96	13.04	12.68	**12.76**	0.45	3.5
K2O	0.01	0.03	0.03	0.03	**0.03**	0.02	85.5	0.04	0.02	0.02	**0.02**	0.02	79.1	0.11	0.11	0.05	0.03	0.08	**0.08**	0.08	97.7
Total	97.34	96.57	96.68	97.01	**96.90**	0.70	0.7	95.98	96.91	96.75	**96.55**	0.99	1.0	96.42	96.55	97.75	96.70	96.39	**96.76**	1.13	1.2
No. of ions in formula based on 23 O																						
Si	7.96	7.98	8.01	7.98	**7.98**	0.04	0.5	7.95	7.98	8.02	**7.98**	0.07	0.9	8.00	8.00	7.99	8.04	8.06	**8.02**	0.06	0.8
Al	0.03	0.04	0.04	0.02	**0.03**	0.02	55.8	0.04	0.03	0.03	**0.03**	0.01	19.4	0.06	0.06	0.04	0.02	0.04	**0.04**	0.03	75.0
Fe2+	0.09	0.04	0.09	0.05	**0.07**	0.05	75.6	0.07	0.07	0.03	**0.06**	0.05	80.6	0.10	0.06	0.08	0.07	0.08	**0.08**	0.03	35.9
Mg	4.90	4.88	4.85	4.91	**4.88**	0.06	1.2	4.93	4.89	4.87	**4.90**	0.06	1.2	4.83	4.86	4.89	4.85	4.76	**4.84**	0.10	2.1
Ni	0.02	0.00			**0.01**	0.02	333.7									0.02	0.01	0.01	**0.01**	0.02	204.4
Ti	0.00	0.00	0.00	0.00	**0.00**	0.00	37.6	0.00	0.00	0.00	**0.00**	0.00	44.9	0.00	0.00		0.00	0.00	**0.00**	0.00	158.0
Cr	0.00	0.00	0.00	0.00	**0.00**	0.00	37.8	0.00		0.00	**0.00**	0.00	219.9	0.00	0.00	0.00		0.00	**0.00**	0.00	137.1
Ca	2.00	2.00	1.93	2.01	**1.98**	0.07	3.5	2.00	1.99	1.98	**1.99**	0.02	1.2	1.86	1.85	1.89	1.91	1.87	**1.87**	0.05	2.9
K	0.00	0.01	0.01	0.01	**0.00**	0.00	85.7	0.01	0.00	0.00	**0.00**	0.00	80.6	0.02	0.02	0.01	0.00	0.01	**0.01**	0.01	98.3
Total	15.04	15.04	15.01	15.04	**15.03**	0.03	0.2	15.07	15.04	14.98	**15.03**	0.09	0.6	15.07	15.08	15.08	14.97	15.00	**15.04**	0.11	0.7
Mg#	98.27	99.16	98.13	98.99	**98.64**	1.03	1.0	98.56	98.51	99.35	**98.81**	0.95	1.0	98.04	98.82	98.43	98.50	98.39	**98.44**	0.56	0.6

Chl-serpentinite									**Atg-Chl-Opx-Ol rock**							
Tr-1 (large subhedral grains growing over Ol-2)									**Tr-1 (analyses of one grain)**							
Alm06-113	Alm06-113	Alm06-113	Alm06-113	Alm06-113	**Average**	2stdev	2stdev%		Alm06-087	Alm06-087	Alm06-087	Alm06-087	Alm06-087	**Average**	2stdev	2stdev%
57.36	57.85	57.98	57.42	57.70	**57.66**	0.54	0.9		57.74	57.71	57.91	57.38	57.56	**57.66**	0.40	0.7
0.22	0.12	0.16	0.30	0.29	**0.22**	0.16	70.7		0.15	0.05	0.09	0.19	0.12	**0.12**	0.11	88.5
1.53	1.24	1.29	1.55	1.70	**1.46**	0.39	26.4		1.12	1.35	1.18	1.55	1.25	**1.29**	0.33	25.8
23.95	24.33	24.01	23.98	23.79	**24.01**	0.39	1.6		23.63	24.18	24.13	23.56	23.86	**23.87**	0.56	2.4
	0.05	0.02	0.00		**0.02**	0.05	185.6			0.05		0.07		**0.06**	0.02	29.2
0.03		0.01	0.01	0.01	**0.02**	0.02	123.3		0.02	0.00		0.04	0.01	**0.02**	0.03	194.7
12.91	12.88	13.06	12.75	12.54	**12.83**	0.39	3.0		13.15	13.07	13.22	13.05	13.08	**13.11**	0.14	1.1
0.05	0.02	0.03	0.12	0.12	**0.07**	0.10	146.0		0.08	0.04	0.07	0.01	0.05	**0.05**	0.06	115.7
96.05	96.49	96.56	96.13	96.15	**96.28**	0.46	0.5		95.90	96.46	96.61	95.85	95.93	**96.15**	0.72	0.7
7.95	7.96	7.98	7.95	7.98	**7.96**	0.03	0.4		8.00	7.96	7.97	7.97	7.97	**7.97**	0.03	0.3
0.04	0.02	0.03	0.05	0.05	**0.04**	0.03	71.1		0.02	0.01	0.01	0.03	0.02	**0.02**	0.02	89.1
0.18	0.14	0.15	0.18	0.20	**0.17**	0.05	26.9		0.13	0.16	0.14	0.18	0.14	**0.15**	0.04	26.2
4.95	4.99	4.92	4.95	4.90	**4.94**	0.07	1.3		4.88	4.97	4.95	4.88	4.93	**4.92**	0.08	1.7
	0.01	0.00	0.00	0.00	**0.00**	0.00	284.9			0.01		0.01		**0.00**	0.01	276.4
0.00		0.00	0.00	0.00	**0.00**	0.00	174.5		0.00	0.00		0.00	0.00	**0.00**	0.00	238.8
		0.00	0.00	0.00	**0.00**	0.00	447.2				0.00		0.00	**0.00**	0.00	387.1
1.92	1.90	1.93	1.89	1.86	**1.90**	0.05	2.8		1.95	1.93	1.95	1.94	1.94	**1.94**	0.02	0.8
0.01	0.00	0.00	0.02	0.02	**0.01**	0.02	146.3		0.01	0.01	0.01	0.00	0.01	**0.01**	0.01	115.6
15.04	15.03	15.01	15.04	15.01	**15.02**	0.03	0.2		15.00	15.04	15.03	15.01	15.02	**15.02**	0.03	0.2
96.54	97.23	97.07	96.50	96.15	**96.70**	0.89	0.9		97.40	96.96	97.32	96.44	97.15	**97.05**	0.76	0.8

Granular Chl-harzburgite									**Spinifex-textured Chl-harzburgite**								
Tr-1									**Tr-1 (subhedral grains with occasional Ol and Opx inclusions)**								
Alm06-077	Alm06-077	Alm06-077	Alm06-077	Alm06-077	Alm06-077	**Average**	2stdev	2stdev%	Alm06-029	Alm06-029	Alm06-029	Alm06-029	Alm06-029	Alm06-029	**Average**	2stdev	2stdev%
57.90	57.82	58.48	58.55	58.18	58.33	**58.21**	0.60	1.0	57.52	58.22	58.32	58.20	58.24	57.85	**58.06**	0.62	1.07
0.14	0.15	0.20	0.12	0.23	0.27	**0.18**	0.11	61.9	0.12	0.15	0.15	0.22	0.23	0.32	**0.20**	0.15	73.58
0.56	0.72	1.02	1.01	0.86	0.66	**0.80**	0.38	47.3	0.76	0.39	0.90	0.90	0.84	0.94	**0.79**	0.40	51.30
0.04	0.04	0.05	0.05	0.05	0.09	**0.05**	0.04	71.7	0.07	0.06	0.06	0.08	0.07	0.08	**0.07**	0.02	24.23
23.79	23.52	23.91	23.83	23.55	23.62	**23.70**	0.32	1.4	23.81	23.94	24.11	24.01	24.12	24.05	**24.01**	0.23	0.98
0.10	0.06	0.12		0.01		**0.07**	0.10	137.0	0.07		0.25	0.22	0.33	0.13	**0.20**	0.21	103.21
0.00	0.02	0.01	0.00	0.02	0.01	**0.01**	0.02	165.3	0.03	0.00	0.01	0.01		0.03	**0.02**	0.02	141.85
12.87	13.10	12.85	13.52	12.29	12.57	**12.87**	0.85	6.6	12.96	13.27	12.66	12.95	12.54	12.65	**12.84**	0.54	4.24
0.13	0.09	0.13	0.07	0.13	0.02	**0.09**	0.09	90.8	0.06	0.08	0.06	0.01	0.05	0.05	**0.05**	0.05	84.24
95.91	95.89	97.25	97.30	95.64	95.70	**96.28**	1.55	1.6	95.65	96.46	96.83	96.78	96.79	96.47	**96.50**	0.89	0.92
8.01	8.00	7.99	8.00	8.05	8.05	**8.02**	0.05	0.7	7.98	8.00	7.99	7.98	7.99	7.96	**7.99**	0.02	0.31
0.02	0.03	0.03	0.02	0.04	0.04	**0.03**	0.02	62.2	0.02	0.02	0.02	0.04	0.04	0.05	**0.03**	0.02	73.47
0.06	0.08	0.12	0.12	0.10	0.08	**0.09**	0.04	46.2	0.09	0.05	0.10	0.10	0.10	0.11	**0.09**	0.05	51.16
4.90	4.85	4.87	4.85	4.86	4.86	**4.87**	0.04	0.8	4.93	4.90	4.93	4.91	4.93	4.94	**4.92**	0.03	0.51
0.01	0.01	0.01		0.00		**0.01**	0.01	221.5	0.01		0.03	0.02	0.04	0.01	**0.02**	0.03	147.51
0.00	0.00	0.00	0.00	0.00	0.00	**0.00**	0.00	166.0	0.00	0.00	0.00	0.00		0.00	**0.00**	0.00	181.82
	0.00	0.00		0.00	0.00	**0.00**	0.00	284.1	0.00	0.00	0.00	0.00	0.00	0.00	**0.00**	0.00	60.10
1.91	1.94	1.88	1.98	1.82	1.86	**1.90**	0.11	6.0	1.93	1.95	1.86	1.90	1.84	1.87	**1.89**	0.09	4.57
0.02	0.02	0.02	0.01	0.02	0.00	**0.02**	0.02	90.9	0.01	0.01	0.01	0.00	0.01	0.01	**0.01**	0.01	84.34
15.05	15.04	15.06	15.02	14.98	14.94	**15.01**	0.09	0.6	15.04	15.03	15.03	15.02	15.04	15.05	**15.04**	0.02	0.17
98.70	98.32	97.67	97.68	97.99	98.47	**98.14**	0.85	0.9	98.24	99.09	97.96	97.95	98.07	97.86	**98.19**	0.91	0.93

Supplementary Table A2. Major element compositions of olivine (representative measurements)

Lithology	**Atg-serpentinite**															
Mineral growth stage	**Ol-1 (overgrown by Atg-1 blades, associated with metamorphic Cpx-2**															
Sample	Alm06-093	Alm06-093	Alm06-093	Alm06-093	Alm06-093	Alm06-094	Alm06-094	Alm06-094	Alm06-094	Alm06-109	Alm06-109	Alm06-109	Alm06-109	**Average**	2stdev	2stdev%
Wt% oxides																
SiO2	40.27	40.48	41.65	40.99	40.69	40.41	40.31	40.22	40.18	40.44	40.96	40.91	41.29	**40.68**	0.91	2.2
Al2O3	0.00		0.00	0.01			0.00	0.01	0.00	0.01			0.02	**0.01**	0.01	132.4
FeO_{tot}	8.67	8.46	7.76	6.76	7.50	7.33	7.76	7.75	7.62	7.98	8.88	7.65	7.45	**7.81**	1.15	14.7
MnO	0.29	0.30	0.37	0.39	0.32	0.35	0.33	0.32	0.36	0.28	0.37	0.29	0.38	**0.33**	0.08	22.5
MgO	50.87	50.83	51.43	51.62	50.05	52.13	52.08	51.86	52.07	50.86	49.43	50.42	51.88	**51.19**	1.73	3.4
NiO	0.27	0.18	0.19	0.14	0.26	0.06	0.29	0.23	0.12	0.30	0.21	0.18	0.22	**0.20**	0.14	68.3
TiO2	0.01	0.02			0.01	0.08	0.01	0.02		0.01		0.02	0.01	**0.02**	0.04	232.3
Cr2O3		0.00		0.03	0.03	0.00		0.01		0.01		0.04		**0.02**	0.03	173.0
CaO	0.00	0.01	0.00	0.01	0.00	0.01	0.01	0.01	0.00	0.02	0.01	0.01	0.01	**0.01**	0.01	121.7
Na2O	0.01	0.00	0.00	0.03	0.00	0.02	0.01	0.01	0.01					**0.01**	0.02	171.2
Total	100.41	100.30	101.41	99.97	98.87	100.39	100.82	100.45	100.37	99.90	99.86	99.51	101.26	**100.27**	1.36	1.4
No. of ions in formula based on 4 O																
Si	0.98	0.99	1.00	0.99	1.00	0.98	0.98	0.98	0.98	0.99	1.00	1.00	0.99	**0.99**	0.02	2.0
Al	0.00		0.00	0.00			0.00	0.00	0.00	0.00			0.00	**0.00**	0.00	231.9
Fe2+	0.18	0.17	0.16	0.14	0.15	0.15	0.16	0.16	0.15	0.16	0.18	0.16	0.15	**0.16**	0.02	15.3
Mn	0.01	0.01	0.01	0.01	0.01	0.01	0.01	0.01	0.01	0.01	0.01	0.01	0.01	**0.01**	0.00	21.8
Mg	1.85	1.85	1.84	1.86	1.83	1.88	1.88	1.88	1.88	1.85	1.80	1.83	1.86	**1.85**	0.05	2.6
Ni	0.01	0.00	0.00	0.00	0.01	0.00	0.01	0.00	0.00	0.01	0.00	0.00	0.00	**0.00**	0.00	68.6
Ti	0.00	0.00			0.00	0.00	0.00	0.00		0.00		0.00	0.00	**0.00**	0.00	306.4
Cr		0.00		0.00	0.00	0.00		0.00		0.00		0.00		**0.00**	0.00	298.1
Ca	0.00	0.00	0.00	0.00	0.00	0.00	0.00	0.00	0.00	0.00	0.00	0.00	0.00	**0.00**	0.00	122.1
Na	0.00	0.00	0.00	0.00	0.00	0.00	0.00	0.00	0.00					**0.00**	0.00	244.8
Total	3.02	3.01	3.00	3.01	3.00	3.02	3.02	3.02	3.02	3.01	3.00	3.00	3.01	**3.01**	0.02	0.7
Mg#	91.27	91.46	92.20	93.16	92.25	92.69	92.29	92.27	92.41	91.91	90.84	92.16	92.54	**92.11**	1.23	1.3

Ol-1 (more granular and not overgrown by Atg-1)								**Ol-1 (elliptic Ol, exclusively occurring in sample Alm06-095**											
Alm06-109	Alm06-109	Alm06-109	Alm06-109	Alm06-109	**Average**	2stdev	2stdev%	Alm06-095	Alm06-095	Alm06-095	Alm06-095	Alm06-095	Alm06-095	Alm06-095	Alm06-095	Alm06-095	**Average**	2stdev	2stdev%
40.38	40.53	40.76	40.90	41.08	**40.73**	0.56	1.4	40.48	40.48	40.64	40.46	40.59	40.58	40.43	40.46	40.48	**40.51**	0.15	0.4
0.03	0.00	0.02	0.01	0.02	**0.02**	0.02	132.6	0.00				0.02	0.01				**0.01**	0.02	124.9
9.83	9.43	8.88	8.47	7.87	**8.90**	1.55	17.4	8.39	7.54	8.51	8.11	7.18	8.57	8.93	8.35	7.70	**8.14**	1.12	13.8
0.23	0.34	0.51	0.31	0.34	**0.35**	0.20	57.5	0.40	0.43	0.38	0.40	0.47	0.38	0.37	0.39	0.41	**0.40**	0.06	15.6
49.25	49.48	49.60	49.61	50.17	**49.62**	0.68	1.4	51.08	51.75	50.82	51.01	51.69	50.53	50.33	50.66	51.12	**51.00**	0.97	1.9
0.20	0.30	0.25	0.24	0.26	**0.25**	0.08	30.6	0.31	0.19	0.36	0.21	0.17	0.08	0.22	0.09	0.15	**0.20**	0.19	94.0
	0.01	0.02	0.01		**0.01**	0.01	115.6	0.04			0.02	0.01			0.01	0.01	**0.02**	0.02	126.1
																0.01	**0.00**	0.01	282.8
0.02	0.01	0.02		0.01	**0.01**	0.01	57.3	0.01	0.01	0.01	0.01		0.01	0.00	0.01	0.00	**0.01**	0.01	120.0
		0.00						0.00	0.01		0.01		0.01	0.01	0.01	0.01	**0.01**	0.01	105.0
99.93	100.10	100.06	99.56	99.74	**99.88**	0.45	0.5	100.71	100.41	100.72	100.23	100.16	100.17	100.31	100.00	99.89	**100.29**	0.57	0.6
0.99	0.99	1.00	1.00	1.00	**1.00**	0.01	0.9	0.98	0.98	0.99	0.99	0.98	0.99	0.99	0.99	0.99	**0.99**	0.00	0.5
0.00	0.00	0.00	0.00	0.00	**0.00**	0.00	132.9	0.00				0.00	0.00				**0.00**	0.00	353.6
0.20	0.19	0.18	0.17	0.16	**0.18**	0.03	17.9	0.17	0.15	0.17	0.17	0.15	0.17	0.18	0.17	0.16	**0.17**	0.02	14.1
0.00	0.01	0.01	0.01	0.01	**0.01**	0.00	57.2	0.01	0.01	0.01	0.01	0.01	0.01	0.01	0.01	0.01	**0.01**	0.00	15.3
1.80	1.81	1.81	1.81	1.82	**1.81**	0.02	0.8	1.85	1.87	1.84	1.85	1.87	1.84	1.83	1.84	1.86	**1.85**	0.03	1.5
0.00	0.01	0.00	0.00	0.01	**0.00**	0.00	30.4	0.01	0.00	0.01	0.00	0.00	0.00	0.00	0.00	0.00	**0.00**	0.00	93.7
	0.00	0.00	0.00		**0.00**	0.00	227.6	0.00			0.00	0.00			0.00	0.00	**0.00**	0.00	248.2
																0.00	**0.00**	0.00	600.0
0.00	0.00	0.00		0.00	**0.00**	0.00	128.0	0.00	0.00	0.00	0.00		0.00	0.00	0.00	0.00	**0.00**	0.00	146.9
		0.00			**0.00**	0.00	447.2	0.00	0.00		0.00		0.00	0.00	0.00	0.00	**0.00**	0.00	162.9
3.01	3.01	3.00	3.00	3.00	**3.00**	0.01	0.3	3.02	3.02	3.01	3.02	3.01	3.01	3.01	3.01	3.01	**3.01**	0.00	0.2
89.93	90.34	90.87	91.26	91.91	**90.86**	1.55	1.7	91.56	92.44	91.41	91.81	92.77	91.31	90.95	91.54	92.21	**91.78**	1.17	1.3

Ol-1 (granular Ol associated with Mag and Chl-1)									**Ol-1 (overgrown by Atg-1-blades in the massive sample**								
Alm06-094	Alm06-094	Alm06-094	Alm06-094	Alm06-094	**Average**	2stdev	2stdev%		Alm06-119	Alm06-119	Alm06-119	Alm06-119	Alm06-119	Alm06-119	**Average**	2stdev	2stdev%
41.17	39.72	41.11	41.17	41.48	**40.93**	1.38	3.4		40.55	40.81	40.66	40.56	40.84	40.60	**40.67**	0.25	0.6
0.00	0.00		0.00		**0.00**	0.00	173.3		0.01		0.02	0.04	0.00	0.01	**0.02**	0.03	210.4
9.32	9.10	8.90	8.60	7.81	**8.75**	1.17	13.4		9.81	9.44	9.40	9.06	8.70	7.75	**9.03**	1.46	16.2
	0.28				**0.28**		0.0		0.27	0.21	0.36	0.29	0.28	0.33	**0.29**	0.10	35.6
50.26	51.09	50.16	50.67	51.14	**50.66**	0.91	1.8		50.00	50.17	50.35	50.59	50.97	51.35	**50.57**	1.02	2.0
0.19	0.21	0.18	0.19	0.23	**0.20**	0.04	21.9		0.24	0.27	0.31	0.27	0.28	0.28	**0.27**	0.04	16.2
0.00				0.00	**0.00**	0.00	178.4										
	0.00		0.06	0.07	**0.05**	0.08	173.2		0.03			0.01			**0.02**	0.02	93.4
0.00	0.01	0.00	0.00	0.01	**0.00**	0.01	134.4				0.00		0.00		**0.00**	0.00	188.6
	0.01		0.02	0.00	**0.01**	0.02	160.6			0.01	0.01	0.01			**0.01**	0.01	79.5
100.95	100.43	100.35	100.72	100.74	**100.64**	0.49	0.5		100.90	100.91	101.10	100.83	101.08	100.32	**100.86**	0.57	0.6
1.00	0.97	1.00	1.00	1.00	**0.99**	0.02	2.5		0.99	0.99	0.99	0.99	0.99	0.99	**0.99**	0.00	0.4
0.00	0.00		0.00		**0.00**	0.00	274.5		0.00	0.00	0.00	0.00	0.00	0.00	**0.00**	0.00	246.2
0.19	0.19	0.18	0.17	0.16	**0.18**	0.03	14.1		0.20	0.19	0.19	0.18	0.18	0.16	**0.18**	0.03	16.4
	0.01				**0.00**	0.01	282.8		0.01	0.00	0.01	0.01	0.01	0.01	**0.01**	0.00	35.5
1.81	1.86	1.82	1.83	1.84	**1.83**	0.04	2.1		1.81	1.82	1.82	1.83	1.84	1.86	**1.83**	0.03	1.8
0.00	0.00	0.00	0.00	0.00	**0.00**	0.00	21.7		0.00	0.01	0.01	0.01	0.01	0.01	**0.01**	0.00	16.0
0.00				0.00	**0.00**	0.00	278.6										
	0.00		0.00	0.00	**0.00**	0.00	273.8		0.00			0.00			**0.00**	0.00	334.4
0.00	0.00	0.00	0.00	0.00	**0.00**	0.00	135.5				0.00		0.00		**0.00**	0.00	400.2
	0.00		0.00	0.00	**0.00**	0.00	262.7			0.00	0.00	0.00			**0.00**	0.00	241.1
3.00	3.03	3.00	3.00	3.00	**3.01**	0.02	0.8		3.01	3.01	3.01	3.01	3.01	3.01	**3.01**	0.00	0.1
90.58	90.92	90.95	91.31	92.11	**91.17**	1.17	1.3		90.08	90.45	90.52	90.87	91.26	92.19	**90.90**	1.50	1.7

Chl-serpentinite
Ol-2 (fragmented aggregates)

Alm06-085	Alm06-085	Alm06-085	Alm06-085	**Average**	2stdev	2stdev%	Alm06-113	Alm06-113	Alm06-113	Alm06-113	Alm06-113	Alm06-113	**Average**	2stdev	2stdev%
39.99	40.04	39.89	40.03	**39.99**	0.14	0.3	41.05	40.97	41.04	41.38	40.94	41.08	**41.08**	0.32	0.8
0.04	0.01	0.02	0.02	**0.02**	0.03	125.0		0.01				0.06	**0.03**	0.07	200.5
11.47	11.84	11.36	10.90	**11.39**	0.77	6.8	10.45	10.81	10.16	9.91	10.40	10.03	**10.29**	0.66	6.4
0.23	0.28	0.22	0.16	**0.22**	0.10	43.8	0.22	0.25	0.27	0.28	0.26	0.28	**0.26**	0.04	16.7
49.03	49.06	49.54	49.64	**49.32**	0.64	1.3	50.13	50.39	50.59	51.09	50.02	51.02	**50.54**	0.89	1.8
0.33	0.39	0.41	0.44	**0.39**	0.10	25.0	0.45	0.39	0.40	0.38	0.35	0.31	**0.38**	0.10	26.1
0.02	0.01	0.01	0.01	**0.01**	0.01	99.8	0.01	0.01	0.01	0.03		0.00	**0.01**	0.03	197.8
0.00	0.00		0.00	**0.00**	0.00	64.0	0.01			0.01	0.01		**0.01**	0.00	41.1
	0.01						0.00		0.00		0.01	0.00	**0.00**	0.01	247.1
0.01		0.01		**0.01**	0.00	46.0		0.02			0.03	0.02	**0.02**	0.01	59.8
101.11	101.63	101.47	101.19	**101.35**	0.48	0.5	102.32	102.85	102.48	103.08	102.01	102.79	**102.59**	0.78	0.8
0.98	0.98	0.97	0.98	**0.98**	0.00	0.5	0.99	0.98	0.99	0.99	0.99	0.98	**0.99**	0.00	0.5
0.00	0.00	0.00	0.00	**0.00**	0.00	125.3		0.00				0.00	**0.00**	0.00	410.1
0.24	0.24	0.23	0.22	**0.23**	0.02	6.8	0.21	0.22	0.20	0.20	0.21	0.20	**0.21**	0.01	6.9
0.00	0.01	0.00	0.00	**0.00**	0.00	43.8	0.00	0.01	0.01	0.01	0.01	0.01	**0.01**	0.00	16.2
1.79	1.79	1.80	1.81	**1.80**	0.02	1.1	1.80	1.80	1.81	1.82	1.80	1.82	**1.81**	0.02	0.9
0.01	0.01	0.01	0.01	**0.01**	0.00	24.7	0.01	0.01	0.01	0.01	0.01	0.01	**0.01**	0.00	26.4
0.00	0.00	0.00	0.00	**0.00**	0.00	100.1	0.00	0.00	0.00	0.00		0.00	**0.00**	0.00	232.9
0.00	0.00		0.00	**0.00**	0.00	150.4	0.00			0.00	0.00		**0.00**	0.00	225.4
	0.00			**0.00**	0.00	400.0	0.00		0.00		0.00	0.00	**0.00**	0.00	326.9
0.00		0.00		**0.00**	0.00	236.9		0.00			0.00	0.00	**0.00**	0.00	232.1
3.02	3.02	3.03	3.02	**3.02**	0.00	0.2	3.01	3.02	3.01	3.01	3.01	3.02	**3.01**	0.00	0.2
88.40	88.08	88.60	89.03	**88.53**	0.80	0.9	89.53	89.26	89.87	90.19	89.55	90.07	**89.75**	0.71	0.8

									Ol-2 (strongly overgrown by Atg-1)							
Alm06-111	Alm06-111	Alm06-111	Alm06-111	Alm06-111	Alm06-111	**Average**	2stdev	2stdev%	Alm06-113	Alm06-113	Alm06-113	Alm06-113	**Average**	2stdev	2stdev%	
41.07	40.92	40.83	41.00	40.86	40.94	**40.94**	0.18	0.4	41.16	41.24	41.46	41.40	**41.32**	0.28	0.7	
	0.03		0.03		0.01	**0.02**	0.03	134.1		0.04	0.02		**0.03**	0.02	66.6	
10.19	9.32	9.88	10.26	9.71	9.73	**9.85**	0.69	7.0	8.38	8.57	8.70	8.45	**8.53**	0.28	3.3	
0.25	0.29	0.26	0.22	0.24	0.27	**0.26**	0.05	17.6	0.29	0.27	0.28	0.28	**0.28**	0.02	6.2	
50.33	50.89	50.52	50.51	50.83	50.35	**50.57**	0.48	0.9	52.08	52.09	51.95	52.26	**52.10**	0.25	0.5	
0.31	0.42	0.38	0.41	0.41	0.45	**0.40**	0.09	23.6	0.41	0.37	0.35	0.35	**0.37**	0.06	15.5	
		0.02		0.00		**0.01**	0.02	190.1		0.00	0.00	0.00	**0.00**	0.00	157.6	
	0.01	0.00				**0.01**	0.01	141.4	0.00				**0.00**			
0.01	0.01		0.01	0.00	0.01	**0.01**	0.01	76.2		0.01	0.00	0.01	**0.01**	0.00	73.9	
	0.00	0.01		0.00		**0.01**	0.01	136.6								
102.17	101.89	101.90	102.43	102.07	101.76	**102.04**	0.49	0.5	102.32	102.58	102.77	102.75	**102.60**	0.42	0.4	
0.99	0.99	0.99	0.99	0.98	0.99	**0.99**	0.00	0.4	0.98	0.98	0.99	0.98	**0.98**	0.00	0.3	
	0.00		0.00		0.00	**0.00**	0.00	277.0		0.00	0.00		**0.00**	0.00	243.5	
0.21	0.19	0.20	0.21	0.20	0.20	**0.20**	0.01	6.9	0.17	0.17	0.17	0.17	**0.17**	0.01	3.1	
0.01	0.01	0.01	0.00	0.00	0.01	**0.01**	0.00	17.8	0.01	0.01	0.01	0.01	**0.01**	0.00	6.2	
1.81	1.83	1.82	1.81	1.82	1.81	**1.82**	0.02	0.9	1.85	1.85	1.84	1.85	**1.85**	0.01	0.6	
0.01	0.01	0.01	0.01	0.01	0.01	**0.01**	0.00	23.7	0.01	0.01	0.01	0.01	**0.01**	0.00	15.9	
		0.00		0.00		**0.00**	0.00	401.4		0.00	0.00	0.00	**0.00**	0.00	217.4	
	0.00	0.00				**0.00**	0.00	363.2	0.00				**0.00**	0.00	400.0	
0.00	0.00		0.00	0.00	0.00	**0.00**	0.00	127.8		0.00	0.00	0.00	**0.00**	0.00	155.9	
	0.00	0.00		0.00		**0.00**	0.00	279.2								
3.01	3.01	3.01	3.01	3.02	3.01	**3.01**	0.00	0.1	3.02	3.02	3.01	3.02	**3.02**	0.00	0.1	
89.80	90.68	90.11	89.77	90.32	90.22	**90.15**	0.68	0.8	91.72	91.55	91.41	91.68	**91.59**	0.28	0.3	

Atg-Chl-Opx-Ol rock

Ol-2 (colorless, granular, associated with Opx-1, enclosing Chl-3-flakes											**Ol-3 (brown olivine)**							
Alm06-086	Alm06-086	Alm06-086	Alm06-086	Alm06-086	Alm06-086	Alm06-086	**Average**	2stdev	2stdev%		Alm06-087	Alm06-087	Alm06-087	Alm06-087	Alm06-087	**Average**	2stdev	2stdev%
40.67	40.64	40.39	40.72	40.31	40.09	40.38	**40.46**	0.46	1.1		40.45	40.18	40.59	40.42	40.49	**40.43**	0.30	0.8
0.01	0.01					0.02	**0.01**	0.01	101.3		0.01	0.01	0.02	0.02		**0.02**	0.01	76.9
10.25	9.47	10.34	9.83	10.34	10.23	10.28	**10.11**	0.66	6.5		10.30	10.41	10.25	10.29	10.51	**10.35**	0.21	2.1
0.16	0.15	0.15	0.15	0.20	0.16	0.17	**0.16**	0.03	21.6		0.12	0.12	0.12	0.14	0.12	**0.12**	0.02	13.4
50.02	50.23	49.90	50.12	49.70	49.76	50.02	**49.96**	0.38	0.8		50.01	49.99	49.80	49.83	49.70	**49.87**	0.26	0.5
0.19	0.31	0.28	0.31	0.17	0.32	0.24	**0.26**	0.12	45.8		0.42	0.40	0.38	0.39	0.45	**0.41**	0.06	13.7
0.02							**0.02**					0.01	0.00	0.01	0.00	**0.01**	0.01	172.5
0.00					0.01		**0.01**	0.01	130.5		0.00	0.02		0.00		**0.01**	0.02	261.5
0.01		0.00	0.00		0.01		**0.00**	0.01	163.5		0.00	0.00		0.00		**0.00**	0.00	71.3
0.00		0.01	0.01	0.00	0.02	0.02	**0.01**	0.01	125.2		0.03		0.01			**0.02**	0.03	190.7
101.33	100.82	101.08	101.14	100.73	100.59	101.12	**100.97**	0.53	0.5		101.34	101.14	101.16	101.11	101.28	**101.21**	0.20	0.2
0.99	0.99	0.98	0.99	0.99	0.98	0.98	**0.99**	0.01	0.5		0.98	0.98	0.99	0.98	0.99	**0.98**	0.01	0.6
0.00	0.00					0.00	**0.00**	0.00	284.4		0.00	0.00	0.00	0.00	0.00	**0.00**	0.00	139.3
0.21	0.19	0.21	0.20	0.21	0.21	0.21	**0.21**	0.01	6.9		0.21	0.21	0.21	0.21	0.21	**0.21**	0.00	2.2
0.00	0.00	0.00	0.00	0.00	0.00	0.00	**0.00**	0.00	22.0		0.00	0.00	0.00	0.00	0.00	**0.00**	0.00	13.5
1.81	1.82	1.81	1.81	1.81	1.82	1.82	**1.81**	0.01	0.4		1.81	1.82	1.81	1.81	1.80	**1.81**	0.01	0.6
0.00	0.01	0.01	0.01	0.00	0.01	0.00	**0.01**	0.00	45.8		0.01	0.01	0.01	0.01	0.01	**0.01**	0.00	13.7
0.00							**0.00**	0.00	529.2		0.00	0.00	0.00	0.00	0.00	**0.00**	0.00	217.7
0.00					0.00		**0.00**	0.00	389.9		0.00	0.00		0.00		**0.00**	0.00	358.4
0.00		0.00	0.00		0.00		**0.00**	0.00	275.7		0.00	0.00		0.00		**0.00**	0.00	201.1
0.00		0.00	0.00	0.00	0.00	0.00	**0.00**	0.00	160.2		0.00		0.00			**0.00**	0.00	363.0
3.01	3.01	3.02	3.01	3.01	3.02	3.02	**3.01**	0.01	0.2		3.02	3.02	3.01	3.01	3.01	**3.02**	0.01	0.2
89.69	90.44	89.59	90.09	89.55	89.66	89.66	**89.81**	0.66	0.7		89.64	89.54	89.65	89.62	89.40	**89.57**	0.21	0.2

Ol-4 (colorless rims on Ol-3)									Granular Chl-harzburgite Ol-2 (colorless, granular olivine, inclusion-free grains								
Alm06-087	Alm06-087	Alm06-087	Alm06-087	Alm06-087	Alm06-087	**Average**	2stdev	2stdev%	Alm09-001	Alm09-001	Alm06-058	Alm06-058	Alm06-077	Alm06-077	Alm06-077	Alm06-077	Alm06-077
40.57	40.66	40.86	40.44	40.84	41.09	**40.74**	0.47	1.1	40.37	40.49	40.54	40.36	40.34	40.51	40.72	40.43	40.77
0.03	0.02	0.00				**0.02**	0.03	170.4			0.00		0.01	0.03	0.01		0.04
10.28	10.26	10.31	10.51	10.39	10.16	**10.32**	0.24	2.3	10.34	9.81	9.68	9.67	9.72	9.17	8.96	9.99	10.20
0.13	0.15	0.13	0.14	0.11	0.13	**0.13**	0.02	18.5	0.08	0.10	0.10	0.11	0.02		0.18	0.24	0.18
50.22	50.01	50.04	49.81	49.97	50.56	**50.10**	0.52	1.0	48.92	49.68	49.45	49.41	49.91	51.06	50.71	49.49	49.68
0.42	0.40	0.43	0.41	0.43	0.44	**0.42**	0.03	8.0	0.32	0.33	0.41	0.36	0.27	0.31	0.28	0.30	0.26
0.01		0.02	0.00	0.01	0.01	**0.01**	0.02	162.9	0.01			0.03	0.01	0.03		0.03	0.02
		0.01	0.00		0.00	**0.01**	0.01	182.3	0.10	0.01			0.01		0.07	0.02	0.08
	0.01		0.02	0.01	0.02	**0.01**	0.01	47.4	0.02		0.01	0.00	0.01	0.01		0.01	0.01
0.01	0.01	0.00				**0.01**	0.01	125.2	0.01				0.01	0.01	0.01	0.04	
101.67	101.51	101.81	101.33	101.76	102.41	**101.75**	0.74	0.7	100.17	100.42	100.20	99.95	100.32	101.12	100.93	100.54	101.24
0.98	0.99	0.99	0.98	0.99	0.99	**0.99**	0.00	0.4	0.99	0.99	0.99	0.99	0.99	0.98	0.99	0.99	0.99
0.00	0.00	0.00				**0.00**	0.00	307.3			0.00		0.00	0.00	0.00		0.00
0.21	0.21	0.21	0.21	0.21	0.20	**0.21**	0.01	3.1	0.21	0.20	0.20	0.20	0.20	0.19	0.18	0.20	0.21
0.00	0.00	0.00	0.00	0.00	0.00	**0.00**	0.00	18.8	0.00	0.00	0.00	0.00	0.00		0.00	0.00	0.00
1.81	1.81	1.80	1.81	1.80	1.81	**1.81**	0.01	0.5	1.79	1.81	1.81	1.81	1.82	1.84	1.83	1.80	1.80
0.01	0.01	0.01	0.01	0.01	0.01	**0.01**	0.00	7.3	0.01	0.01	0.01	0.01	0.01	0.01	0.01	0.01	0.00
0.00		0.00	0.00	0.00	0.00	**0.00**	0.00	200.4	0.00			0.00	0.00	0.00		0.00	0.00
		0.00	0.00		0.00	**0.00**	0.00	318.0	0.00	0.00			0.00		0.00	0.00	0.00
	0.00		0.00	0.00	0.00	**0.00**	0.00	164.4	0.00		0.00	0.00	0.00	0.00		0.00	0.00
0.00	0.00	0.00				**0.00**	0.00	270.4	0.00				0.00	0.00	0.00	0.00	
3.02	3.01	3.01	3.02	3.01	3.01	**3.01**	0.00	0.1	3.01	3.01	3.01	3.01	3.01	3.02	3.01	3.01	3.01
89.70	89.68	89.64	89.42	89.55	89.87	**89.64**	0.30	0.3	89.40	90.03	90.11	90.11	90.15	90.85	90.98	89.83	89.67

Ol-2 (colorless, granular olivine, inclusion-rich grains							**Ol-2 (colorless, granular olivine, inclusion-free rim of inclusion-rich grain**						
Alm06-058	Alm06-058	Alm06-058	Alm09-001	Alm09-001	Alm09-001	Alm09-001	Alm06-058	Alm06-058	Alm06-058	Alm06-058	**Average**	2stdev	2stdev%
40.19	40.59	40.68	39.81	39.57	40.23	40.64	40.31	40.21	40.69	40.70	**40.41**	0.61	1.5
	0.01			0.01	0.01			0.01	0.00		**0.01**	0.03	239.6
9.69	9.75	9.66	9.99	10.26	9.85	9.56	9.64	9.65	9.72	9.64	**9.75**	0.65	6.6
0.12	0.14	0.12	0.03	0.10	0.05	0.13	0.10	0.12	0.12	0.12	**0.11**	0.10	86.5
49.54	49.15	49.19	49.27	49.29	49.70	48.50	49.33	49.47	49.35	49.25	**49.52**	1.12	2.3
0.38	0.16	0.44	0.31	0.26	0.33	0.27	0.32	0.30	0.14	0.29	**0.30**	0.14	47.3
0.03		0.01		0.02	0.01	0.02		0.01	0.00		**0.02**	0.02	104.8
	0.00		0.10	0.05				0.01		0.01	**0.04**	0.08	191.5
0.01	0.00		0.01	0.01	0.02	0.00	0.01	0.01	0.01	0.00	**0.01**	0.01	99.1
		0.00		0.01	0.02		0.01		0.00		**0.01**	0.02	163.6
99.96	99.81	100.12	99.51	99.58	100.23	99.13	99.73	99.78	100.04	100.01	**100.14**	1.06	1.1
0.99	1.00	1.00	0.98	0.98	0.99	1.00	0.99	0.99	1.00	1.00	**0.99**	0.01	1.2
	0.00			0.00	0.00		0.00	0.00	0.00	0.00	**0.00**	0.00	328.2
0.20	0.20	0.20	0.21	0.21	0.20	0.20	0.20	0.20	0.20	0.20	**0.20**	0.01	7.2
0.00	0.00	0.00	0.00	0.00	0.00	0.00	0.00	0.00	0.00	0.00	**0.00**	0.00	86.0
1.81	1.80	1.80	1.82	1.82	1.82	1.79	1.81	1.81	1.80	1.80	**1.81**	0.03	1.5
0.01	0.00	0.01	0.01	0.01	0.01	0.01	0.01	0.01	0.00	0.01	**0.01**	0.00	47.3
0.00		0.00		0.00	0.00	0.00	0.00	0.00	0.00	0.00	**0.00**	0.00	197.5
	0.00		0.00	0.00			0.00	0.00	0.00	0.00	**0.00**	0.00	313.7
0.00	0.00		0.00	0.00	0.00	0.00	0.00	0.00	0.00	0.00	**0.00**	0.00	137.3
		0.00		0.00	0.00		0.00	0.00	0.00	0.00	**0.00**	0.00	304.6
3.01	3.00	3.00	3.01	3.02	3.01	3.00	3.01	3.01	3.00	3.00	**3.01**	0.01	0.4
90.11	89.99	90.08	89.79	89.54	89.99	90.04	90.12	90.14	90.05	90.11	**90.05**	0.72	0.8

Spinifex-textured Chl-harzburgite

Ol-2 (colorless cores rimmed by brown Ol-3)										**Ol-2 (colorless cores rimmed by brown Ol-3)**								
Alm06-099	Alm06-099	Alm06-099	Alm06-099	Alm06-099	Alm06-099	**Average**	2stdev	2stdev%		Alm06-141	Alm06-141	Alm06-141	Alm06-141	Alm06-141	Alm06-141	**Average**	2stdev	2stdev%
40.02	40.21	40.62	40.32	40.46	40.53	**40.36**	0.44	1.1		40.83	40.65	40.78	41.14	41.00	40.52	**40.82**	0.45	1.1
0.02	0.05	0.01	0.04	0.04	0.02	**0.03**	0.03	90.1		0.07	0.04	0.02	0.02	0.03		**0.03**	0.05	132.3
11.82	10.53	9.49	10.84	11.08	9.75	**10.59**	1.73	16.3		8.87	8.89	8.58	8.76	9.10	8.76	**8.83**	0.35	3.9
0.34	0.16	0.15	0.10	0.22	0.06	**0.17**	0.20	114.7		0.24	0.15	0.05	0.14	0.24	0.18	**0.16**	0.14	84.9
47.89	49.27	49.91	49.06	49.22	49.85	**49.20**	1.46	3.0		50.83	50.25	50.78	50.94	50.60	50.49	**50.65**	0.51	1.0
0.28	0.30	0.33	0.34	0.25	0.29	**0.30**	0.06	21.5		0.31	0.29	0.33	0.38	0.35	0.29	**0.33**	0.07	22.5
	0.02	0.01		0.01		**0.01**	0.01	70.8			0.00	0.02			0.02	**0.01**	0.01	108.5
0.05				0.08		**0.07**	0.05	73.9		0.03	0.05	0.04	0.01			**0.03**	0.03	96.1
0.01	0.01			0.01		**0.01**	0.00	34.6			0.00		0.00	0.00	0.01	**0.00**	0.00	151.4
	0.01				0.00	**0.01**	0.01	166.5						0.02				
100.43	100.57	100.53	100.71	101.38	100.51	**100.69**	0.70	0.7		101.18	100.33	100.59	101.40	101.33	100.26	**100.85**	1.03	1.0
0.99	0.99	0.99	0.99	0.99	0.99	**0.99**	0.00	0.4		0.99	0.99	0.99	0.99	0.99	0.99	**0.99**	0.00	0.3
0.00	0.00	0.00	0.00	0.00	0.00	**0.00**	0.00	89.9		0.00	0.00	0.00	0.00	0.00	0.00	**0.00**	0.00	172.4
0.24	0.22	0.19	0.22	0.23	0.20	**0.22**	0.04	17.1		0.18	0.18	0.17	0.18	0.18	0.18	**0.18**	0.01	3.8
0.01	0.00	0.00	0.00	0.00	0.00	**0.00**	0.00	115.7		0.00	0.00	0.00	0.00	0.00	0.00	**0.00**	0.00	84.6
1.76	1.80	1.81	1.79	1.79	1.81	**1.80**	0.04	2.1		1.83	1.83	1.84	1.83	1.82	1.84	**1.83**	0.01	0.6
0.01	0.01	0.01	0.01	0.00	0.01	**0.01**	0.00	21.5		0.01	0.01	0.01	0.01	0.01	0.01	**0.01**	0.00	21.7
	0.00	0.00		0.00		**0.00**	0.00	237.0			0.00	0.00			0.00	**0.00**	0.00	258.4
0.00				0.00		**0.00**	0.00	324.6		0.00	0.00	0.00	0.00			**0.00**	0.00	191.6
0.00	0.00			0.00		**0.00**	0.00	223.1			0.00		0.00	0.00	0.00	**0.00**	0.00	234.7
	0.00				0.00	**0.00**	0.00	382.2						0.00		**0.00**	0.00	489.9
3.01	3.01	3.01	3.01	3.01	3.01	**3.01**	0.00	0.1		3.01	3.01	3.01	3.01	3.01	3.01	**3.01**	0.00	0.1
87.84	89.29	90.36	88.97	88.79	90.11	**89.23**	1.85	2.1		91.08	90.97	91.34	91.20	90.84	91.13	**91.09**	0.35	0.4

Ol-2 (colorless cores rimmed by brown Ol-3)										**Ol-3 (brown spinifex-textured olivine)**										
Alm06-142	Alm06-142	Alm06-142	Alm06-142	Alm06-142	Alm06-142	**Average**	2stdev	2stdev%		Alm06-099	Alm06-099	Alm06-141	Alm06-141	Alm06-142	Alm06-142	Alm06-142	Alm06-142	**Average**	2stdev	2stdev%
39.40	39.67	40.88	40.21	40.22	40.33	**40.12**	1.04	2.6		40.40	40.39	40.26	39.68	39.93	40.40	40.36	40.75	**40.27**	0.65	1.6
		0.01	0.01	0.02	0.03	**0.02**	0.02	127.6		0.02	0.04	0.01	0.03	0.03		0.01	0.02	**0.02**	0.02	95.0
9.01	9.31	9.23	9.46	9.20	9.08	**9.22**	0.32	3.5		9.97	9.44	8.74	9.91	9.55	9.52	8.70	8.53	**9.30**	1.13	12.1
0.02	0.25	0.02	0.02		0.39	**0.14**	0.35	251.2		0.15	0.11	0.14	0.17	0.29	0.09	0.17	0.11	**0.15**	0.12	79.7
50.53	50.18	50.51	50.14	49.86	50.33	**50.26**	0.51	1.0		49.50	50.08	50.56	49.57	49.73	49.59	50.24	49.99	**49.91**	0.75	1.5
0.39	0.45	0.31	0.35	0.37	0.34	**0.37**	0.09	24.7		0.33	0.38	0.26	0.45	0.50	0.56	0.50	0.44	**0.43**	0.20	45.7
0.01				0.01	0.01	**0.01**	0.01	73.2		0.08			0.04	0.09	0.09	0.11	0.02	**0.07**	0.07	98.7
				0.15	0.14	**0.14**	0.01	9.8		0.09	0.13		0.67	0.12	0.30		0.09	**0.23**	0.46	197.5
0.01		0.01	0.01	0.01		**0.01**	0.01	98.3				0.01		0.00	0.02			**0.01**	0.02	147.2
0.01		0.00			0.01	**0.01**	0.01	151.9			0.01						0.01	**0.01**	0.00	3.1
99.38	99.85	100.97	100.20	99.84	100.65	**100.15**	1.17	1.2		100.55	100.59	99.99	100.52	100.23	100.56	100.09	99.95	**100.31**	0.55	0.5
0.97	0.98	0.99	0.98	0.99	0.98	**0.98**	0.01	1.4		0.99	0.99	0.98	0.97	0.98	0.99	0.99	1.00	**0.99**	0.01	1.2
		0.00	0.00	0.00	0.00	**0.00**	0.00	214.5		0.00	0.00	0.00	0.00	0.00		0.00	0.00	**0.00**	0.00	128.8
0.19	0.19	0.19	0.19	0.19	0.19	**0.19**	0.01	3.6		0.20	0.19	0.18	0.20	0.20	0.19	0.18	0.17	**0.19**	0.02	12.3
0.00	0.01	0.00	0.00		0.01	**0.00**	0.01	286.4		0.00	0.00	0.00	0.00	0.01	0.00	0.00	0.00	**0.00**	0.00	80.2
1.86	1.84	1.82	1.83	1.82	1.83	**1.83**	0.03	1.5		1.80	1.82	1.84	1.81	1.82	1.81	1.83	1.82	**1.82**	0.03	1.4
0.01	0.01	0.01	0.01	0.01	0.01	**0.01**	0.00	25.9		0.01	0.01	0.01	0.01	0.01	0.01	0.01	0.01	**0.01**	0.00	45.7
0.00				0.00	0.00	**0.00**	0.00	238.3		0.00			0.00	0.00	0.00	0.00	0.00	**0.00**	0.00	166.1
				0.00	0.00	**0.00**	0.00	310.2		0.00	0.00		0.01	0.00	0.01		0.00	**0.00**	0.01	255.0
0.00		0.00	0.00	0.00		**0.00**	0.00	191.4				0.00		0.00	0.00			**0.00**	0.00	346.5
0.00		0.00			0.00	**0.00**	0.00	292.5			0.00						0.00	**0.00**	0.00	370.4
3.03	3.02	3.01	3.02	3.01	3.02	**3.02**	0.01	0.5		3.01	3.01	3.02	3.02	3.02	3.01	3.01	3.00	**3.01**	0.01	0.3
90.91	90.57	90.70	90.43	90.62	90.81	**90.67**	0.34	0.4		89.85	90.44	91.16	89.92	90.27	90.28	91.15	91.26	**90.54**	1.14	1.3

Ol-4 (colorless rims on brown spinifex-textured olivine and individual colorless grains

Alm06-029	Alm06-029	Alm06-099	Alm06-099	Alm06-141	Alm06-142	Alm06-142	**Average**	2stdev	2stdev%
40.64	40.69	40.39	40.24	40.89	39.93	40.72	**40.50**	0.66	1.6
0.03	0.02	0.02	0.00	0.05	0.01	0.01	**0.02**	0.03	174.6
9.06	8.96	9.73	9.85	8.30	9.00	9.37	**9.18**	1.05	11.4
0.12	0.16	0.11	0.18	0.05	0.17	0.21	**0.14**	0.11	73.7
50.72	50.70	50.11	49.82	50.95	50.10	49.78	**50.31**	0.94	1.9
0.44	0.39	0.33	0.42	0.44	0.57	0.48	**0.44**	0.15	34.3
0.01		0.00	0.01	0.00	0.00		**0.01**	0.01	174.1
			0.08	0.02	0.04	0.05	**0.05**	0.05	101.1
	0.01		0.00	0.01	0.00	0.02	**0.01**	0.01	163.1
	0.00								
101.03	100.93	100.69	100.60	100.73	99.82	100.64	**100.63**	0.78	0.8
0.99	0.99	0.99	0.98	0.99	0.98	0.99	**0.99**	0.01	0.8
0.00	0.00	0.00	0.00	0.00	0.00	0.00	**0.00**	0.00	173.9
0.18	0.18	0.20	0.20	0.17	0.18	0.19	**0.19**	0.02	12.0
0.00	0.00	0.00	0.00	0.00	0.00	0.00	**0.00**	0.00	74.1
1.83	1.83	1.82	1.82	1.84	1.84	1.81	**1.83**	0.02	1.2
0.01	0.01	0.01	0.01	0.01	0.01	0.01	**0.01**	0.00	34.9
0.00		0.00	0.00	0.00	0.00		**0.00**	0.00	240.9
			0.00	0.00	0.00	0.00	**0.00**	0.00	225.3
	0.00		0.00	0.00	0.00	0.00	**0.00**	0.00	231.1
	0.00						**0.00**	0.00	529.2
3.01	3.01	3.01	3.02	3.01	3.02	3.01	**3.01**	0.01	0.2
90.89	90.98	90.18	90.02	91.63	90.85	90.45	**90.71**	1.09	1.2

Supplementary Table A2. Major element compositions of orthopyroxene (representative measurements)

Lithology	**Atg-Chl-Opx-Ol rock**								
Mineral growth stage	**Opx-1**								
Sample	Alm06-086	Alm06-086	Alm06-086	Alm06-087	Alm06-087	Alm06-087	**Average**	2stdev	2stdev%
Wt% oxides									
SiO2	58.21	57.76	57.70	57.84	57.46	57.67	**57.77**	0.50	0.9
Al2O3	0.14	0.19	0.33	0.07	0.30	0.07	**0.18**	0.22	122.9
FeO_{tot}	7.02	7.26	7.50	6.75	7.23	7.08	**7.14**	0.51	7.1
MnO	0.15	0.19	0.17	0.15	0.16	0.13	**0.16**	0.04	26.5
MgO	35.34	35.31	35.28	35.79	35.66	35.96	**35.56**	0.57	1.6
NiO	0.05	0.05	0.06	0.08	0.07	0.08	**0.07**	0.03	40.6
TiO2	0.02	0.01	0.01	0.01	0.02	0.02	**0.02**	0.01	65.9
Cr2O3	0.06	0.08	0.15	0.04	0.06	0.00	**0.07**	0.10	150.5
CaO	0.03	0.04	0.06	0.03	0.03	0.03	**0.04**	0.02	62.1
Na2O	0.01	0.00	0.03	0.03			**0.02**	0.03	187.1
Total	101.02	100.89	101.29	100.79	101.00	101.04	**101.00**	0.34	0.3
No. of ions in formula based on 6 O									
Si	1.99	1.98	1.97	1.98	1.97	1.97	**1.98**	0.01	0.7
Al	0.01	0.01	0.01	0.00	0.01	0.00	**0.01**	0.01	122.9
Fe2+	0.20	0.21	0.21	0.19	0.21	0.20	**0.20**	0.01	7.1
Mn	0.00	0.01	0.00	0.00	0.00	0.00	**0.00**	0.00	26.7
Mg	1.80	1.81	1.80	1.83	1.82	1.84	**1.82**	0.03	1.7
Ni	0.00	0.00	0.00	0.00	0.00	0.00	**0.00**	0.00	40.6
Ti	0.00	0.00	0.00	0.00	0.00	0.00	**0.00**	0.00	66.0
Cr	0.00	0.00	0.00	0.00	0.00	0.00	**0.00**	0.00	150.4
Ca	0.00	0.00	0.00	0.00	0.00	0.00	**0.00**	0.00	62.1
Na	0.00	0.00	0.00	0.00			**0.00**	0.00	267.0
Total	4.01	4.01	4.02	4.02	4.02	4.02	**4.02**	0.01	0.3
Mg#	89.97	89.66	89.35	90.43	89.79	90.05	**89.88**	0.74	0.8

Granular Chl-harzburgite

Opx-1

Alm06-077	Alm06-077	Alm06-077	Alm06-077	Alm06-077	Alm06-077	Alm09-001	Alm09-001	Alm09-001	Alm06-058	Alm06-058	Alm06-058	Alm06-058	Alm06-058	Alm06-058	**Average**	2stdev	2stdev%
57.63	58.00	57.72	57.60	57.38	56.46	57.82	58.06	58.12	58.22	57.99	58.13	57.83	57.44	56.63	**57.67**	1.04	1.8
0.03	0.01	0.03	0.03	0.04	0.01	0.05	0.07	0.05	0.15	0.10	0.05	0.24	0.26	0.17	**0.09**	0.16	185.3
6.70	6.78	7.42	7.13	6.31	6.56	6.83	7.08	7.11	7.00	6.61	7.30	6.98	6.77	6.71	**6.89**	0.59	8.6
0.24	0.14	0.22	0.21		0.09	0.04	0.27	0.08	0.11	0.06	0.19	0.20	0.19	0.07	**0.15**	0.15	101.7
35.24	34.44	33.75	34.54	35.63	35.50	34.97	35.00	34.92	35.55	36.07	35.21	35.76	35.65	35.87	**35.21**	1.24	3.5
0.04	0.03	0.06	0.05	0.04	0.09	0.04	0.05	0.06	0.04	0.03	0.05	0.06	0.08	0.03	**0.05**	0.03	70.0
0.01	0.01	0.01	0.01	0.02	0.02	0.01		0.01	0.03	0.03	0.01	0.02	0.04	0.03	**0.02**	0.02	105.7
			0.13							0.03	0.11	0.02	0.07	0.10	**0.08**	0.09	116.4
0.05	0.06	0.06	0.06	0.07	0.08	0.07	0.08	0.07	0.06	0.08	0.07	0.08	0.10	0.08	**0.07**	0.02	33.9
		0.02					0.00	0.00		0.02		0.04	0.00		**0.01**	0.03	223.4
99.94	99.48	99.28	99.76	99.50	98.81	99.82	100.61	100.43	101.16	101.02	101.12	101.24	100.60	99.68	**100.16**	1.54	1.5
1.99	2.01	2.01	2.00	1.99	1.97	2.00	1.99	2.00	1.99	1.98	1.99	1.98	1.97	1.96	**1.99**	0.03	1.3
0.00	0.00	0.00	0.00	0.00	0.00	0.00	0.00	0.00	0.01	0.00	0.00	0.01	0.01	0.01	**0.00**	0.01	184.8
0.19	0.20	0.22	0.21	0.18	0.19	0.20	0.20	0.20	0.20	0.19	0.21	0.20	0.19	0.19	**0.20**	0.02	8.5
0.01	0.00	0.01	0.01		0.00	0.00	0.01	0.00	0.00	0.00	0.01	0.01	0.01	0.00	**0.00**	0.00	101.6
1.81	1.78	1.75	1.78	1.84	1.85	1.80	1.79	1.79	1.81	1.84	1.80	1.82	1.83	1.85	**1.81**	0.06	3.2
0.00	0.00	0.00	0.00	0.00	0.00	0.00	0.00	0.00	0.00	0.00	0.00	0.00	0.00	0.00	**0.00**	0.00	70.6
0.00	0.00	0.00	0.00	0.00	0.00	0.00		0.00	0.00	0.00	0.00	0.00	0.00	0.00	**0.00**	0.00	121.9
			0.00							0.00	0.00	0.00	0.00	0.00	**0.00**	0.00	308.0
0.00	0.00	0.00	0.00	0.00	0.00	0.00	0.00	0.00	0.00	0.00	0.00	0.00	0.00	0.00	**0.00**	0.00	33.4
		0.00					0.00	0.00		0.00		0.00	0.00		**0.00**	0.00	418.1
4.01	3.99	3.99	4.00	4.01	4.03	4.00	4.00	4.00	4.01	4.02	4.01	4.02	4.02	4.03	**4.01**	0.02	0.6
90.36	90.05	89.02	89.62	90.96	90.61	90.13	89.81	89.75	90.05	90.68	89.58	90.13	90.37	90.50	**90.11**	1.00	1.1

Spinifex-textured Chl-harzburgite

Opx-1

Alm06-099	Alm06-099	Alm06-140	Alm06-140	Alm06-140	Alm06-141	Alm06-141	Alm06-141	**Average**	2stdev	2stdev%
57.45	56.59	56.74	57.47	56.81	57.36	57.45	55.84	**56.96**	1.16	2.0
0.08	0.12	0.16	0.16	0.17	0.09	0.12	0.06	**0.12**	0.08	67.8
6.85	6.65	6.86	7.15	7.09	6.47	6.32	6.51	**6.74**	0.60	8.9
	0.10	0.20	0.16	0.15	0.11	0.03	0.01	**0.11**	0.14	124.4
35.71	35.61	35.36	35.26	35.05	35.01	34.88	35.83	**35.34**	0.70	2.0
0.05	0.09	0.02	0.01	0.08	0.10	0.03	0.07	**0.06**	0.07	122.6
0.01	0.02	0.01	0.07	0.03	0.01	0.00	0.01	**0.02**	0.05	218.9
0.01	0.24	0.21	0.07	0.31				**0.17**	0.25	147.7
0.05	0.09	0.06	0.06	0.05	0.04	0.07	0.04	**0.06**	0.03	58.2
0.02	0.01	0.00	0.00					**0.01**	0.02	186.4
100.24	99.52	99.62	100.41	99.73	99.19	98.90	98.38	**99.50**	1.34	1.3
1.98	1.97	1.97	1.98	1.97	1.99	2.00	1.96	**1.98**	0.02	1.3
0.00	0.00	0.01	0.01	0.01	0.00	0.00	0.00	**0.00**	0.00	67.4
0.20	0.19	0.20	0.21	0.21	0.19	0.18	0.19	**0.20**	0.02	8.2
	0.00	0.01	0.00	0.00	0.00	0.00	0.00	**0.00**	0.00	124.2
1.83	1.85	1.83	1.81	1.81	1.81	1.81	1.88	**1.83**	0.05	2.5
0.00	0.00	0.00	0.00	0.00	0.00	0.00	0.00	**0.00**	0.00	122.8
0.00	0.00	0.00	0.00	0.00	0.00	0.00	0.00	**0.00**	0.00	217.8
0.00	0.01	0.01	0.00	0.01				**0.00**	0.01	243.9
0.00	0.00	0.00	0.00	0.00	0.00	0.00	0.00	**0.00**	0.00	58.2
0.00	0.00	0.00	0.00					**0.00**	0.00	323.9
4.02	4.03	4.02	4.01	4.02	4.01	4.00	4.04	**4.02**	0.02	0.6
90.28	90.52	90.18	89.79	89.81	90.61	90.77	90.75	**90.34**	0.78	0.9

Supplementary Table A2. Major element compositions of clinopyroxene (representative measurements)

Lithology	**Atg-serpentinite**									
Mineral growth stage	**Cpx-1 (relic, dusty cores)**									
Sample	Alm06-109	Alm06-109	Alm06-109	Alm06-094	Alm06-093	Alm06-093	Alm06-093	**Average**	2stdev	2stdev%
Wt% oxides										
SiO2	53.89	54.84	52.20	56.56	55.89	56.09	56.03	**55.07**	3.11	5.7
Al2O3	0.97	0.73	1.34	0.01	0.00		0.03	**0.51**	1.16	225.7
FeO_{tot}	1.61	1.66	3.32	0.93	0.86	0.87	1.14	**1.48**	1.75	118.1
MnO	0.09	0.01	0.24					**0.11**	0.23	204.1
MgO	18.08	17.63	18.26	18.17	18.03	17.93	17.85	**17.99**	0.42	2.3
NiO	0.02	0.07	0.03	0.02	0.02	0.01	0.01	**0.02**	0.04	171.2
TiO2	0.06	0.10	0.13		0.00			**0.07**	0.11	152.9
Cr2O3	0.09	0.32	0.95	0.11			0.01	**0.30**	0.77	259.7
CaO	23.89	24.90	22.69	25.33	26.03	25.96	25.66	**24.92**	2.46	9.9
Na2O	0.32	0.27	0.29	0.02	0.01	0.00	0.03	**0.13**	0.30	222.4
Total	99.01	100.52	99.46	101.15	100.84	100.86	100.76	**100.37**	1.62	1.6
No. of ions in formula based on 6 O										
Si	1.97	1.98	1.92	2.02	2.00	2.01	2.01	**1.99**	0.07	3.4
Al	0.04	0.03	0.06	0.00	0.00		0.00	**0.02**	0.05	256.9
Fe2+	0.05	0.05	0.10	0.03	0.03	0.03	0.03	**0.05**	0.05	121.1
Mn	0.00	0.00	0.01					**0.00**	0.01	372.0
Mg	0.99	0.95	1.00	0.97	0.96	0.96	0.95	**0.97**	0.04	3.9
Ni	0.00	0.00	0.00	0.00	0.00	0.00	0.00	**0.00**	0.00	171.3
Ti	0.00	0.00	0.00		0.00			**0.00**	0.00	266.6
Cr	0.00	0.01	0.03	0.00			0.00	**0.01**	0.02	329.1
Ca	0.94	0.96	0.90	0.97	1.00	1.00	0.99	**0.96**	0.07	7.7
Na	0.02	0.02	0.02	0.00	0.00	0.00	0.00	**0.01**	0.02	223.1
Total	4.02	4.01	4.04	3.98	4.00	3.99	3.99	**4.00**	0.04	1.0
Mg#	95.24	94.98	90.74	97.20	97.41	97.34	96.55	**95.64**	4.75	5.0

Cpx-2 (metamorphic, inclusion-poorer rims on relic dusty Cpx-1)

Alm06-093	Alm06-093	Alm06-093	Alm06-093	Alm06-093	Alm06-109	Alm06-109	Alm06-109	Alm06-109	**Average**	2stdev	2stdev%
55.96	55.70	56.37	55.89	56.10	55.46	55.52	55.07	55.41	**55.72**	0.80	1.4
0.03	0.02				0.02	0.04	0.05		**0.03**	0.02	70.2
0.76	1.27	0.66	0.59	0.56	0.86	0.52	1.29	1.13	**0.85**	0.61	72.3
0.19	0.16	0.00		0.07	0.06		0.10		**0.10**	0.14	141.7
18.36	18.32	17.99	18.16	18.26	18.22	18.45	18.07	18.31	**18.24**	0.29	1.6
0.02	0.03				0.05	0.01	0.04		**0.03**	0.03	93.3
0.03	0.01		0.01		0.01	0.01	0.01		**0.01**	0.02	141.2
	0.05		0.11		0.10	0.02	0.26	0.05	**0.10**	0.17	170.6
25.72	25.68	26.08	26.27	26.03	25.17	25.64	25.02	25.23	**25.65**	0.87	3.4
0.02	0.01	0.02		0.01	0.02	0.02	0.04	0.03	**0.02**	0.02	101.3
101.10	101.25	101.12	101.02	101.04	99.96	100.23	99.95	100.16	**100.65**	1.11	1.1
2.00	1.99	2.01	2.00	2.01	2.00	2.00	2.00	2.00	**2.00**	0.01	0.5
0.00	0.00				0.00	0.00	0.00		**0.00**	0.00	210.2
0.02	0.04	0.02	0.02	0.02	0.03	0.02	0.04	0.03	**0.03**	0.02	72.9
0.01	0.00	0.00		0.00	0.00		0.00		**0.00**	0.00	224.8
0.98	0.98	0.96	0.97	0.97	0.98	0.99	0.98	0.99	**0.98**	0.02	2.0
0.00	0.00				0.00	0.00	0.00		**0.00**	0.00	224.3
0.00	0.00		0.00		0.00	0.00	0.00		**0.00**	0.00	224.0
	0.00		0.00		0.00	0.00	0.01	0.00	**0.00**	0.00	252.7
0.99	0.99	1.00	1.01	1.00	0.97	0.99	0.97	0.98	**0.99**	0.02	2.4
0.00	0.00	0.00		0.00	0.00	0.00	0.00	0.00	**0.00**	0.00	131.2
4.00	4.00	3.99	4.00	4.00	3.99	4.00	4.00	4.00	**4.00**	0.01	0.2
97.72	96.26	97.99	98.22	98.30	97.42	98.44	96.15	96.65	**97.46**	1.79	1.8

Cpx-2 (metamorphic, columnar Cpx in sample with no relic dusty Cpx-1)									
Alm06-119	Alm06-119	Alm06-119	Alm06-119	Alm06-119	Alm06-119	Alm06-119	**Average**	2stdev	2stdev%
55.47	55.12	54.97	54.91	54.44	55.59	55.58	**55.15**	0.85	1.5
0.02	0.01	0.02	0.02	0.00	0.02		**0.02**	0.02	99.6
0.75	0.80	1.00	1.40	0.71	0.77	0.81	**0.89**	0.48	54.3
	0.10	0.01	0.05	0.10	0.19	0.06	**0.09**	0.13	148.9
18.07	18.14	17.97	18.07	18.26	18.03	18.15	**18.10**	0.19	1.0
		0.03	0.01	0.05	0.01	0.02	**0.03**	0.03	127.5
0.01	0.01	0.05	0.02	0.04	0.02		**0.03**	0.03	126.2
	0.25	0.07	0.06			0.03	**0.10**	0.20	194.8
25.41	25.55	25.49	25.09	25.63	25.81	25.71	**25.53**	0.47	1.8
0.02	0.06	0.04	0.06		0.03	0.01	**0.04**	0.04	108.1
99.75	100.05	99.66	99.70	99.23	100.48	100.36	**99.89**	0.88	0.9
2.01	1.99	2.00	2.00	1.99	2.00	2.00	**2.00**	0.01	0.6
0.00	0.00	0.00	0.00	0.00	0.00		**0.00**	0.00	137.8
0.02	0.02	0.03	0.04	0.02	0.02	0.02	**0.03**	0.01	54.8
	0.00	0.00	0.00	0.00	0.01	0.00	**0.00**	0.00	180.8
0.97	0.98	0.97	0.98	0.99	0.97	0.97	**0.98**	0.02	1.7
		0.00	0.00	0.00	0.00	0.00	**0.00**	0.00	200.7
0.00	0.00	0.00	0.00	0.00	0.00		**0.00**	0.00	161.2
	0.01	0.00	0.00			0.00	**0.00**	0.01	304.9
0.99	0.99	0.99	0.98	1.00	1.00	0.99	**0.99**	0.02	1.6
0.00	0.00	0.00	0.00		0.00	0.00	**0.00**	0.00	145.3
3.99	4.00	4.00	4.00	4.01	4.00	4.00	**4.00**	0.01	0.3
97.72	97.59	96.98	95.83	97.86	97.67	97.56	**97.32**	1.42	1.5

Cpx-2 (metamorphic, individual clear neoblasts in samples with relic Cpx-1)									
Alm06-093	Alm06-093	Alm06-093	Alm06-094	Alm06-093	Alm06-094	**Average**	2stdev	2stdev%	
56.22	55.52	56.11	55.83	56.00	55.27	**55.83**	0.73	1.3	
0.01		0.01			0.02	**0.01**	0.01	110.0	
1.16	0.57	0.68	1.06	1.20	1.02	**0.95**	0.53	55.6	
0.02	0.02	0.08		0.02		**0.04**	0.06	158.1	
17.70	17.72	17.93	18.00	17.98	18.05	**17.90**	0.30	1.7	
0.01				0.01	0.03	**0.02**	0.02	121.2	
	0.00	0.01				**0.00**	0.01	258.5	
		0.06							
25.81	26.15	26.25	24.96	25.76	24.71	**25.61**	1.26	4.9	
	0.01	0.01	0.02	0.01	0.02	**0.01**	0.01	91.2	
100.93	100.00	101.13	99.88	100.99	99.12	**100.34**	1.60	1.6	
2.01	2.01	2.01	2.02	2.01	2.01	**2.01**	0.01	0.4	
0.00		0.00			0.00	**0.00**	0.00	260.9	
0.03	0.02	0.02	0.03	0.04	0.03	**0.03**	0.02	55.4	
0.00	0.00	0.00		0.00		**0.00**	0.00	239.7	
0.95	0.95	0.96	0.97	0.96	0.98	**0.96**	0.02	2.5	
0.00				0.00	0.00	**0.00**	0.00	268.8	
	0.00	0.00				**0.00**	0.00	464.8	
		0.00				**0.00**	0.00	489.9	
0.99	1.01	1.01	0.97	0.99	0.96	**0.99**	0.04	4.1	
	0.00	0.00	0.00	0.00	0.00	**0.00**	0.00	138.9	
3.99	3.99	3.99	3.98	3.99	3.99	**3.99**	0.01	0.2	
96.44	98.23	97.92	96.79	96.38	96.92	**97.11**	1.56	1.6	

Supplementary Table A2. Major element compositions of Ti-clinohumite (representative measurements)

Lithology	**Atg-serpentinite**																			
Mineral growth stage	**Ti-Chu-1**																			
Sample	Alm06-093	Alm06-093	Alm06-093	Alm06-093	Alm06-093	Alm06-093	Alm06-093	Alm06-093	Alm06-094	Alm06-094	Alm06-094	Alm06-094	Alm06-094	Alm06-094	Alm06-094	Alm06-094	Alm06-094	**Average**	2stdev	2stdev%
Wt% oxides																				
SiO2	37.07	37.22	37.92	37.44	37.71	37.18	37.15	37.02	37.95	37.82	38.40	37.90	38.17	37.62	37.65	37.71	37.84	**37.63**	0.80	2.1
Al2O3	0.02				0.03				0.03		0.02	0.04	0.05		0.02	0.00		**0.03**	0.03	112.2
FeO_{tot}	7.29	6.83	6.25	6.83	6.57	7.30	7.20	7.33	8.00	7.77	7.95	7.78	7.88	7.79	7.97	7.72	7.82	**7.43**	1.08	14.5
MnO					0.01					0.01	0.02			0.02	0.00		0.01	**0.01**	0.01	126.3
MgO	48.25	48.36	48.97	48.17	48.70	47.88	47.96	48.09	48.13	47.66	48.55	47.80	48.58	48.10	47.87	47.61	47.97	**48.16**	0.75	1.6
NiO	0.17	0.13	0.13	0.13	0.15	0.18	0.24	0.15	0.16	0.18	0.14	0.15	0.13	0.15	0.16	0.16	0.18	**0.16**	0.05	34.5
TiO2	4.92	4.72	5.14	5.19	5.01	5.09	5.09	4.89	4.92	5.03	4.28	5.11	5.00	5.16	5.14	5.09	5.24	**5.00**	0.45	9.0
Cr2O3			0.11			0.06	0.01					0.05	0.08			0.08		**0.07**	0.07	104.6
CaO	0.00	0.01	0.01	0.00	0.01	0.02	0.01	0.01	0.00	0.01	0.02	0.01	0.01		0.01	0.00	0.00	**0.01**	0.01	144.1
Na2O			0.02	0.01	0.00	0.02	0.00	0.01	0.00	0.02			0.02	0.04			0.01	**0.01**	0.02	166.6
K2O	0.01	0.01	0.01	0.01	0.01	0.01		0.00	0.01	0.02		0.00		0.02		0.00	0.00	**0.01**	0.01	137.5
Total	97.74	97.28	98.56	97.78	98.19	97.74	97.66	97.49	99.21	98.51	99.37	98.83	99.93	98.89	98.82	98.38	99.08	**98.44**	1.50	1.5
No. of ions in formula based on 17.4 O																				
Si	4.04	4.06	4.07	4.06	4.07	4.05	4.05	4.04	4.08	4.09	4.11	4.08	4.07	4.06	4.06	4.08	4.07	**4.07**	0.04	0.9
Al	0.00				0.00				0.00		0.00	0.00	0.01		0.00	0.00		**0.00**	0.00	229.6
Fe2+	0.66	0.62	0.56	0.62	0.59	0.66	0.66	0.67	0.72	0.70	0.71	0.70	0.70	0.70	0.72	0.70	0.70	**0.67**	0.09	14.0
Mn					0.00					0.00	0.00			0.00	0.00		0.00	**0.00**	0.00	285.5
Mg	7.83	7.87	7.84	7.79	7.83	7.77	7.79	7.83	7.71	7.68	7.75	7.68	7.72	7.73	7.70	7.68	7.69	**7.76**	0.13	1.7
Ni	0.02	0.01	0.01	0.01	0.01	0.02	0.02	0.01	0.01	0.02	0.01	0.01	0.01	0.01	0.01	0.01	0.02	**0.01**	0.00	35.2
Ti	0.40	0.39	0.42	0.42	0.41	0.42	0.42	0.40	0.40	0.41	0.34	0.41	0.40	0.42	0.42	0.41	0.42	**0.41**	0.04	9.2
Cr			0.01			0.01	0.00					0.00	0.01			0.01		**0.00**	0.01	234.2
Ca	0.00	0.00	0.00	0.00	0.00	0.00	0.00	0.00	0.00	0.00	0.00	0.00	0.00		0.00	0.00	0.00	**0.00**	0.00	144.4
Na			0.00	0.00	0.00	0.00	0.00	0.00	0.00	0.00			0.00	0.01			0.00	**0.00**	0.00	200.1
K	0.00	0.00	0.00	0.00	0.00	0.00		0.00	0.00	0.00		0.00		0.00		0.00	0.00	**0.00**	0.00	193.0
Total	12.96	12.95	12.91	12.91	12.92	12.93	12.93	12.96	12.92	12.90	12.94	12.90	12.93	12.93	12.92	12.90	12.91	**12.93**	0.04	0.3
Mg#	92.2	92.7	93.3	92.6	93.0	92.1	92.2	92.1	91.5	91.6	91.6	91.6	91.7	91.7	91.5	91.7	91.6	**92.0**	1.1	1.2

Supplementary Table A2. Major element compositions of talc (representative measurements)

Lithology	**Chl-serpentinite**									**Atg-Chl-Opx-Ol rock**						**Granular Chl-harzburgite**						
Mineral growth stage	**Talc (fine-grained intersticial talc)**									**Talc (pseudomorphically replaces Opx-1)**						**Talc (pseudomorphically replaces Opx-1)**						
Sample	Alm06-085	Alm06-085	Alm06-085	Alm06-085	Alm06-085	Alm06-085	**Average**	2stdev	2stdev%	Alm06-086	Alm06-086	Alm06-086	**Average**	2stdev	2stdev%	Alm06-077	Alm06-077	Alm06-077	Alm06-077	**Average**	2stdev	2stdev%
Wt% oxides																						
SiO2	62.86	59.87	62.31	60.93	61.98	62.23	**61.70**	2.19	3.6	61.91	62.16	62.17	**62.08**	0.29	0.5	62.32	61.89	62.57	63.01	**62.45**	0.94	1.5
Al2O3	0.16	0.22	0.12	0.10	0.19	0.09	**0.15**	0.11	74.9	0.22	0.12	0.36	**0.23**	0.25	106.5	0.12	0.11	0.11	0.09	**0.11**	0.02	20.9
FeO_{tot}	0.24	0.43	1.29	1.32	1.25	1.18	**0.95**	0.97	101.7	1.10	0.83	0.97	**0.97**	0.28	28.6	0.99	1.00	1.04	0.95	**0.99**	0.08	7.6
MnO	0.06		0.04				**0.05**	0.03	66.1													
MgO	30.35	30.27	30.23	30.44	30.67	31.09	**30.51**	0.65	2.1	30.83	31.05	30.97	**30.95**	0.22	0.7	30.55	31.15	31.04	30.65	**30.85**	0.58	1.9
NiO	0.14	0.04	0.10	0.15	0.18	0.12	**0.12**	0.10	80.0	0.08	0.06	0.08	**0.07**	0.02	27.3	0.13	0.06	0.15	0.05	**0.10**	0.10	107.1
TiO2	0.02	0.03	0.03	0.01	0.04	0.01	**0.02**	0.02	89.7	0.03	0.01	0.02	**0.02**	0.02	101.4	0.02		0.04	0.03	**0.03**	0.01	41.7
Cr2O3	0.04	0.04			0.89	3.26	**1.06**	3.05	288.1		3.88	0.90	**2.39**	4.22	176.6		2.37	3.39		**2.88**	1.44	50.1
CaO	0.01	0.02	0.02	0.22	0.17	0.04	**0.08**	0.18	232.6	0.08	0.05	0.00	**0.04**	0.08	190.2	0.10	0.05	0.01	0.02	**0.05**	0.08	176.8
Na2O	0.08	0.08	0.03	0.11	0.07	0.11	**0.08**	0.06	74.7	0.06	0.09	0.10	**0.09**	0.04	50.2	0.01	0.04	0.04	0.04	**0.03**	0.03	89.4
K2O	0.02	0.00	0.02	0.01	0.02	0.02	**0.01**	0.01	100.4	0.03	0.01		**0.02**	0.04	202.7	0.01		0.02	0.00	**0.01**	0.01	112.7
Total	93.98	91.00	94.17	93.28	95.46	98.14	**94.34**	4.74	5.0	94.34	98.25	95.57	**96.05**	4.00	4.2	94.26	96.67	98.40	94.85	**96.04**	3.75	3.9
No. of ions in formula based on 22 O																						
Si	8.05	7.94	8.01	7.93	7.90	7.77	**7.93**	0.19	2.4	7.95	7.76	7.90	**7.87**	0.20	2.5	7.99	7.82	7.79	8.02	**7.91**	0.24	3.0
Al	0.02	0.03	0.02	0.01	0.03	0.01	**0.02**	0.02	77.4	0.03	0.02	0.05	**0.03**	0.04	107.2	0.02	0.02	0.02	0.01	**0.02**	0.00	21.9
Fe2+	0.03	0.05	0.14	0.14	0.13	0.12	**0.10**	0.10	101.0	0.12	0.09	0.10	**0.10**	0.03	31.3	0.11	0.11	0.11	0.10	**0.11**	0.01	5.9
Mn	0.01	0.00	0.00	0.00	0.00	0.00	**0.00**	0.01	322.1	0.00	0.00	0.00	**0.00**	0.00		0.00	0.00	0.00	0.00	**0.00**	0.00	
Mg	5.79	5.99	5.79	5.91	5.83	5.79	**5.85**	0.16	2.7	5.90	5.78	5.86	**5.85**	0.13	2.2	5.84	5.86	5.76	5.82	**5.82**	0.09	1.5
Ni	0.01	0.00	0.01	0.02	0.02	0.01	**0.01**	0.01	79.2	0.01	0.01	0.01	**0.01**	0.00	29.7	0.01	0.01	0.01	0.00	**0.01**	0.01	106.2
Ti	0.00	0.00	0.00	0.00	0.00	0.00	**0.00**	0.00	90.3	0.00	0.00	0.00	**0.00**	0.00	103.9	0.00	0.00	0.00	0.00	**0.00**	0.00	140.0
Cr	0.00	0.00	0.00	0.00	0.09	0.32	**0.07**	0.26	367.1	0.00	0.38	0.09	**0.16**	0.40	253.9	0.00	0.24	0.33	0.00	**0.14**	0.34	237.5
Ca	0.00	0.00	0.00	0.03	0.02	0.00	**0.01**	0.03	233.7	0.01	0.01	0.00	**0.01**	0.01	191.9	0.01	0.01	0.00	0.00	**0.01**	0.01	178.4
Na	0.02	0.02	0.01	0.03	0.02	0.03	**0.02**	0.01	74.1	0.02	0.02	0.03	**0.02**	0.01	49.0	0.00	0.01	0.01	0.01	**0.01**	0.01	88.1
K	0.00	0.00	0.00	0.00	0.00	0.00	**0.00**	0.00	98.9	0.00	0.00	0.00	**0.00**	0.01	277.7	0.00	0.00	0.00	0.00	**0.00**	0.00	180.1
Total	13.95	14.05	13.99	14.07	14.05	14.07	**14.03**	0.10	0.7	14.04	14.05	14.04	**14.05**	0.01	0.1	14.00	14.06	14.04	13.97	**14.02**	0.08	0.6
Mg#	99.6	99.2	97.7	97.6	97.8	97.9	**98.3**	1.7	1.8	98.0	98.5	98.3	**98.3**	0.5	0.5	98.2	98.2	98.2	98.3	**98.2**	0.1	0.1

Supplementary Table A3.
Reactive bulk rock major element composition

	Atg-serpentinites (wt-%)	**Chl-harzburgites** (wt-%)
SiO_2	40.85	43.40
TiO_2	0.07	0.06
Al_2O_3	2.05	2.65
Cr_2O_3	0.39	0.39
FeO	3.07	6.01
MnO	0.13	0.11
NiO	0.29	0.26
MgO	41.48	42.61
CaO	0.86	0.08
Na_2O	0.004	0.01
K_2O	0.002	0.002
P_2O_5	0.003	0.010
LOI[a]	10.80	4.41
Total	100.00	100.00
Mg#[b]	96.0	92.7

Notes:

[a] LOI: loss on ignition determined by heating the dried sample powder at 1050 °C during 1.5 hours
[b] $[Mg/(Mg+Fe)]_{molar}$